

Application of Electrical Vehicle Energy Storage Nonaqueous Sodium-Ion Full Cells: Status, Approaches, and Prospects

P. Raj Kumar*¹, B. Prem Anand²

*Department of Mechanical Engineering, Engine Research Laboratory, Faculty of
Engineering and Technology, Annamalai University, Annamalainagar – 608 002, Tamil
Nadu, India*

Abstract

Sodium-ion full cells (SIFCs), as a novel bridging technology between sodium-ion half-cells (SIHCs) and commercial batteries, have recently garnered a great deal of attention in response to the increasing energy for Electrical vehicle application energy storage into sodium-ion batteries (SIBs). It is crucial to get a thorough and in-depth understanding of the major concerns and research status of SIFCs in order to effectively encourage their growth. This Review summarises the modification strategies to improve their electrochemical performance, such as interface modification, cathode/anode matching, capacity ratio, electrolyte optimisation, and sodium compensation, and focuses primarily on the interface issues, major challenges, and recent advances in SIFCs based on diverse electrolytes (i.e., nonaqueous liquid electrolytes, quasi-solid-state electrolytes, and all-solid-state electrolytes). Future research directions for constructing superior SIFCs are also discussed, along with outlooks and thoughts on those approaches.

1. Introduction

The fast growth of contemporary society means that the traditional energy supply from fossil fuels is insufficient to fulfil the rising demands. In the meanwhile, there has been a surge of interest in renewable energy sources like wind, solar, and geothermal as a solution to the environmental problems caused by the use of fossil fuels and the depletion of their supplies.[1] However, the output of these renewable sources of power varies over time and is dispersed geographically. In order to mitigate the intermittent nature of renewable energy sources, large-scale electrical energy storage (EES) technology is employed. One of the electrochemical energy storage technologies, lithium-ion batteries (LIBs) have found widespread application in portable electronic gadgets, electric automobiles, and hybrid electric vehicles [2,3]. Lithium-ion batteries (LIBs) are in high demand as the electric sector grows, even though lithium supplies are scarce. Novel rechargeable batteries including sodium-ion batteries (SIBs), aluminumion batteries, and others are being developed to ease the need for LIBs. SIBs are prospering after a slump due of their plentiful resources and low salt prices. Although adopting a similar working principle, SIBs are lazier in kinetics than LIBs because the radius of sodium ion (0.102 nm) is significantly bigger than that of lithium ion (0.076 nm)[4]. This has been one of the key reasons for its silence for many years. Fortunately, nanotechnology's quick progress and LIBs' research expertise have revived SIBs.

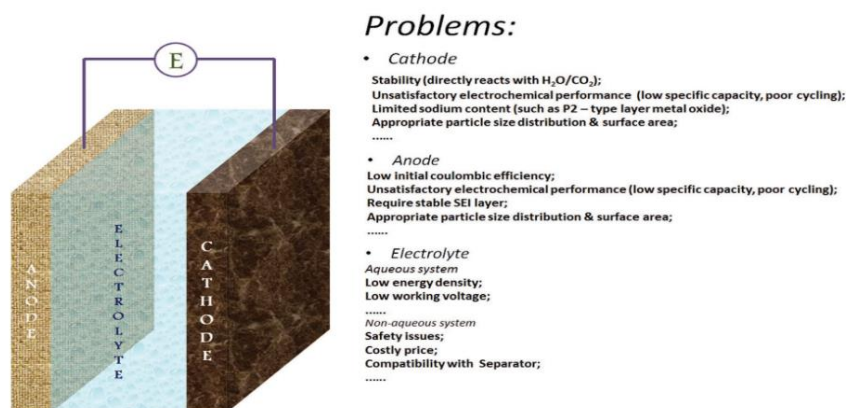
Academic research has always focused on cathode, anode, and electrolyte, which dominate battery cost and weight [5,6]. Oxides, polyanionic compounds, organics, Prussian blue, and its analogues are described SIB cathode materials. Despite their poor electronic/ionic conductivity, low specific capacity, structural instability, etc., many colourful and effective modification strategies like surface coating, encapsulation, composite-mixing, dimension reduction, doping, and morphology design have been widely proposed, and many Reviews have systematically summarised research on these aspects.[7–8] Generally anode materials have a substantially larger capacity than cathode materials because of the unique sodium storage method (such as alloying, conversion reaction, adsorption, and intercalation). Carbonaceous materials, titanates, chalcogenides, and organics are the four most investigated anode materials. It is the anode's difficulties, over and above those of the cathode, which restrict battery performance. These include, but are not limited to, high volume growth, poor cycle stability, low initial Coulombic efficiency, etc. These problems have been handled to a certain extent, and the related development may be completely comprehended in certain Reviews, in a manner not dissimilar to the methods used by cathode materials. [9,10–16] Nonaqueous liquid, quasi-solid, and all-solid electrolytes are the categories into which electrolytes fall. Electrolytes play a crucial role in the movement of sodium ions, and several studies have shown that electrolytes also affect the stability, Coulombic efficiency, and rate capacity of electrode materials. [5, 17–35] Furthermore, unlike LIBs, the sodium metal does not create an alloy with aluminium, therefore a cheaper aluminium current collector may be chosen in SIBs instead of a costly copper, further reducing the cost of the battery's construction. This is seen by the annual output of articles (Figure 1b). Although it only accounts for a small percentage of research activity on SIBs, related work on sodium-ion full cells (SIFCs) has quietly begun, with a focus on electrode materials and electrolytes. A pouch type complete cell with a $\text{NaNi}_{0.3}\text{Fe}_{0.4}\text{Mn}_{0.3}\text{O}_2$ cathode and hard carbon (HC) anode was first described in 2013 by Sumitomo Chemical Co. Ltd (Japan).[36] In 2015, the Sharp laboratory in the United States created a prototype complete cell using Prussian blue analogues for the cathode and HC for the anode, yielding a nominal voltage of 3 V.[37] Using a layered oxide cathode and an HC anode, Faradion (UK) was able to construct a whole cell with an energy density of over 120 W h kg^{-1} in the same year, which they then successfully integrated into electric bicycles. The first cylindrical type 18650 SIBs with an energy density of over 90 W h kg^{-1} and a cycle life of more than 2000 cycles are being developed by TIAMAT (France). This cell was developed collaboratively by CNRS and RS2E (France). In addition, two pouch type cells based on $\text{NaNi}_{1/3}\text{Fe}_{1/6}\text{Mn}_{1/3}\text{Mg}_{1/12}\text{Sn}_{1/12}\text{O}_2$ cathode and HC anode were proven by the Sharp laboratory (UK) in 2017. These cells have capacities of 3.3 and 4.2 Ah, respectively.[38] Recent advances in low-speed electric cars based on SIFCs have also been developed at the Institute of Physics, Chinese Academy of Science. Despite these advancements, there are still many reports on the prototype SIFCs; however, in terms of current industrialization status, the mostly used electrode materials are still oxides and HC, indicating that the other cathode or anode materials reported in literature are far away from real application for SIFCs.

The rational matching of different cathodes, anodes, and electrolytes, and especially the interface between them, is crucial to increasing performance in solid oxide fuel cells (SIFCs), as the four basic components—architecture, anode, cathode, electrolyte, and separator—have undefined and unexpected effects on the electrochemical properties of SIFCs. Thus, in stark contrast to the aforementioned Reviews, which all focused on a single electrode or electrolyte,[39] New perspectives (interface, whole cells instead of half-cells, etc.) and modification procedures for SIFCs are studied here. This Review focuses on: 1) In addition to the hottest nonaqueous liquid SIFCs (NALSIFCs), quasi-solid-state (QSSSIFCs) and all-solid-state (ASSSIFCs) electrolytes are also comprehensively discussed; 2) Half-cell interface discrepancies and major concerns are suggested and compared to full cells; 3) To further understand SIFC study, electrode materials, electrolytes, separators, binders, and conductive additives were statistically analysed; 4) The theoretical calculation of capacity, average voltage, Coulombic efficiency, mass ratio, energy density, and power density provides direction for developing high-performance SIFCs; 5) More crucially, sodium compensation solutions are first summarised fully. To power mid-range electric automobiles, CATL will start adding sodium cells to lithium battery packs. To make up for the reduced energy density, the business plans to exchange the two parts in production. San Diego researchers are helping the business develop safer, more energy-dense solid-state sodium batteries. CATL's first generation of sodium-ion cells has a gravimetric energy density of 160Wh/kg, compared to the Tesla Model 3 and Model Y's 2170 Li-ion cells' 250Wh/kg. Na-ion batteries in the new CATL will survive thousands of charging cycles and power an electric motor. These batteries also provide EVs ample range for most usage. The Chinese battery company believes that optimised sodium-ion cells might outperform Li-ion batteries in safety, charging speed, and cold-weather operability. Faradion, the global leader in non-aqueous sodium-ion cell technology, is helping Reliance Industries deliver sodium-ion batteries in India. Reliance acquired Faradion for USD135 million to commercialise sodium-ion battery technology through integrated and end-to-end Giga scale production in India. For cost-conscious buyers in India and other emerging nations, improved batteries would make EVs cheaper. Faradion has focused on sodium-ion batteries for over a decade, which now offer 160-170 watt-hours per kilogramme commercially and are anticipated to reach 200 soon. To encourage electrification and cut carbon emissions, India has subsidised electric vehicles, making them cheaper than petrol guzzlers. New electric motorcycles and rising gasoline prices will boost India's USD300 million EV storage. 4 million cars will be sold in India by 2025, including 5% EVs. As adoption rises, battery consumption will skyrocket, requiring large-scale imports to meet local demand. Thus, the Reliance acquisition of Faradion will help meet electric car battery storage needs in the future. Battery makers are aggressively investing on cheaper, denser, and lighter batteries by twisting existing battery chemistries. Ultra Fast Carbon Electrode, NAWA Technologies' battery technology, is projected to revolutionise the battery business. Vertically aligned carbon nanotubes (VACNTs) like the Ultra Fast Carbon Electrode can raise battery power ten-fold, energy storage by three, and battery lifespan by five. SVOLT has developed cobalt-free EV batteries without sacrificing energy density. Electric automobiles might have an 800-km (500-mile) range with the cobalt-free battery. More similar advances might improve electric car batteries.

1. Nonaqueous Sodium-Ion Full-Cell System

A sodium-ion battery with sufficient energy density, safety, rate capability, and cycle life will be an important component of future energy storage systems. The qualities of the active materials, cathode and anode compatibility, binder and separator choice, and electrolyte optimisation are the primary sources of these features. The active materials used in the cathode and anode of the nonaqueous sodium-ion full-cell devices may be broken down into two distinct categories: symmetric and asymmetric. In what follows, we'll compare and contrast these two distinct models.

Problem Identification



1.1 Symmetric Full-Cell Sodium-Ion Batteries

The symmetric sodium-ion full-cell system, in which the cathode and anode are made from the same active materials, is one of the most promising alternatives to the typical lithium-ion battery. Recent studies have focused on proposing the symmetric full-cell system for vanadium or titanium-based phosphate-type materials, with the two redox couples being M^{3+}/M^{2+} and M^{4+}/M^{3+} (M V, Ti, Cr, or Ni).

2. Full-Cell Sodium Ion Asymmetry Utilising Presodiated Anodes

The asymmetric full-cell system offers benefits due to its high energy density and low operating voltage in comparison to the symmetric sodium-ion full-cell system. Some alloy-based anode materials, meantime, can show extraordinarily high specific capacity of up to several hundred $mA\ h\ g^{-1}$, which can theoretically boost the energy density for future practical implementation. The commercialization of the sodium-ion battery is hindered by the full-cell system's irreversible capacity limitations with regard to the anode material and the lack of cyclable sodium ions. The foregoing issues have prompted the development of solutions such as the presodiation procedure and the sodium compensation method. Sacrifice salts, such as NaN_3 , Na_3P , and Na_2CO_3 , which break down into sodium ions at a particular potential, are one idea for offsetting the sodium ions in a complete cell system.

2.1 Features of the Interfaces of Chemical Reactors for SIFCs,

The interface characteristics are crucial due to the proximity of all electrochemical reaction sites at the interface of the electrochemical system. Nonaqueous liquid solid interface heterogeneous cultures (NALSIFCs), quaternary solid-state SIFCs (QSSSIFCs), and aqueous solid-state SIFCs (ASSSIFCs) interface characteristics.

2.2 Electrode-Electrolyte Interactions

Inactive sodium is mostly consumed irreversibly at this contact. Sodium is lost at a different rate in NALSIFCs and QSSSIFCs when liquid solvents like ethylene carbonate (EC), propylene carbonate (PC), and fluoroethylene carbonate (FEC) are present; this is because these solvents react with the anode and cathode to form solid/cathode electrolyte interphase (SEI/CEI) films. In contrast, in ASSSIFCs, under an appropriate electrochemical window, the electrode/electrolyte contact does not immediately induce irreversible consumption of active sodium. However, low cycle stability and rate capability result from their high interface resistance (R_{in}) and incompatibility due to solid electrode/solid electrolyte contact.

2.3 Electrolyte-Separator Interaction

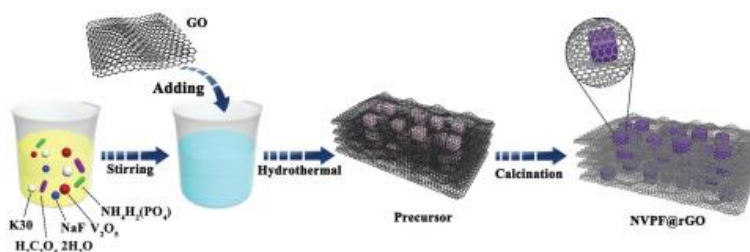
The traditional Celgard membranes show poor compatibility with many electrolyte systems (such as PC-FEC and EC-PC), which can lead to large polarisation or failure of the battery, but glass fibre is the most widely used separator among the reported NALSIFCs because of its good wettability and capability to uptake a large amount of electrolyte. Given the expensive price and limited mechanical strength of glass fibre, it is crucial for the advancement of SIFCs to modify electrolyte contents to increase compatibility with Celgard membranes.

2.4 Interparticle Interface

This primarily involves two interfaces: those between the particles of the active substance and those between the particles of the electrolyte. Ion migration and electron transmission are facilitated by the contact between particles at the interparticle (electrode) interface, which is present in all systems. To this goal, many methods, such as coating, composite, or morphological design (1D-3D), have been proposed to deal with such difficulties. Fast sodium ion transport is needed at the interparticle (electrolyte) contact, whereas electronic transmission should be minimised. The same holds true for the electrode/electrolyte interface, where a significant interface or grain boundary impedance has long been the stumbling block for solid-state electrolytes and, potentially, the tipping point for the game-changing development of solid-state batteries like ASSSIFCs.

3. Limited Cathode Type

In complete cells, $\text{Na}_3\text{V}_2(\text{PO}_4)_3$ is a preferred cathode material due to its strong cycle stability and acceptable operating voltage plateau (3.4 V for $\text{V}^{4+}/\text{V}^{3+}$). Full cells with an average voltage of 3 V may be made by matching with carbonaceous materials like HC.



Combining a graphene anode with a graphene-coated $\text{Na}_3\text{V}_2(\text{PO}_4)_3$ cathode, Liang et al. report a cell voltage of 2.7 V. The capacity retention after 200 cycles at 0.1 C is 77.1%, based on the initial discharge capacity of $109.2 \text{ mA h g}^{-1}$. [40]

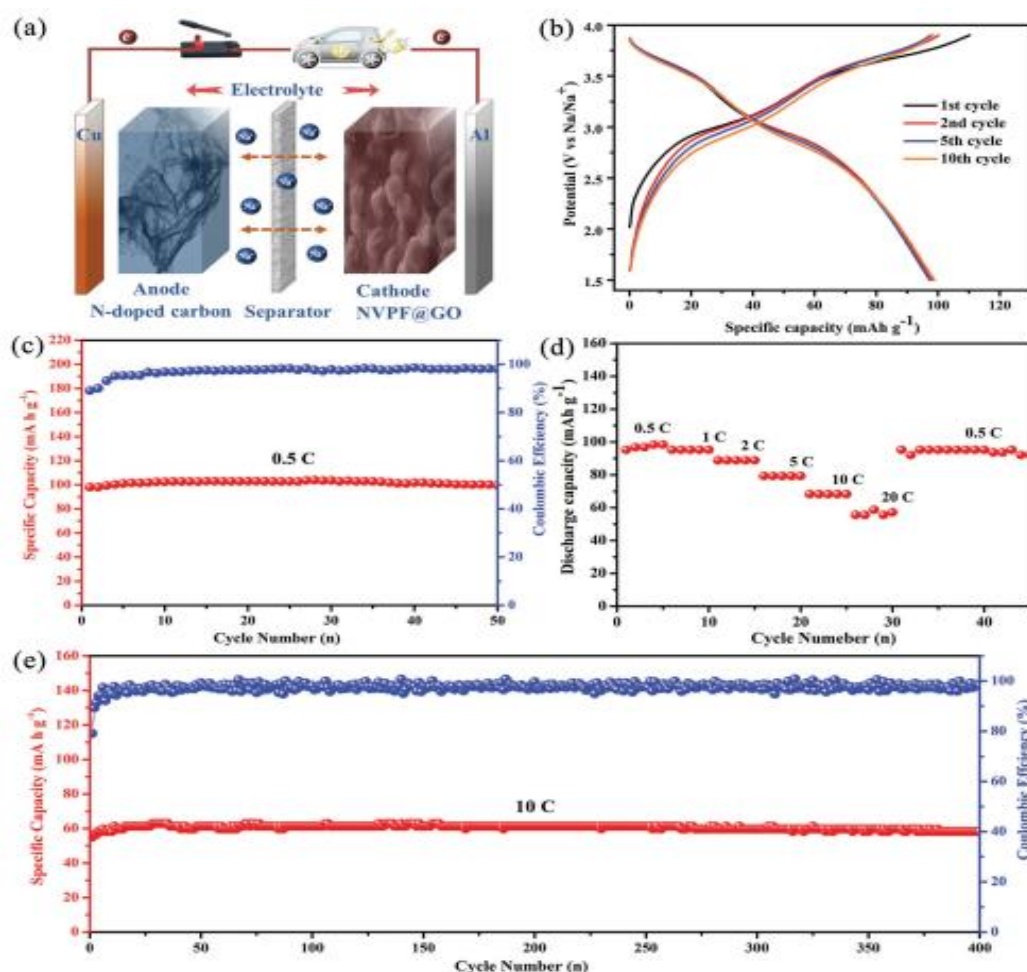


Figure 1 Electrochemical performance of NVPF@rGO cathode in sodium-ion full-cell. a) Schematic of the sodium-ion full-cell (NVPF@rGO || N-doped carbon); b) the charge/discharge profiles of the selected cycles at the current density of 0.5 C; c) the cycling performance at 0.5 C; d) the rate performance from 0.5 to 20 C; e) the long cycling performance at 10 C.

Phosphate-based whole cells (cathode material weights). This NVPF@rGON-doped carbon full-cell has 291 W h kg^{-1} energy density and 192 W kg^{-1} power density. Power density of 6144 W kg^{-1} does not change energy density of 139 W h kg^{-1} . The NVPF@rGO is ideal for high-power SIBs applications like hybrid electric vehicles, electric vehicles, and large-scale ESSs, despite having a lower energy density than $\text{VOPO}_4/\text{Na}_2\text{Ti}_3\text{O}_7$ at 100 W kg^{-1} [41].

Na extraction/addition. CV and GITT show the NVPF@rGO electrode's favourable Nadiiffusion kinetics. The sodium-ion full-cell with NVPF@rGO cathode and N-doped carbon anode has very reversible sodium storage and desired power performance. These positive results may inspire micro-/nanoscale electrode material research and engineering for SIBs. The average cell voltage based on HC anode was increased from 2.8 to 3.3 V by modifying $\text{Na}_3\text{V}_2(\text{PO}_4)_3$ particle size. [45] Anodes often use chalcogenides and elements. Cao et al. built a complete cell using a Sb anode and a $\text{Na}_3\text{V}_2(\text{PO}_4)_3$, graphene composite cathode, achieving an average voltage of 2.6 V and an energy density of 240 W h kg^{-1} at 0.1 C. [46]

Developed a scalable sol-gel technique to synthesise carbon-coated $\text{Na}_3\text{V}_2(\text{PO}_4)_3$ (NVP) and $\text{NaTi}_2(\text{PO}_4)_3$ (NTP) (NTP) composites with a porous structure. The simple synthesis process allows mass production of cathode and anode components. Despite their low carbon content, NVP/C and NTP/C electrodes demonstrated excellent electrochemical performance, including high power capability and cycle stability. NTP//NVP complete cells had 80% energy efficiency, 94% retention after 5000 cycles, and 85 mAh g^{-1} at 2.4 A g^{-1} depending on cathode power. [47] Tarascon et al. showed that a microsized Sn anode can perform better than an HC anode in terms of energy density and volumetric energy density.[48]

Faradion's first cathode materials were polyanionic materials, which Valence Technology has shown to have rich Na-ion chemistry, indicating considerable promise for high-voltage and high-capacity Na-ion cathodes. In September 2011, Faradion filed a patent on condensed mixed-phosphate polyanions, sulphate-based cathodes.[51] These patents covered prominent Na-ion cathodes such $\text{Na}_4\text{M}_3(\text{PO}_4)_2(\text{P}_2\text{O}_7)$ with Mn or Fe, [52] $\text{Na}_7\text{V}_4(\text{P}_2\text{O}_7)_4(\text{PO}_4)$ [52] or $\text{Na}_2\text{Fe}_2(\text{SO}_4)_3$. Due to their high energy density, vanadium-based phosphates and fluorophosphates like $\text{Na}_3\text{V}_2(\text{PO}_4)_3$ and $\text{Na}_3\text{V}_2(\text{PO}_4)_2\text{F}_3$ are the most attractive polyanionic molecules.

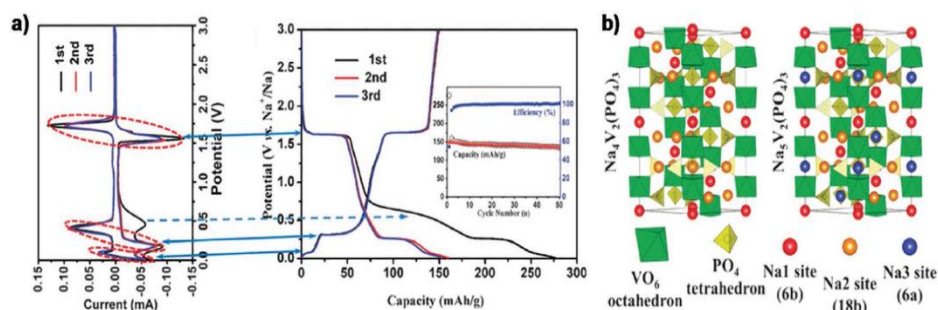


Figure 2 CV curves of $\text{Na}_3\text{V}_2(\text{PO}_4)_3/\text{C}$ cycled between 0–3 V. b) Charge/discharge curves of $\text{Na}_3\text{V}_2(\text{PO}_4)_3/\text{C}$ at a current rate of 0.1 C. The inset shows the capacity retention over 50 cycles. c) Structures of $\text{Na}_4\text{V}_2(\text{PO}_4)_3$ (left) and $\text{Na}_5\text{V}_2(\text{PO}_4)_3$ (right). Reproduced with permission.[235] Copyright 2015, Royal Chemical Society.

In addition to the cathode material's inherent qualities, such as structural and electrochemical stability, the electrolyte and the anode component play key roles in the construction of a well-functioning Na-ion battery. Polyanionic anode materials (such V- and Ti-based phosphates) have attractive electrochemical properties in both half cells (such as $\text{NaTi}_2(\text{PO}_4)_3/\text{Na}_{0.44}\text{MnO}_2$) and full cells. There is also a lot of research being done on new, more stable electrolyte systems, although detailing such systems would be beyond the scope of this introduction.

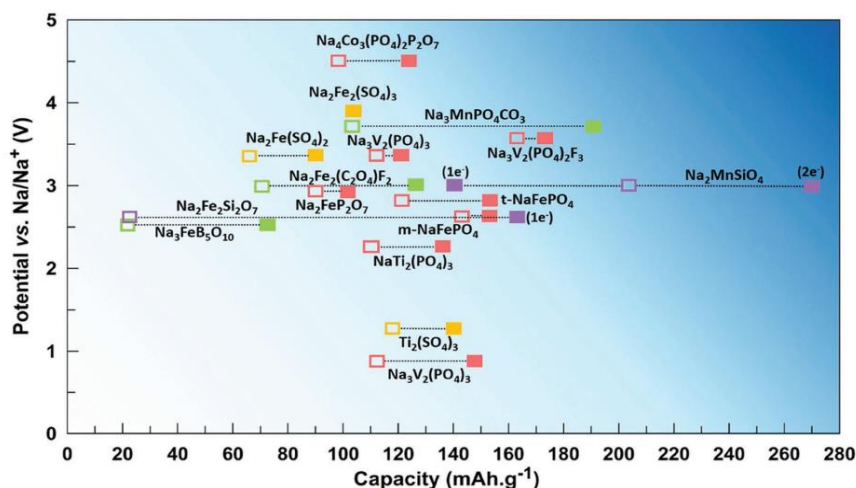


Figure 3. Overview of polyanionic cathode materials described in this review in terms of voltage and capacity. The red, orange and red squares represent phosphates, sulfates, and oxysalts including borates and silicates, respectively. The filled squares show the theoretical capacity, while the empty ones mark the experimental capacity.

Their once-widespread industrial use has been hampered by vanadium's toxicity and expensive price. Similarly fascinating is the pyrophosphate $\text{Na}_2\text{FeP}_2\text{O}_7$ because to its high power capacity, safety, and cycle stability; nevertheless, its low working voltage (3.0 V versus Na/Na) limits its practical value in terms of energy density. Alluaudite $\text{Na}_2\text{Fe}_2(\text{SO}_4)_3$ seems like a good option due to the high voltage it can produce and the wide variety of elements it is composed of. Sulfate's strong hygroscopicity, however, requires special care while handling it and limits its usefulness. [53] Illustrations of electrochemical cycling of such materials are shown in ESI figures S1a and S1b. Although these materials may display a high average discharge voltage (>3 V vs. Na/Na⁺), great cycling stability and rate performance, and a high degree of safety, the reported reversible capacities in full Na-ion cells were below 100 mA h g⁻¹. In an attempt to improve reversible capacities, Faradion investigated several oxide cathode materials and, in March 2012, filed a patent on metallate electrodes of the type $\text{Na}_a\text{M}_b\text{X}_c\text{O}_d$, where X is Sb, Ni, Se, Te, Ta, and/or Bi. Subsequently, Na-based layered oxides with O³⁻, P²⁻, and P³⁻-type structures were investigated by Faradion as promising active materials [55].

Layer oxides with formula AxMO_2 where M is a transition element with two oxidation states or a mixture of tetravalent and trivalent (or divalent) elements are generated for $0.5 \leq x \leq 1$. In a trigonal prismatic or octahedral setting, edge-sharing MO_6 octahedra hold alkali ions.

A_2MO_3 oxides have alkali ions between $(A_{1/2} M_{2/3}) O_2$ sheets, according to Delmas et al.[60] Oxide cathodes are possible.[61]

O3-type oxides have larger capacities because to their higher Na content (x value in $Na_x(TM)O_2$ is typically ~ 1), hence early investigations focused on materials with this structure. Na-based layered oxides provide an electrochemically stable voltage window for the $Ni^{2+} \rightleftharpoons Ni^{4+}$ redox potential. Na-ion full cells are ineffective if they can't enhance discharge capacity. To capitalise on this occurrence, Faradion includes a redox active element in a high oxidation state and "activated" it during primary discharge or cycling. This design accommodates multiple anomalous capacity methods.

The high oxidation state metal would be diminished during discharge if any $O^{2-} \rightleftharpoons O^{(2-n)-} + ne^-$ redox had a large hysteresis or wasn't totally reversible. In the event that any $O^{2-} \rightleftharpoons O^{(2-n)-} + ne^-$ redox generated an unacceptable fading in capacity, the metal with the originally high oxidation state would buffer it. Following such design concepts resulted in countless failed attempts.

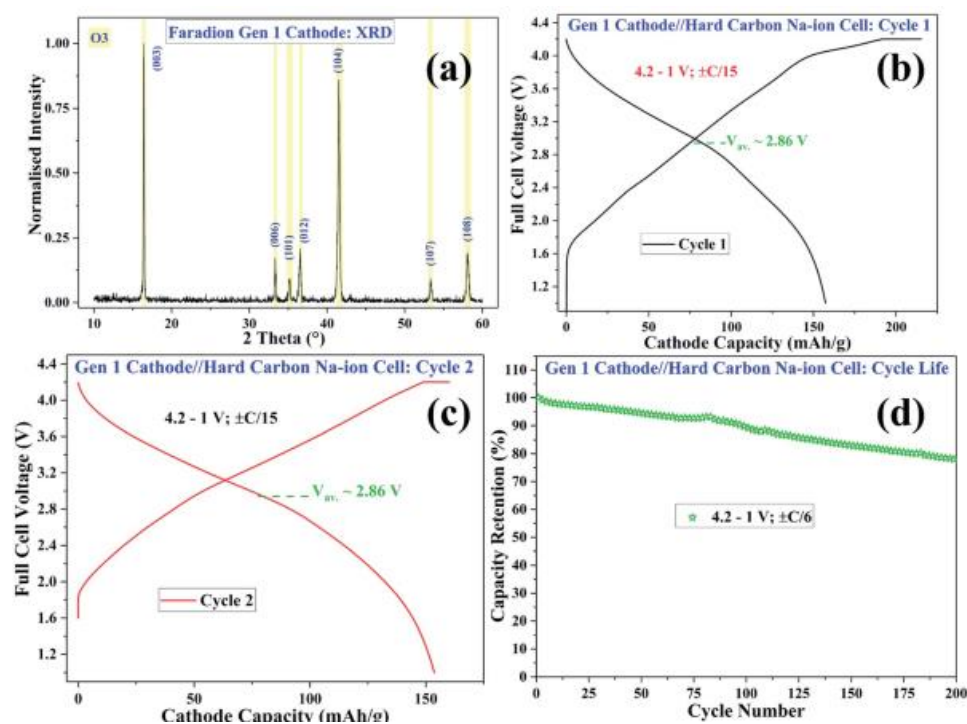
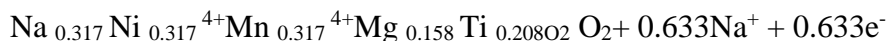
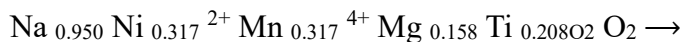


Fig. 4 Overview of Faradion's Gen 1 cathode material. (a) XRD plot confirming a typical O3 phase. (b) Cycle 1 of a full Na-ion cell paired with commercial hard carbon. (c) Cycle 2 of such a Na-ion cell illustrating smooth charge–discharge curves. (d) Cycling stability over 200 cycles at C/6 rate.

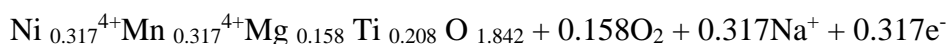
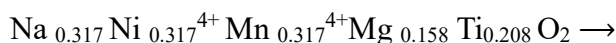
The simplified example below shows a system that can extract and reintroduce all Na with a minimum amount of Ni for low cost and high sustainability. This example assumes the extreme case of O^{2-} oxidation only, with no O_2^- : $O^{2-} \rightleftharpoons O^{(2-n)-} + ne^-$ redox, and it should be stressed that the example below is theoretical to aid understanding, since a first cycle loss is not taken into account and it is highly unlikely that acceptable cycle life could be achieved if all Na-ions were removed from the structure. O^{2-}

In Faradion's IP portfolio, the technique described here can be utilised more practically.

Charge. Step (1): Na⁺ extraction via Ni²⁺ oxidation to Ni⁴⁺



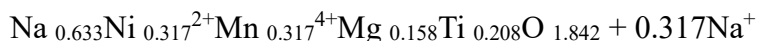
Step (2): Na⁺ extraction via O²⁻ oxidation to O₂



Discharge. Step (1): Na⁺ insertion via Ni⁴⁺ reduction to Ni²⁺



Step (2): Na⁺ insertion via Mn⁴⁺ reduction to Mn³⁺



The X-ray diffraction (XRD) pattern in Fig. 1a reveals that the stoichiometry of the first of Faradion's materials to be scaled up to multi-kilogramme level (referred to as 'Gen 1' cathode material) was Na_{0.950} Ni_{0.317} Mn_{0.317} Mg_{0.158} Ti_{0.208}- O₂, with a typical O3 phase. The material and its use in devices are protected under U.S. Patent 9774035[62]. An electrode according to the present invention includes an active material made up of one or more of the following: a transition metal chosen from titanium, vanadium, niobium, tantalum, hafnium, chromium, molybdenum, tungsten, manganese, iron, osmium, cobalt, nickel, palladium, platinum, copper, silver, gold, zinc, and cadmium; an optional non-transition metal chosen from magnesium, calcium. The finest electrodes in the present innovation employ a mixed phase material with Na⁺ and Li⁺ or K⁺. Instead, b=0 is active. Two or more simple anions form a negatively charged condensed polyanion. Species have octahedral, tetrahedral, or mixed structures. Homopolyanions (iso-condensed) and heteropolyanions (mixed) contain two or more core atoms that may be the same or different.

The centre atoms may include titanium, vanadium, chromium, molybdenum, tungsten, manganese, aluminium, boron, carbon, silicon, nitrogen, and phosphorus. Hetero-condensed polyanions include $V_2W_4O_{19}^{4-}$, $NiMo_2O_8^{2-}$, $CoMo_2O_8^{2-}$ and $MnMo_2O_8^{2-}$.

The core atoms may be linked to oxygen, hydroxide, sulphur, fluorine, chlorine, bromine, and iodine ligands. Since the dependent ligands attached to the central atom may be various kinds, condensed polyanions may be either iso-ligand or hetero-ligand. A hetero-ligand condensed polyanion with oxygen and a halogen in one or more ligands, such as $Mn_2F_6(P_2O_7)^{4-}$ is preferred.

In a preferred electrode embodiment, condensed polyanions including at least one of phosphorous, boron, titanium, vanadium, molybdenum, and sulphur are employed. Condensed phosphorous polyanions like $P_2O_7^{4-}$, $P_3O_9^{5-}$ and $P_4O_{10}^{6-}$, are useful active materials for electrodes. Compact phosphate polyanions are anionic entities made from corner-sharing PO_4 tetrahedra with an O/P ratio of $5/2 < O/P < 4$. Condensed phosphate moieties should not be confused with oxyphosphates, which contain oxygen atoms that do not belong in the anionic entity. $O/P > 4$ is a characteristic of all oxyphosphate anion instances.[62] The remarkable ability describes a version without O. The material's anomalous capacity was attributed to irreversible O₂-oxidation, hence the stoichiometry was chosen. [63]

The Faradion Gen 2 material is a mixed-phase material that averages the stoichiometries of the company's O3- and P2-type chemicals. We used a P2-type material with the stoichiometry $Na_{0.667}Ni_{0.300}Mn_{0.600}Mg_{0.033}Ti_{0.067}O_2$ and an O3-type material based on a version of the Gen 1 material for this experiment. Averaging the stoichiometries resulted in a target material with a Na content of < 1 , removing the requirement to avoid Na 1.0 materials. $NaNi_{0.333}Mn_{0.333}Mg_{0.167}Ti_{0.167}O_2$ might be used as the O3- dopant.

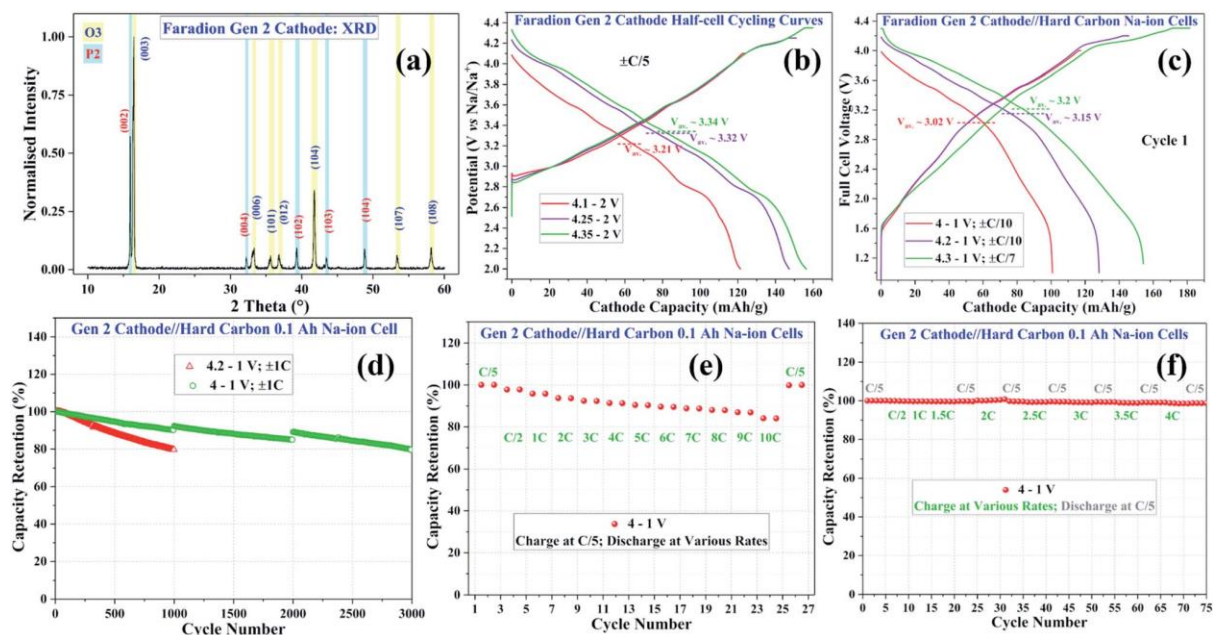


Fig. 5 Overview of Faradion's Gen 2 cathode. (a) XRD plot indicating presence of O3 as well as P2 phases. (b) Half-cell cycling at C/5 at various voltage windows.

Typical cycling performances of Gen 2 cathode in full Na-ion cells when paired with commercial hard carbon, showing (c) typical Cycle 1 curves using various voltage windows, (d) cycling stability at 4–1 V highlighting excellent cycling stabilities over 3000 cycles (please note that the capacity jumps seen after every 1000 cycles were due to cell relaxation for a few days after each thousand cycles: as the cycling programme was scheduled in batches of 1000 cycles, there was some delay in restarting the cycling programme), along with cycling stability at 4.2–1 V, (e) rate performance capabilities – response at a fast 10C rate (6 min) possible with 84% capacity retention, and (f) fast charge capabilities of Faradion's Na-ion cells with charge acceptance possible at 4C (15 min) without any drop in capacity

Numerous trials were performed with various mixtures of O3- and P2-type end members to determine their effects on stoichiometry, with results ranging from (25% O3, 75% P2) to (50% O3, 50% P2) to (75% O3, 25% P2). Note that it was not anticipated that these mixed-phase materials would necessarily have discrete phases with certain end-member stoichiometries. To do this, it is possible to synthesise each phase separately and then physically blend them, a process that is also protected by Faradion's intellectual property. However, the elemental ratio within each phase is influenced by a number of parameters, including the relative thermodynamic stabilities of each cation in the various structural types and the synthesis conditions. that demonstrated the best overall performance, synthesised directly, is now known as Faradion's Gen 2 material and has been scaled up by our commercial partner Haldor Topse A/S. The precursor material is prepared at the tonne level, and this can be fired under different conditions to provide active materials with a wide range of properties. Half-cell cycling of Faradion's Gen 2 cathode material at various voltage windows and utilising our standard CCCV At the most expanded 4.35–2 V window, the material delivers a near-theoretical capacity of 156 mA h g⁻¹ at $\pm C/5$ rate (theoretical capacity of the Gen 2 material is 165 mA h g⁻¹ based on the Ni²⁺ \rightleftharpoons Ni⁴⁺ redox couple); under de-rated conditions, such as 4.25–2 V or 4.1–2 V, reversible capacities of 147 mA h g⁻¹ or 121 mA h g⁻¹, respectively, can still be obtained. Fig. 5c presents galvanostatic cycling curves of full Na-ion pouch cells containing Gen 2 cathode//commercially available hard carbon anode using three different voltage windows to illustrate such flexibility of operation. At the most expanded voltage window of 4.3–1 V, a reversible capacity of 154 mA h g⁻¹ is obtained with an average discharge voltage of 3.2 V, In a slightly smaller 4.2–1 V window, reversible capacities of 130 mA h g⁻¹ are attained at a rather high average discharge voltage of 3.15 V. A cycling curve for the 4–1 V window shows 101 mA h g⁻¹ reversible capacity at 3.02 V under de-rated circumstances. Lee et al. found that intergrowth between the O3/P2 phases enhances sodium storage in mixed Na–Li oxide systems. Such stacking morphology suggests a high chance of such intergrowth.[82] As with any battery system, the cycle life of Gen 2 cathode/hard carbon complete Na-ion systems depends on the voltage window and cathode:anode mass balance. As shown in Fig. 5d, cycle lifetimes in excess of 3000 cycles can be produced to 20% capacity fade in 0.1 A h pouch cells at relatively rapid 1C rate between 4–1 V. Our current cell design has a cycle life of 1000 cycles at 4.2–1 V at 1C in prototype 0.1 A h cells, as shown in Fig. 5d. Li-ion literature shows that as the voltage window of cycling expands, cycle life decreases due to a combination of factors, including increased electrolyte reactivity at higher potentials, increased cathode (and/or anode) polarisation, and increased volume change of the cathode or anode.

On the last point, we expect the volume change of our mixed-phase O3/P2 Gen 2 cathode material during sodium (de-)intercalation.[64] and/or because to the projected lower TMO6 bond length distortion. [65]

Faradion's Na-ion cell architecture is optimised for high energy density; nonetheless, our energy cells can still react at relatively fast rates. A 0.1 A h pouch cell cycled through 4-1 V (the associated cycling curves are given in Fig. S4) is shown in Fig. 5e, illustrating the cycling stabilities at different rates up to 10C (charging being performed at C/5). At a rapid 4C pace (15 min discharge), our cells retain over 91% of their original capacity, and at a faster 10C rate (6 min discharge), we get 84%. In light of these quick reactions, Faradion cells can be used in a wide variety of high-power applications, such as in moderate-range electric vehicles and power equipment. Faster charging capability is crucial for many applications, especially consumer-facing ones like electric vehicles or consumer electronics, where customers prefer batteries capable of charging quickly in response to consumer demand. It can be seen in Fig. 2f that the C/5 capacity after charging at 4C is the same as the C/5 cycling in the first part of the experiment, proving that there was no loss of Na inventory from the cell due to plating, even though the total charge time was only 15 minutes.

Fewer studies have focused on full cells based on sulphate and pyrophosphate cathode materials, despite their abundant resources and environmentally friendly nature. Fe₃O₄@graphite//Na₂Fe_{1.8}(SO₄)₃ full cell with an average voltage of 3.2 V can deliver an energy density of 224 W h kg⁻¹ at 0.1 C with a capacity retention of 70% after 500 cycles.[66] The average voltage of sulfate-based complete cells can be increased further by picking the anode materials for Na-ion batteries with care. Having a firm grasp on their structure is crucial for maximising their Na storage capacities and, by extension, their performance. In this work, carbon nanofibers (CNFs) are generated using electrospinning, and their microstructure, texture, and surface functionality are modified via carbonization at temperatures ranging from 650 to 2800 °C.

In order to establish a connection between the properties of the CNFs and Na storage behaviour, we will be monitoring the relevant electrochemical performance as the heteroatoms are progressively removed and the graphitization degree is increased through a stepwise carbonization process. Na uptake plateaus at 0.1 V with capacities of 200 mAh g⁻¹ are discovered for CNFs carbonised at temperatures above 2000 °C, which is an impressive finding. This enhanced performance may be rooted in the fact that CNFs at these temperatures have a more graphitized structure, less active surface area, and a more porous texture. While the benefit of such CNFs electrode for increasing the energy density of full Na-ion cells has been demonstrated through the assembly of a CNF/Na₂Fe₂(SO₄)₃cell (such as carbonaceous materials [67]), difficulties due to their inherent poor thermal stability and crystallinity are bound to affect their practical application.

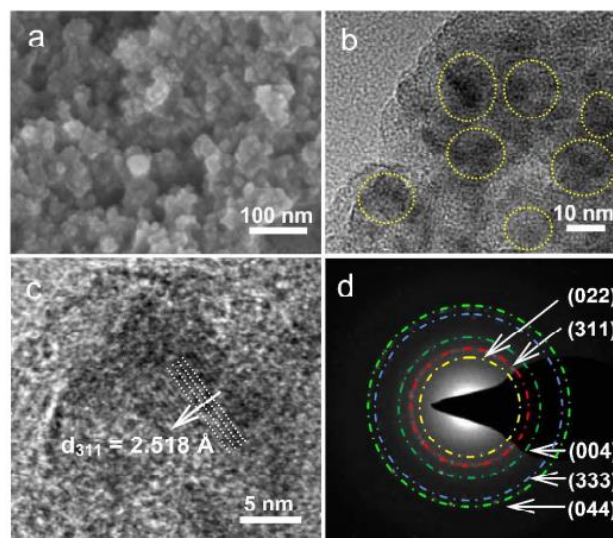


Fig. 6 The exposed lattice distance of 2.518 Å well correspond to the Fe₃O₄ planes of (311) (Fig. 6c). Besides, the indexed diffraction patterns of (002), (311), (004), (333) and (044) in selected area electron diffraction (SAED) were in good accordance with the XRD result, as shown in Figure 2a. Except the pattern of (422), which was too weak to observe in SAED and also not obvious in XRD (Fig. 1d, Fig. 2a). The crystal structure of Fe₃O₄ belongs to the space group of FD-3MZ (ICSD#633020),³³ in which the octahedral FeO₆ were corner connected by bridged O and the cell parameters of a, b and c were 8.3528 Å, as characterized by the Rietveld results of XRD pattern (Fig. 6b).³⁴ The main visual structure of PC-Fe₃O₄ was shown in Figure 1d, in which the Fe₃O₄ nanocrystals we .[68,69]

Many studies have looked into the electrochemical behaviour of different pyrophosphate cathode materials, however so far only iron-based pyrophosphate complete cells have been reported. However, because to reduced operating voltages and capacities, these complete cells are less competitive in real-world applications. It was proven by scanning electron microscopy (SEM), transmission electron microscopy (TEM), and high-resolution transmission electron microscopy (HRTEM) that the PC-Fe₃O₄ composite consists of Fe₃O₄ nanocrystals between 10-15 nm in size contained within the porous carbon (Fig. 6 a-c, yellow circle).

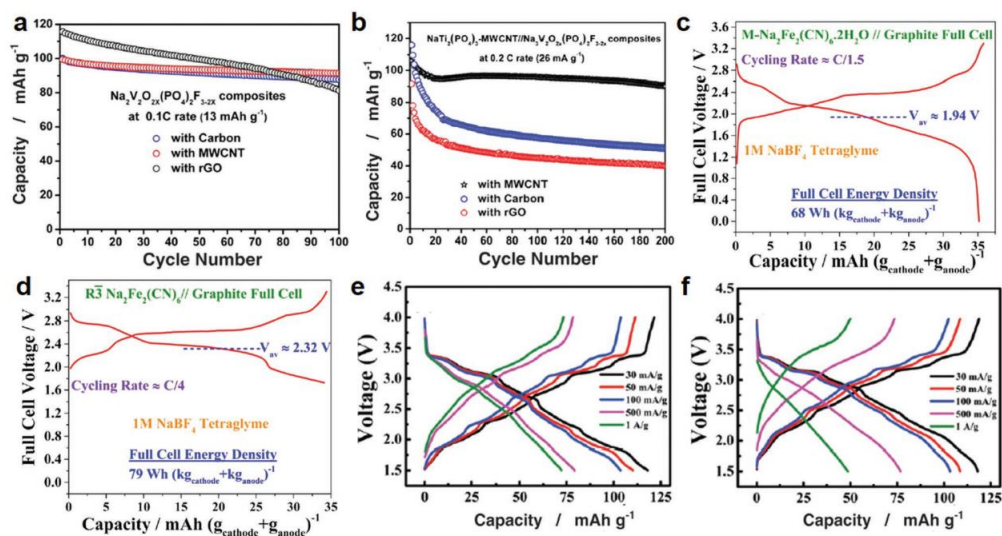


Figure 7. Cycling stability of $\text{Na}_3\text{V}_2\text{O}_2\text{x}(\text{PO}_4)_2\text{F}_{3-2\text{x}}$ in a) half- and b) full cells with different carbon polymorphs, respectively. a,b) Reproduced with permission [70] Copyright 2017, Springer. Charge–discharge profiles of c) graphite//monoclinic (M)- $\text{Na}_2\text{Fe}_2(\text{CN})_6 \cdot 2\text{H}_2\text{O}$ and d) graphite//rhombohedral (R)- $\text{Na}_2\text{Fe}_2(\text{CN})_6$ full cell. c,d) Reproduced with permission [71] Copyright 2017, The Electrochemical Society. Charge–discharge profiles of HC// $\text{Na}_{0.44}\text{MnO}_2$ full cells in e) ionic liquid and f) conventional organic electrolyte at various current densities, respectively. e,f) Reproduced with permission [72] Copyright 2016, Royal Society of Chemistry.

Based on Oxides: As reported in literatures, P2 and O3 layered oxide cathodes are commonly used in full cells with higher energy density. For example, the energy density of Sb-C//P2-Na_{0.6}Ni_{0.22}Fe_{0.11}Mn_{0.66}O₂, [73] Sb@Graphene//P2-Na_{2/3}Ni_{1/3}Mn_{7/12}Fe_{1/12}O₂, [74] CuSbS₂//P2-Na_{2/3}Ni_{1/3}Mn_{1/2}Ti_{1/6}O₂, [75] SnS/mutiwalled carbon nanotube (MWCNT)//P2-Na_{2/3}Ni_{1/3}Mn_{1/2}Ti_{1/6}O₂ [76] and HC//Al₂O₃ coated O3-Na[Ni_{0.6}Co_{0.2}Mn_{0.2}]O₂ [77] can reach to 185, 260, 200, 262, and 216 W h kg⁻¹, respectively. Their high energy densities are mainly attributed to the high-capacity characteristics of oxide cathodes. Preparation of NMO/CNTs nanotubes.

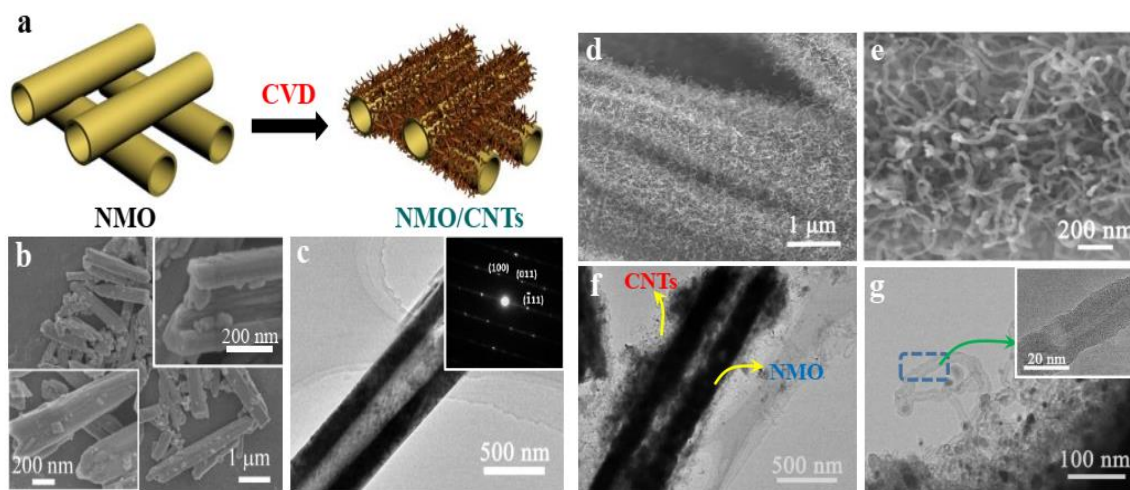


Fig. 8 (a) Schematic illustration of synthesis of NMO/CNTs composite; (b, c) SEM images of NMO and NMO/CNTs composites; (d,e) SEM images of NMO/CNTs; (f,g) TEM-HRTEM images of NMO/CNTs composite (HRTEM image in inset).

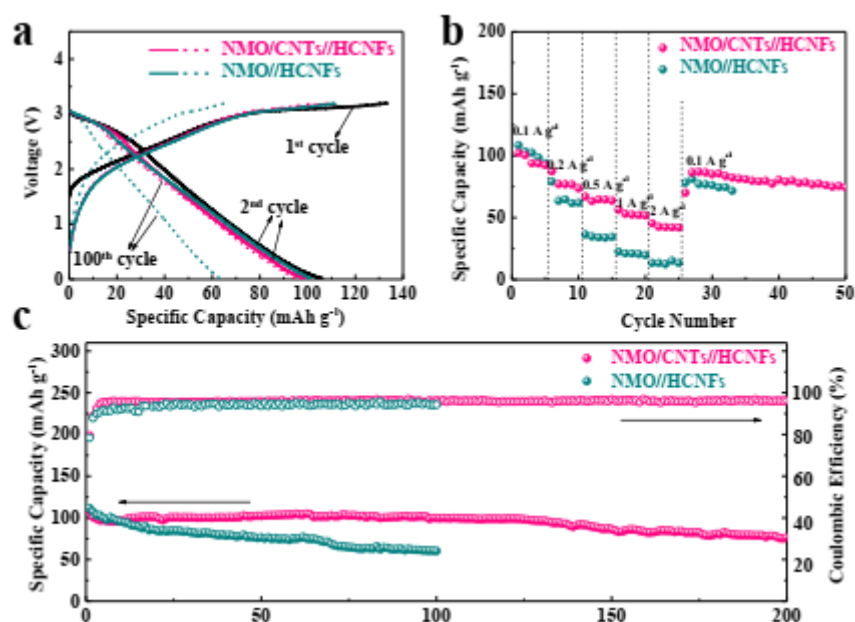


Fig. 9 (a) Discharge/charge voltage profiles of NMO/CNTs//HCNFs full cell at 0.1 A g^{-1} at the 1st, 2nd and 100th cycles and NMO//HCNFs full cell at the 2nd and 100th cycles. (b) Rate capability. (c) Cycling performance at 0.1 A g^{-1}

First, β -MnO₂ nanotubes were hydrothermally synthesised. HCNF CVD tech prep. This study generated HCNFs utilising a modified CVD technique at 250 °C using acetylene as a carbon source and copper nanoparticles as catalysts, followed by a 2-h annealing treatment at 800 °C. After 100 cycles, the Na_{0.7}MnO_{2.05}/CNTs core/branch cathode, maintains 88% of its original discharge capacity of 158.2 mAh g⁻¹ at 100 mA. We also built a high-performance helical carbon nanofibre anode to complement the Na_{0.7}MnO_{2.05}/CNTs cathode for Mn-based SIBs. The literature states that this integrated technology improves cell performance and capacity.[79] to boost complete cell cycle retention at 0.1 A g^{-1} from 54% after 100 cycles to 71% after 200 cycles and capacity by 200% at 2 A g^{-1} .

[80] Instead, doping, interface modification, and multiphase mixing [81–83] Based on: Prussian blue analogues and organics are also complete cell cathode materials. organic sodium ion complete cell employing PTCDA-based polyimide and disodium terephthalate (pre-sodiated) redox active molecules as cathode and anode, respectively. As a cathode for rechargeable sodium batteries, as-synthesized PI has a maximum energy density of 254 Whkg^{-1} and a maximum power density of $1,624 \text{ Wkg}^{-1}$ when cycled against Na. While the half-cell experiments on PI electrode demonstrated steady reversible capacity of 126 mAhg^{-1} with high capacity retention and rate capability, the all-organic sodium ion whole cell gave an initial capacity of 73 mAhg^{-1} . Perylene polyimide material's strong electrochemical performance is due to its structural stability and electrode insolubility in the electrolyte. With PTCDA-based PI material's attractive performance, [87.88] Although organics are green electrode materials, their lower cathode voltage restricts their practical use. Prussian blue analogues are attractive SIFC materials because to their high voltage, high capacity, and inexpensive cost.

3.1 Cathode slurry and coating

Two steps make cathode slurry. First, a high torque mixer model disperses the active material and carbon conductive additives in N-Methyl-2-pyrrolidone (NMP) under dynamic vacuum. This technique processes high-viscosity mixes with high solid content. The container-mixer shear forces are optimised for mixing and dispersing. High shear mixing of the slurry is the second step. Under dynamic vacuum, lumps are broken and the paste is agglomerate-free. The paste is mixed for 2 hours with a stabilised polymer polyvinylidene fluoride (PVDF) solution. The reel-to-reel coater feeding tank receives the slurry. A three-zone drier with air-impingement nozzles set at three temperatures coats cathode slurry onto an aluminium substrate using the comma-bar or slot-die coating technique. The cathode is then cured overnight at 120°C under dynamic vacuum.

4. Limited-Type Anode

Faradion basic work on hard carbon: the economic value of addressing the sodiation process. Hard carbon is a kind of carbon with three major structural properties:

Thermal treatment may create sp^2 - and sp^3 -hybridized carbon structures from non-volatile carbonaceous precursors with high carbon and oxygen concentration and low hydrogen content. Non-graphitizable carbon frequently possesses strongly cross-linked and highly immobilised crystallites that cannot be thermally rearranged into well-aligned graphitic structures from their turbostratic state at temperatures up to 3000°C . [89] These immobilised nano-scale domains locally display pseudographitic crystallinity and are bridged to create a structure with closed microporosity (1–2 nm) and ultramicroporosity (<1 nm).

Lithium-ion anodes may employ hard carbon. owing to hard carbon's higher average potential during (de-)lithiation (owing to a stronger contribution from the "sloping" rather than the "plateau" component of the potential profile) and somewhat lower capacities, graphite anodes are nevertheless favoured in Li-ion systems with higher energy density. [90,91,92] Hard carbon is attractive for Na-ion cells due to its adjustable closed and open porosity and pseudographitic layers' enhanced d-spacing.

These are better than graphite and graphitisable (soft) carbon because (a) Na-ion has a highly restricted electrochemical activity towards graphite, and (b) graphitisable carbon cannot be purified at moderately low temperatures to achieve low oxygen content (excessive surface oxygen causes irreversible capacity loss).

Since Stevens and Dahn's landmark paper, other sodiation techniques for hard carbon have been developed. Morikawa et al. [94], Alvin et al. [95], and Stratford et al. [96] did recent study in this field. An anode limited type full cell uses cathode material at a rate comparable to that of a cathode limited type full cell. The main difference between the two kinds of cells is the anode material. The HC anode allows the associated whole cell to have a high energy density, but its low voltage plateaus are a double-edged sword.

However, because to the extra cathode material, sodium dendrites may easily develop, which poses health and safety risks. As a result, it's crucial to regulate the cathode material's concentration. For reasons of security, it's preferable to use chalcogenides, elements, and alloys as an anode because of their somewhat higher voltages in the entire cell. Including $\text{Fe}_3\text{O}_4@\text{FeS}/\text{Na}_3\text{V}_2(\text{PO}_4)_2\text{O}_2\text{F}$ (207 W h kg^{-1}), [97] Pie-like $\text{FeS}@C/\text{Na}_3\text{V}_2(\text{PO}_4)_2\text{O}_2\text{F}$ (236 W h kg^{-1}), [98] $\text{P}@C/\text{Na}_3\text{V}_2(\text{PO}_4)_2\text{F}_3/\text{C}$ (281 W h kg^{-1}), [99] $\text{Se}_4\text{P}_4/\text{Na}_3(\text{VO}_{0.5})_2(\text{PO}_4)_2\text{F}_2$ (190 W h kg^{-1}). [100], Ionic liquid complete cells with superior thermal stability, broad electrochemical window, and nonflammability have also been investigated. $\text{HC}/\text{Na}_{0.44} \text{MnO}_2$ complete cell in ionic liquid electrolyte has superior rate capability and capacity retention than in organic electrolyte.

4.1 Anode slurry and coating

The active material and carbon additives are first dispersed in the polymer PVDF binder solution in a high torque mixer for five hours to make anode slurry. This distributes active material and carbon additives throughout the solution. Slurry viscosity may be adjusted by adding NMP. Degassing the anode slurry takes an hour. On a reel-to-reel coater, the anode slurry is coated onto an aluminium substrate like the cathode.

4.2 Faradion proprietary anode materials

The half-cells and complete cells with 0.1 A h Na-ion pouches that use Faradion's patented hard carbon grades Fig. 3 is a summary of representative data for both half-cells and complete cells with 0.1 A h Na-ion pouches that use Faradion's patented hard carbon grades. Figure 3a demonstrates that despite using carbonate ester solvents (rather than glyme-based solvents, which typically result in higher first cycle coulombic efficiencies for Na-ion anodes), the specific capacity of Faradion's proprietary hard carbon is typically in excess of 330 mA h g^{-1} at C/20. On the other hand, a commercially available hard carbon anode that provided 285 mA h g^{-1} had a lower first cycle coulombic efficiency of 88.6%, and this was true even while cycling at C/70 to eliminate Na counter electrode polarisation effects. Commercial hard carbon anodes have extremely excellent first cycle efficiencies of 88% in complete Na-ion 0.1 A h pouch cells using Faradion's Gen 2 cathode, resulting in cathode reversible capacities of $128.2 \text{ mA h g}^{-1}$.

When combined with Faradion's proprietary hard carbon, however, the first cycle coulombic efficiency of a full Na-ion cell is increased to 90% (the highest value of a hard carbon anode-based full cell in the literature without pre-sodiation is 87% in a simulated full cell),[101] resulting in higher cathode reversible specific capacities of $134.5 \text{ mA h g}^{-1}$ (refer to Fig. 10b).

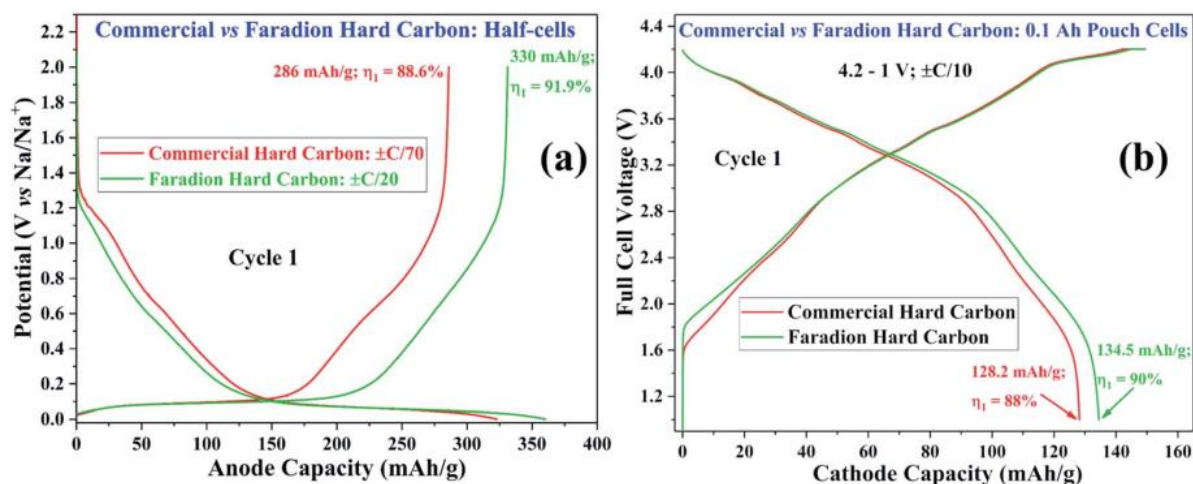


Fig. 10 Electrochemical performance of Faradion's proprietary hard carbon. (a) Half-cell cycling curves illustrating higher capacities with a higher first cycle coulombic efficiency (η_1) compared with those obtained from commercial hard carbon. (b) The more efficient Faradion hard carbon results in unprecedented first cycle efficiencies in full Na-ion cells (90%) when paired with Faradion's Gen 2 cathode. In both sets of experiments, all other experimental conditions were the same; thus, comparisons can be made with confidence.

Faradion's strong carbon also improves cycling stability and rate performance, as described in a forthcoming paper. In a range of cell footprints and capacities up to 12 A h, such results have been reported. Faradion is integrating the next generation of proprietary carbon and hard carbon + X (X $\frac{1}{4}$ non-carbonaceous materials) composite anode active grades into its commercial products. These materials will have faster charge acceptance, lower manufacturing costs, and world-leading coulombic and round-trip efficiencies in Na-ion full cells.

5. Electrolyte optimisation

The electrolyte in a solid oxide fuel cell (SOFC) may be optimised to enhance its electrochemical characteristics by maintaining a stable interface on the electrode surface and avoiding corrosion between the electrolyte and the electrode throughout cycles.[104] You may find electrolytes in liquid, semi-solid, and solid forms. Electrolytes that are useful in the real world have desirable properties such high ionic conductivity, a large working voltage window, good thermal stability, minimal environmental impact, and cheap cost. Many scientists have studied electrolytes and offered advice on how to wisely choose among them. [105,106, 107,108] To determine the best electrolytes for each system, we utilise their full-cell applications.

5.1 Liquid Electrolytes

NALSIFCs are the most extensively reported since various electrode materials are created and changed with liquid electrolytes as evaluation systems. To maintain cell stability, the cathode and anode materials' energy levels should be lower and greater than the electrolyte's LUMO and HOMO levels, respectively (Figure 11a). Interfacial films and side reactions are unavoidable when lower voltage anodes and higher voltage cathodes are used to build cells with higher energy and power densities. [108] Esters, ethers, and ionic liquids are nonaqueous liquid electrolytes. Esters are the most frequent NALSIFC electrolytes (Figure 11b). Ethers are more compatible with most anodes than esters because they create stable SEI layer, but their high voltage faults make them unsuitable for complete cells. High safety allows ionic liquids to work across a wide temperature range, but high viscosity, poor ion mobility, and high cost limit their use.

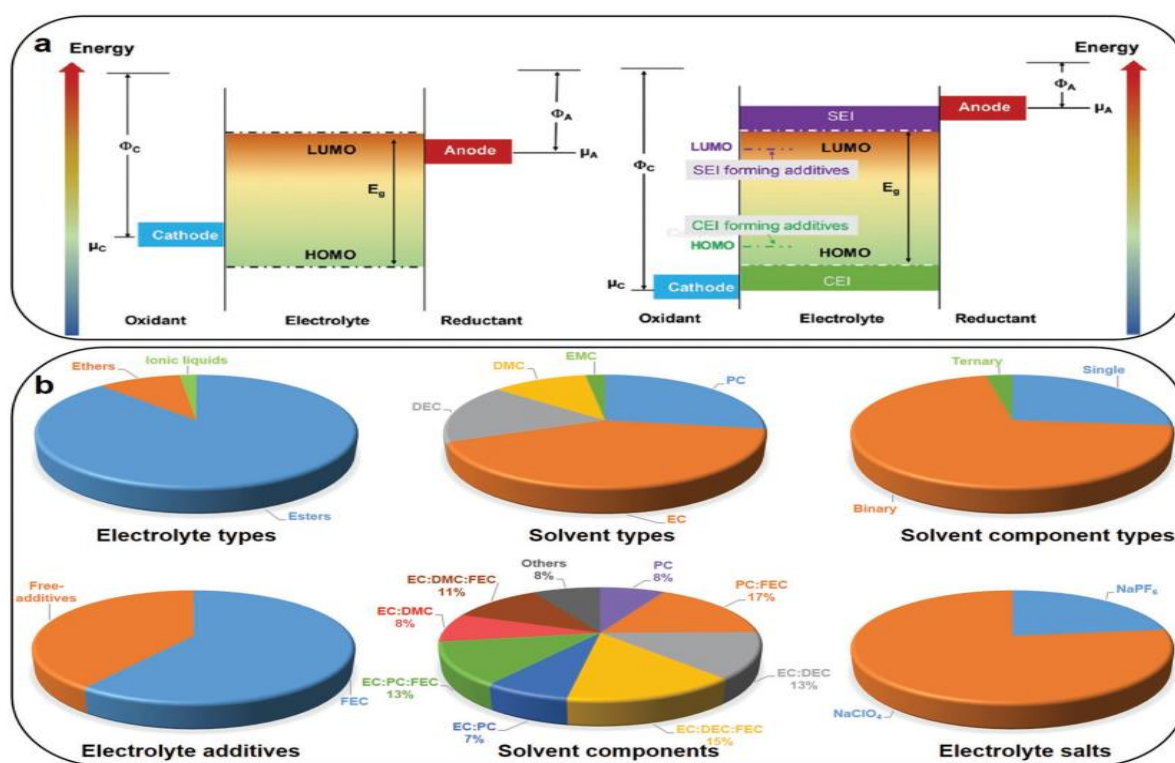


Figure 11. a) Schematic open-circuit energy diagram of ideal electrolytes and practical electrolytes in the presence of functional additives. Φ_A and Φ_C are the anode and cathode work functions, respectively, E_g is the window of the electrolyte for thermodynamic stability. Reproduced with permission. [108] Copyright 2018, Wiley-VCH. b) Summary of the proportion of various electrode solvents, component types, additives and salts in the SIFCs.

5.2 Electrolyte Solvents

Ionic conductivity is related to solvent viscosity and dielectric constant. High viscosity slows ions, whereas high dielectric constant dissolves electrolyte salts. Strong ion conductivity requires low viscosity and high dielectric constant in an electrolyte. Unfortunately, these two parameters frequently have similar values for the same solvent, therefore many solvents must be used with other solvents.

Figure 11b indicates that EC, PC, and DEC solvents dominate entire cells. Due to their high viscosity and inability to create a thick interfacial layer, PC solvents are often used with other solvents or additives to improve cycle stability. Due to its high dielectric constant and film-forming characteristics, EC is the most widely utilised liquid electrolyte matrix.[109]

5.3 Electrolyte Additives

The electrochemical performance of SIFCs may be altered by introducing various additives, such as film-forming additives, solvents, and electrolyte salts. In order to improve the film-forming quality of the interface film, the optimum film-forming additive should have a lower LUMO level and a higher HOMO level than solvents, electrolyte salts, etc. (Figure 12a). FEC, tris(trimethylsilyl) phosphate (TMSP), vinyl carbonate (VC), radium perfluoride (RbPF₆), cesium perfluoride (CsPF₆), etc.,[108] are among the most commonly cited examples of such additions; nonetheless, practically all complete cells employ FEC due to its universal compatibility and its ability to be modified for both cathode and anode. The addition of FEC can cause the creation of a thick and stable interface coating, protecting the electrode from electrolyte erosion.[110] In tandem with the production of by-products such as alkyl compounds, NaF, and Na₂CO₃ (Figure 12a).[111] Since the FEC additive forms an interface film with high-impedance components like NaF or Na₂CO₃, the film is highly polarised. Synergistic effects can be achieved when TMSP, RbPF₆, and CsPF₆ are used in tandem with one another. By adding a little quantity of RbPF₆ or CsPF₆ to the electrolyte containing FEC, Ma et al. were able to decrease the NaF level in the SEI layer, hence enhancing the ionic conductivity and the SEI stability on HC surfaces.

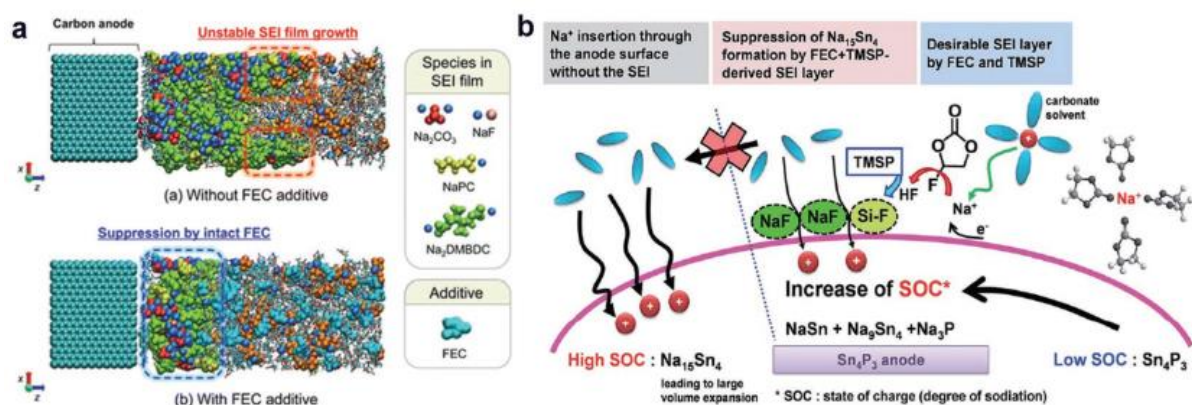


Figure 12. a) Typical snapshots of the SEI films and NaPF₆-PC electrolytes visualized without and with FEC additives. Reproduced with permission.[176] Copyright 2015, American Chemical Society. b) Schematic diagram of FEC and TMSP as coadditives for improving the performance of Sn₄P₃. Reproduced with permission.[32] Copyright 2015, Royal Society of Chemistry

The stability of the HC anode cycle was considerably enhanced.[112] Choi et al. present the advancements in the electrolyte additives for room temperature Na-based rechargeable batteries, including Na-ion, Na-O₂/air, Na-S, and Na-intercalated ions, to prevent the conversion of Sn₄P₃ anode to Na₁₅Sn₄ phase with larger volume during electrochemical sodiation and to reduce the NaF content in the interface film.

In order to improve the performance of Sn4P3 anodes, FEC has been tried in conjunction with tris(trimethylsilyl) phosphate (TMSP). Notably, FEC helps mitigate the volume expansion issue by preventing the production of Na15Sn4. In this situation, a Na9Sn4 species with a reduced sodiation degree is produced, which results in a loss in capacity. The extremely resistive NaF in the SEI layer can be reduced because to TMSP's reaction with the HF produced during FEC breakdown (Figure 4). (Shown in Figure 12b).[113] These successes highlight the importance of additive diversity in stabilising electrode/electrolyte interface properties, although equivalent investigations are currently missing in entire cells.

6. Research and Development of Nonaqueous Electrolytes for Full-Cell Sodium-Ion Batteries Electric Vehicle Application

The organic electrolytes for SIBs are obtained by dissolving a sodium salt (NaPF₆, NaClO₄, sodium trifluoromethane sulfonate (NaTf), sodium bis(fluorosulfonyl)imide (NaFSI), and sodium bis(trifluoromethanesulfonyl)imide (NaTFSI)) into a basic solvent system.[114,115,116] A functional electrolyte is often made using an ingredient like fluoroethylene carbonate (FEC), transdifluoroethylene carbonate (DFEC), ethylene sulfite (ES), or vinylene carbonate (VC) to improve the cell's performance.[117] Electrolytes used in SIBs need to meet a number of criteria, including having high ionic conductivity, excellent electrochemical and thermal stabilities, and being non-toxic and inexpensive to produce. Full-cell SIBs' electrochemical performance is significantly impacted by the organic electrolytes used in their construction. This includes the devices' initial coulombic efficiency, cycle life, rate capability, energy/power density, and safety/operational conditions. The cycling performance of a complete HC//Na[Ni_{0.5} Mn_{0.5}]O₂ cell was studied by Komaba et al. using 1 m PC solutions of various salts (NaClO₄, NaPF₆, or NaTFSI).[118] After 50 cycles, cells containing NaPF₆ or NaTFSI were able to preserve 70% of their original capacity, but NaClO₄-containing cells had starting capacities below 200 mA h g⁻¹ based on the hard carbon at 1 C. Using 1 m NaClO₄ or NaPF₆ in EC_{0.45}:PC_{0.45}:DMC_{0.10} as the electrolyte, Ponrouch et al. generated HC//Na₃V₂(PO₄)₂F₃ complete cells with an average voltage of 3.75 V and a theoretical energy density equivalent to graphite//LiFePO₄ LIB cells.[199]

Several research groups employ complete SIBs with ionic liquid electrolytes because to their excellent thermal and electrochemical stabilities, little volatility, and nonflammability.[120–122] Wang et al. suggested a hard carbon// Na_{0.44}MnO₂ complete cell with an ionic liquid electrolyte that had 117 mA h g⁻¹ at 0.1 C and 97% capacity retention after 100 cycles.[122] Ionic liquid electrolytes' high room-temperature viscosity and high manufacturing cost restrict their use in SIBs.

The thermal and chemical stability of gel polymer electrolytes, as well as their versatility in cell manufacturing, make them ideal for application in SIBs.[123] Using a cross-linked poly(methyl methacrylate) (PMMA) composite gel-polymer electrolyte, Goodenough et al. recently developed a sodium-ion full-cell Sb//Na₃V₂(PO₄)₃ battery that has more cycle stability than a battery using the more common liquid electrolyte.[157] All-solid-state SIBs, known for their excellent safety, extended cycle life, and adaptable geometries, have recently included inorganic solid electrolytes.

[124–127] An all-solid-state rechargeable Na-Sn/Na₃PS₄/TiS₂ SIB was made by Hayashi et al.[124] Even though the all-solid-state cell's capacity was just 40% of what it might have been, excellent charge-discharge reversibility is theoretically possible. Na/Na₃Zr₂(Si₂PO₁₂)/Na₃V₂(PO₄)₃ sodium-ion batteries with a solid electrolyte and capacity retention of more than 100 cycles at the 5 C rate were recently manufactured by Goodenough's team.[127]

The use of non-aqueous electrolytes in SIBs that operate at or near room temperature is discussed here. Although some ideas on electrolytes that can withstand high temperatures will be mentioned briefly, we won't be focusing on electrolytes for the following battery types:

Batteries with aqueous electrolytes. Na-air or Na-O₂ batteries, Na-S batteries, Na-NiCl₂ (ZEBRA) batteries.

6.1 Sodium salts

The salt used is one of the two main components of any SIB electrolyte, and its impact on performance is significant. To create an electrolyte with enough charge carriers present, the salt chosen must first be soluble in the solvent(s) being used; (ii) it must be stable against reduction and oxidation; (iii) it must be chemically stable against the other materials of the electrolyte, the electrodes, and the current collectors; and (iv) it must be non-toxic and safe in other respects. Unfortunately, due to characteristics (i) and (ii), the pool of potential salts is somewhat narrow. The traditional method for discovering weakly coordinating anions (WCAs) in inorganic compounds involves searching for central atoms with ligands that remove electron density to form delocalized negative charge.[128] This type of anion is likewise more likely to be stable than unstable. oxidation (due to the high HOMO energies they possess). The majority of the promising anions for SIB electrolytes have been used for many years in the field of LIB electrolytes ClO₄⁻, BF₄⁻, PF₆⁻, CF₃SO₃⁻ (Tf), and [N(CF₃SO₂)₂] (TFSI).

The benefits and downsides are essentially the same, as many of the ensuing qualities depend more on the anion than the cation. In conclusion, as has been shown in LIB cells, all of the aforesaid anions have drawbacks.[129] A strong oxidant, ClO₄⁻ is effectively off-limits for practical cell development; BF₄⁻ results in less conductive electrolytes due to a stronger interaction with the cation, leading to fewer charge carriers; PF₆⁻ while being the anion of choice (the best compromise candidate) for LIBs - has severe safety issues, especially at elevated temperatures and in the presence of moisture, suffering hydrolysis to yield PF₅, POF₃, and HF; The fundamental issue with Tf, like BF₄⁻ (less conductive electrolytes), is that it corrodes the aluminium current collectors. This is also the main issue with the well-studied TFSI anion.

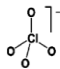
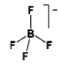
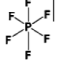
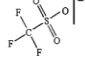
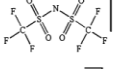
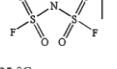
Corrosion in a LIB electrolyte begins at around 2.7 V vs. Li⁺/Li for Tf.[130]

The solubility issue is one that can be addressed by switching from SIBs to LIBs, whereas ESW and Al corrosion are more intrinsic aspects of anions.

The greater melting points and thermal stability of sodium salts over their Li equivalents are predicted to have positive effects on safety. Sodium salts are also simpler to dry than their Li counterparts. **Table 2** provides a summary of the most common physicochemical parameters of sodium salts used in SIB electrolytes.

NaClO₄ is the most widely utilised salt (in around two-thirds of the published SIB articles), perhaps due to a combination of historical and cost considerations (see above). Apart from the obvious safety concerns, these salts are notoriously difficult to dry [131] (despite being less hygroscopic). Even after drying the powder at 80 C under vacuum overnight, NaClO₄- based electrolytes do usually exhibit higher water contents (>40 ppm) as compared to e.g. NaPF₆ based ones (<10 ppm).

Table 2 Basic properties of the most commonly used Na-salts for SIB electrolytes

Salt	Anion chemical structure	M_w [g mol ⁻¹]	T_m [°C] (Li-salt)	σ [mS cm ⁻¹] ^a (Li-salt)
NaClO ₄		122.4	468 (236)	6.4 (5.6)
NaBF ₄		109.8	384 (293)	(3.4)
NaPF ₆		167.9	300 (200)	7.98 (5.8)
NaTf		172.1	248 (>300)	(1.7)
NaTFSI		303.1	257 (234)	6.2 (5.1)
NaFSI		203.3	118 (130)	

^a 1 M NaX (LiX) in PC at 25 °C.

NaPF₆ is the second most common salt, and it is compatible with several LIB experiments. NaTFSI and NaFSI are gaining traction as potential Na-salt of choice options (despite the Al corrosion problems) because of the roles these anions play in generating acceptable ionic liquid matrices. Their non-toxicity, greater thermal stabilities than both NaPF₆ and NaBF₄, and the associated higher conductivities than when employing NaTf are clearly promising, however it is unclear if NaTFSI and NaFSI can be employed as single salts for SIB electrolytes (Al corrosion). It is important to note that the current state of FSI with regards to corrosion concerns is not apparent. Initially, it was thought to erode Al, but researchers eventually determined that the corrosion was caused by Cl impurities left over from the salt's manufacture.[132]

Few research have compared the effects of various Na-salts. Using the same EC: DMC matrix, Bhide et al. [133] examined the ionic conductivity as a function of the salt concentration for NaPF₆, NaClO₄, NaTf, and NaTFSI. Dependence was quite noticeable for NaTf and NaClO₄, but not so much for NaPF₆. The highest values of conductivity found were 6.8 mS cm⁻¹ for 0.6 M (NaPF₆) and 5.0 mS cm⁻¹ for 1 M (NaClO₄), whereas the value for 0.8 M NaTf was too low.

Developing novel salts for battery electrolytes (SIBs and LIBs alike) is a niche academic research area, and new anions reach the field of electrolyte studies only very slowly. This is because of the stringent conditions that must be satisfied, and the limited number of atoms available for forming an anion of suitable size. However, once the Li-salt has been generated, it is typically easy to make the Na-salt (or vice versa), especially when compared to the field of electrode materials. A few instances of novel anions/Na-salts are shown below; nevertheless, it is frequently impossible to judge their complete set of promises and challenges because they now only exist on an academic or, at most, semi-commercial scale.

The framework structure of heterocyclic rings for anion has been investigated as a possible route.[134,135] Both the NaTDI salt and the related NaPDI salt were just recently reported to fall under this category.[136] They have the same electrochemical stability guarantee against oxidation, >4 V vs. Na/Na⁺, as other heterocyclic anions as DCTA (TADC) [62] and comparable [N5Cn]⁻ anions, and both salts have conductivities of around 4 mS cm⁻¹ (at 1 M concentration in PC at ambient temperature).⁵⁸ The NaTDI and NaPDI salts also have excellent stability against moisture, which bodes well for their manageability and potential applications. NaTDI also has a higher melting point than LiTDI (about 330 degrees Celsius vs. 160 degrees Celsius).[137] Recent LIB salt research has also focused on replacing the electro-withdrawing F atom with the pseudo-halogen ⁻CN group. In order to make F-free electrolytes, the BF₄⁻ anion analogue [B(CN)₄]⁻ has recently been used.[138] Surprisingly, while its salts are insoluble in common organic solvents like PC, they are soluble in PEGDME. The electrochemistry is complex, and the use of more than about 4 V looks risky.

In a computational study by Jonsson et al. [65], pseudo-delocalized anions with a central positive core and negatively charged extremities were targeted to create new Na-salts without F atoms. Experimental confirmation is needed, however several of the recommended anions appear to be competitive with those employed today in terms of ion-ion interaction weakness and anion oxidation potential.

Finally, Na-salt characteristics may affect more than only SIB electrolyte development. The two alkaliion battery ideas' SEI can differ greatly because to the Na₂CO₃ salt's greater solubility in electrolytes than the Li₂CO₃ salt.

6.2 Solvents

In the same way that LIBs necessitate electrolyte solvents with large ESWs, SIBs with their strongly reducing negative electrodes and strongly oxidising positive electrodes necessitate electrolyte solvents with large ESWs (hence non-aqueous should indeed more correctly be aprotic). Most of the criteria established for Na-salts also apply to the solvents, such as being stable, non-toxic, affordable, etc. In addition, polar groups must be present in enough numbers for the Na-salt to dissolve. However, there are other methods to achieve this whole set of features using various sorts of solvent ideas, each with its own promises and drawbacks, as we detail in the following sections. Although LIBs and SIBs may use different salt and solvent combinations, no dedicated solvent for SIBs has yet been created, hence the majority of the following applies to both.

6.3 Organic solvents

The organic carbonate (linear and cyclic), ester, and ether families that were studied are quite similar to those that are employed for LIBs (see **Table 3** for a summary of their most important features). Since a solvent's ESW is affected by its Lewis acidity/basicity (i.e., electron acceptor/donor ability), this idea is crucial. Acceptor (AN) and donor (DN) numbers are related to the HOMO/LUMO energy levels of a solvent. Also, the solvent's acidity (basicity) will dictate its solvation qualities; solvents with a high acidity (low basicity) will dissolve anions and cations with relative ease (difficulty), respectively.⁶⁶ All ion-solvent and solvent-solvent interactions are governed by the idea of hard and soft acids and bases (HSAB)[139]. Recent DFT work has also demonstrated that the strength of the acidity of an ion, in this case Li⁺ as opposed to Na⁺, should affect the ion-solvent interactions, particularly the solvation shell and solvation energy.[140]

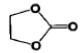
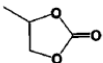
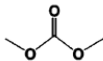
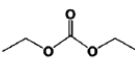
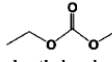
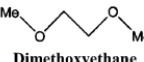
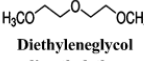
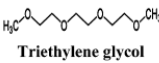
Solvent	T_m (°C)	T_b (°C)	T_f (°C)	η (cP) 25 °C	ϵ 25 °C	AN (DN)
 Ethylene carbonate (EC)	36.4	248	160	1.9 (40 °C)	89.78	(16.4)
 Propylene carbonate (PC)	-48.8	242	132	2.53	64.92	18.3 (15.1)
 Dimethyl-carbonate (DMC)	4.6	91	18	0.59	3.107	
 Diethyl carbonate (DEC)	-74.3	126	31	0.75	2.805	(16.0)
 Ethylmethyl carbonate (EMC)	-53	110		0.65	2.958	
 Dimethoxyethane (DME)	-58	84	0	0.46	7.18	10.9 (18.6)
 Diethyleneglycol dimethylether (Diglyme)	-64	162	57	1.06	7.4	9.9 (19.2)
 Triethylene glycol dimethyl ether (Triglyme)	-46	216	111	3.39	7.53	10.5 (14)

Table 3 Solvents commonly used. T_m , T_b , T_f , η , ϵ and AN/DN stand for the melting point, the boiling point, the flash point, the viscosity, the dielectric constant and the acceptor and donor numbers, respectively

6.4 Ionic liquids

The ionic liquids (ILs) constitute a fully developed scientific branch, whereas their use as matrices for Li-salts or Na-salts is a very modest part of the ILs family tree.[141,142] By definition, ILs are ion-only materials that are liquid at temperatures below 100 °C. It is the subclass of aprotic room temperature ILs (also known as RTILs; from here on out, "ILs") that is of greatest relevance for battery electrolytes. Several characteristics of ILs make them ideal electrolyte solvents. These include a wide liquidus range, thermal and electrochemical stability, and no or very low vapour pressure (making them non-flammable). ILs have naturally high ionic conductivities and are great ionic solvents because of their many beneficial properties. An IL typically comprises of a big organic cation and a WCA family anion. An SIB electrolyte is hence $\text{Na}_x \text{Cation} (1-x) \text{WCA}$, where x is typically in the range of 0.1-0.25, and is made by direct mixing, occasionally aided by heating. The system might contain either one or two WCAs. The two most popular IL cations employed as electrolytes are shown in Fig. 13. Na-salts often use TFSI or FSI for IL anions, although the IL cation chosen might place additional constraints on the electrolyte.

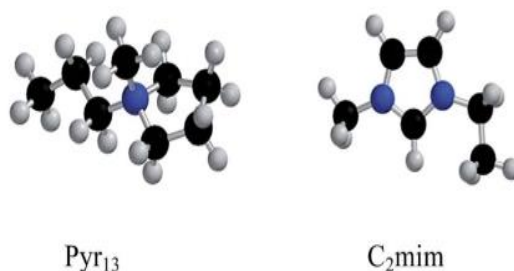


Fig. 13 The two most common IL cations employed in electrolytes: Pyr₁₃ or BMP (left) and C₂mim or EMIm (right).

The imidazolium-based C_nmim (EMIm (n = 2), BMIm (n = 4), etc.) cations have issues with the ESW's cathodic limit, whereas the pyrrolidinium-based Pyr_{1x} family has greater electrochemical stability. ILs for SIB electrolytes have several limitations. The first, and most important, is that practically all ILs have high viscosities, in the range of tens of cP at ambient temperature, and doping with Na-salt often raises them further. Due to increased ion-ion interactions, the mobility of Na-ions is complicated and unresolved (it has been claimed that they move as double negatively charged species).[143] IL prices are the second downside. The anion limits the price, and since the WCA is frequently the same as for the salts used, the overall material cost is significant, sometimes considered too high for practical use. FSI-based ILs, which have a simpler and cheaper synthesis path than TFSI-based ones, can mitigate this issue. The amount of trials with too wet or impure ILs makes some results doubtful and hinders field progress.

6.5 Full Na-ion cell cycling: curves and stability

Full cell cycling profiles at 30°C with a CC/CV (constant current/constant voltage) charging and CC discharging strategy are shown in Figure 14(a). In these conditions, a Faradion complete Na-ion cell may provide 400 Wh/kg cathode in energy density thanks to its 128 mAh/g cathode specific capacity at an average cell voltage of 3.1 V. The profiles of complete cells cycled between 4.3 and 1.0 V at $\pm C/7$ and 30°C are shown in Figure 14(b).

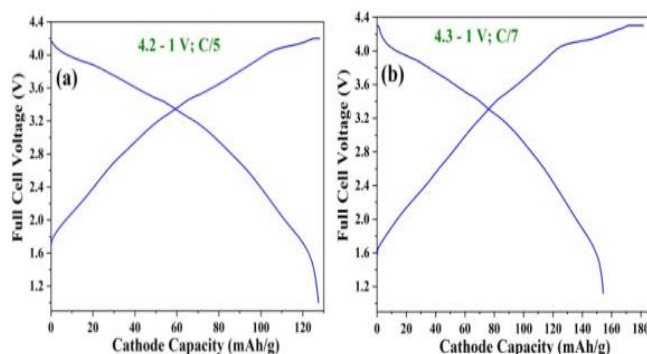


Figure 14. Faradion full Na-ion cell voltage profile at 10 mAh scale.

This wider operating voltage range allows the whole cell to produce about 500 Wh/kg cathode, with an average voltage of close to 3.2 V. These high specific energy density values are proved to be comparable to commercial Li-ion cathodes, suggesting that the energy density of a changeover from Li-ion to Na-ion batteries need not be compromised.

The capacity of faradion complete cells gradually degrades after thousands of cycles at 30 degrees Celsius. Recent studies with optimisation have greatly enhanced this cyclist's efficiency. After 750 cycles between 4.2 and 1.0 V at $\pm C/5$, the cell retains 80% of its initial discharge capacity with steady coulombic efficiencies between 99.9 and 100.0%, as illustrated in Figure 15(a).

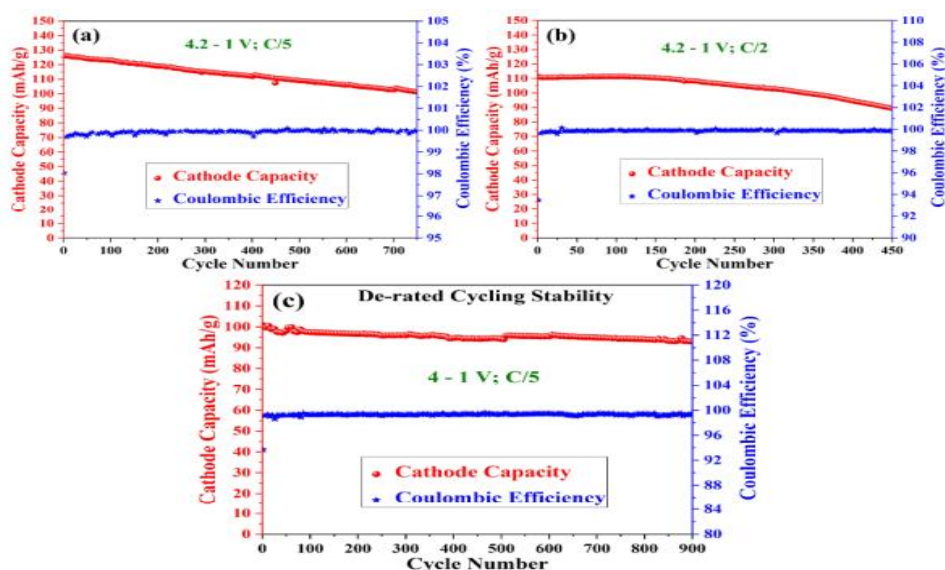


Figure 15. Faradion full Na-ion cell cycling data at (a) C/5 at 4.2–1.0 V, (b) C/2 at 4.2–1.0 V and (c) C/5 at de-rated 4.0–1.0 V.

The cycle life remains high even when the charge/discharge rate is increased. If complete cells are de-rated, cycle life can be extended even more. For instance, Faradion complete cells (refer to Figure 15 (b)) experience just 7% capacity decline over 900 cycles when cycled between 4.0 and 1.0 V at $\pm C/5$. A cycle life of over 3,500 is thus estimated from this.

6.6 Large-scale Na-ion systems

Faradion has been able to scale up its complete cell design from pouch cells with a capacity of < 10 mA h, which corresponds to early stages of research and development, through cells with a capacity of 0.1-3 A h for prototypes, and eventually to pouch cells with a capacity of \$10 A h for mass manufacturing, all without compromising performance. Different cycling results for 12 A h pouch cells are shown in Fig. 16,

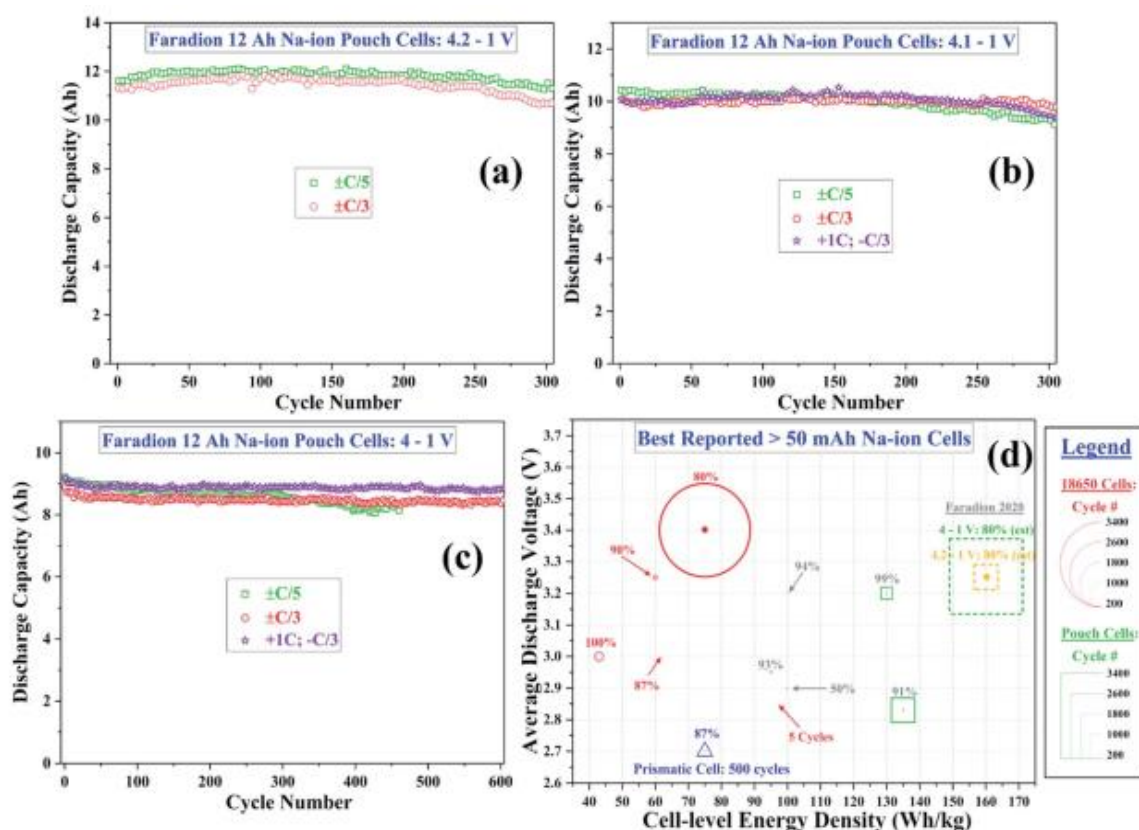


Fig. 16 Cycling of Faradion's first-generation production-category 12 A h Na-ion pouch cells. Cycling stabilities at various voltage windows: (a) 4.2–1 V, (b) 4.1–1 V and (c) 4–1 V. (d) Summary of the best published full Na-ion cells in the literature with a reported capacity of at least 50 mA h. In this plot, the size of the circle or square represents the cycle life reported in the publications with the number above the circle/square being the reported capacity retention. Faradion's specific energy is based on a 32 A h cell at 4.2–1 V, while the cycle life is based on our prototype cells at 4–1 V or 4.2–1 V (refer to Fig. 2d); these cycle lives are currently being confirmed in 32 A h cells. From the figure, it is clear that the Faradion Na-ion technology significantly surpasses that of all prior reports, in terms of specific energies, while still avoiding costly elements such as Co or V.

which are indicative of the first generation of commercial cells produced by Faradion. Three alternative voltage windows (4.2-1 V, 4.1-1 V, and 4-1 V) are depicted in Fig. 16a-c, demonstrating cycle stabilities at $\pm C/5$, $\pm C/3$, and a quicker 1C charge, C/3 discharge. There was hardly any capacity loss seen after 300–600 cycles, and the cycling was found to be fairly stable throughout all voltage windows. It is noteworthy that cells with a nominal capacity of 12 A h may also exhibit quick charge acceptance: performance supplied by cells charged at faster charge rates, such as 1C, was equal to that delivered by cells charged at slower charge rates, such as C/ 5 or C/3 (refer to Fig. 16b and c).

These 12 A h cells also have high RTEE values of 94–95%, comparable to or greater than commercial Li-ion batteries. These 12 A h cycling results show Faradion's first-generation commercial products' scalable cell designs with good performance and safety. To put the above results in perspective and demonstrate how far advanced Faradion's Na-ion technology is compared to the very best reported Na-ion full cells in the literature, we conducted a detailed literature review on large-scale Na-ion full cells with a minimum capacity of at least 50 mA h (a threshold that allowed comparisons with a few academic reports; a higher threshold, such as 10 A h, would have ruled out all reports except one). Fig. 16d shows the cell-level specific energy, average discharge voltage, and cycle life of the best reported large-scale Na-ion cells. Fig. 16d shows three cell types: 18 650 cells [144–148].

6.7 Quasi-Solid-State Electrolytes

The advantages of quasi-solid-state electrolytes over liquid electrolytes include the capacity to function at higher temperatures, compatibility with a larger range of electrode materials, and a wider operating voltage window. Polymers, namely poly(vinylidene fluoride-hexafluoropropylene) (PVDFHFP), make up the majority of the reported quasisolid-state electrolytes for QSSSIFCs. The increased frequency of sodium ion transfers can be attributed, at least in part, to the presence of the polymer framework, which inhibits the activity of anions of bigger size. As a consequence, QSSSIFCs are superior to NALSIFCs in terms of cycle durability and low resistance. Because they are only partially solid, quasi-solid-state electrolytes nonetheless have the same issues as liquid electrolytes. It is interesting to note that the quasi solidification of electrolytes can also hinder the degradation of ethers in the high voltage regions,[149] which may offer a solution for their use in high-voltage battery systems.

6.8 All-Solid-State Electrolytes

Solid-state electrolytes are superior to two other types of electrolytes in terms of safety, operating voltage window, and mechanical strength (Figure 17).

However, the low room temperature ionic conductivity and high interface impedance (especially grain boundary resistance) that result in low capacity, poor cycle retention, and large polarisation mean that these benefits do not provide the expected guarantee for high-performance ASSSIFCs in terms of the aforementioned achievements (Section 3.3). High temperatures are used in many electrochemical studies because they decrease polarisation and improve ionic conductivity. Treatment at high temperatures for extended periods of time is often required for oxide electrolytes to lower the grain boundary resistance, whereas treatment with cold pressing is sufficient for sulphides.

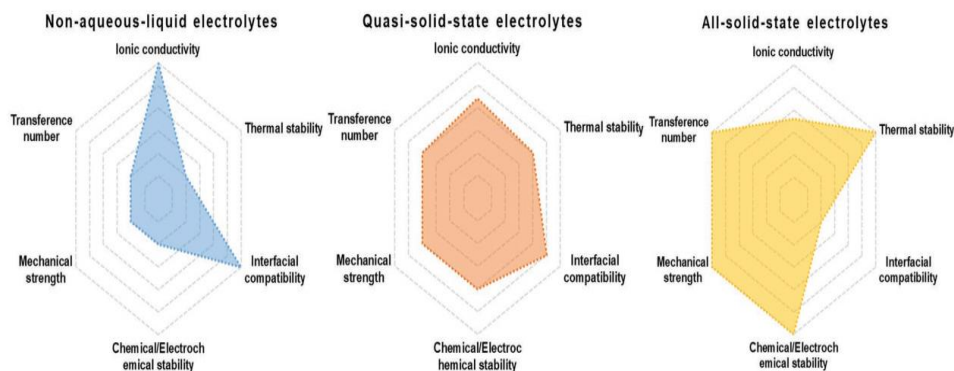


Figure 17. Radar plots of nonaqueous liquid, quasi-solid-state, and all-solid-state electrolytes.

In addition, the sulphides' lower Young's modulus compared to oxides' provides significant benefits in limiting the volume expansion of the electrode during the charge and discharge processes. One of the most active areas of study in solid-state electrolytes is the enhancement of ionic conductivity. The most prevalent processes are purification, doping, and substitution.[150] It is likely that the presence of impurity anions works as a trapping of sodium ions, resulting in resistance to sodium ion conduction; this is why the use of high-purity Na₂S by Hayashi et al. enhanced the ionic conductivity of sulphides from 2.0×10^{-4} to 4.6×10^{-4} S cm⁻¹. [151] Increasing the carrier concentration and the degree of crowding are favourable to enhancing the ionic conductivity of Na₃PS₄, as demonstrated by the doubling of its ionic conductivity upon low-valent heteroatom doping.[152] Substituting a large-radius Se for the S in Na₃PS₄ can have beneficial benefits as well, primarily because Se has the potential to enlarge the ion migration channel and reduce the anionic framework structure's binding capacity to sodium ions. By substituting P with Sb and Sn, for example, not only can the ionic conductivity of the electrolyte be manipulated, but the poor air stability of the sulphide electrolytes may be alleviated as well.[154,155] The fact that tetragonal Na₃SbS₄ has a much lower ionic conductivity than cubic Na₃SbS₄ demonstrates that screening the electrolyte from the standpoint of various crystal structure is also an effective way to increase the ionic conductivity.[156]

One of the most pressing issues in solid-state electrolyte research is finding ways to lower the interfacial impedance between the electrolyte and the electrode. Electrolyte coating, amorphization of electrode materials, and electrolyte component modification are the major approaches used today. Because Na₃SbS₄ is soluble in both water and alcohol, Hong et al. [157] precoated NaCrO₂ with Na₃SbS₄ to boost the full cell's electrochemical performance from 3 to 108 mA h g⁻¹, indicating that a well-thought-out mixing method between the electrode material and the electrolyte is essential. Although amorphization may have a role in reducing interface stress across cycles, it is often not possible to achieve in most high-voltage cathode materials due to their rigid structure and large volume change.[158]

7. Recent Achievements on Sodium-Ion Full-Cell System

Under SIBs' fiery research, more researchers are focusing on SIFCs, which will help its practical implementation. According to published data, QSSSIFCs and ASSSIFCs include mostly electrolytes, unlike NALSIFCs, which have electrode materials, electrolytes, and binders. This section summarises current SIFC research and describes the solutions used to address the concerns described above.

7.1. Based on Nonaqueous Liquid Electrolytes

Nonaqueous liquid electrolytes are used in most SIFC research. As demonstrated in Figure 3, polyanionic compounds and oxides are the most common cathode materials in reported NALSIFCs,

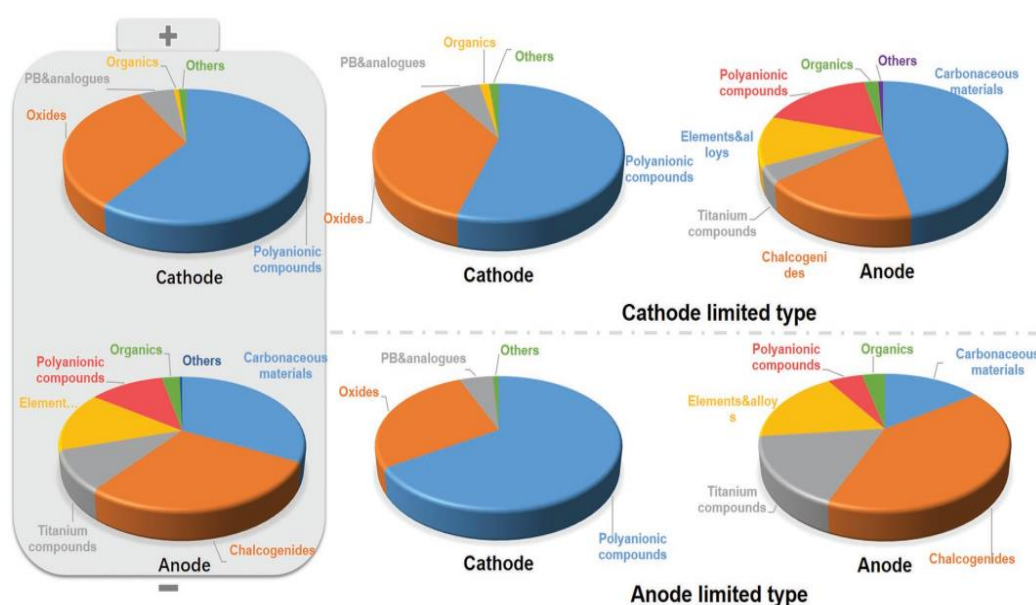


Figure 18. Summary of the proportion of various electrode materials in the NALSIFCs.

Nonaqueous liquid electrolytes are used in most SIFC research. As demonstrated in Figure 3, polyanionic compounds and oxides are the most common cathode materials in reported NALSIFCs, whereas carbonaceous materials and chalcogenides are the most common anode materials. Depending on the kind of complete cell (cathode limited or anode limited), the electrode material's function changes, notably for the anode material.

7.2. Aqueous Sodium-Ion Full-Cell System

The positive aspects of aqueous rechargeable SIBs, which include their cheap cost, excellent rate performance, and environmental friendliness, have caused them to get a lot of interest in recent years. Figure 2 provides a summary of the energy density and the average operating voltage of the aqueous sodium-ion full-cell system, which are based on recent accomplishments that have been published on the system.

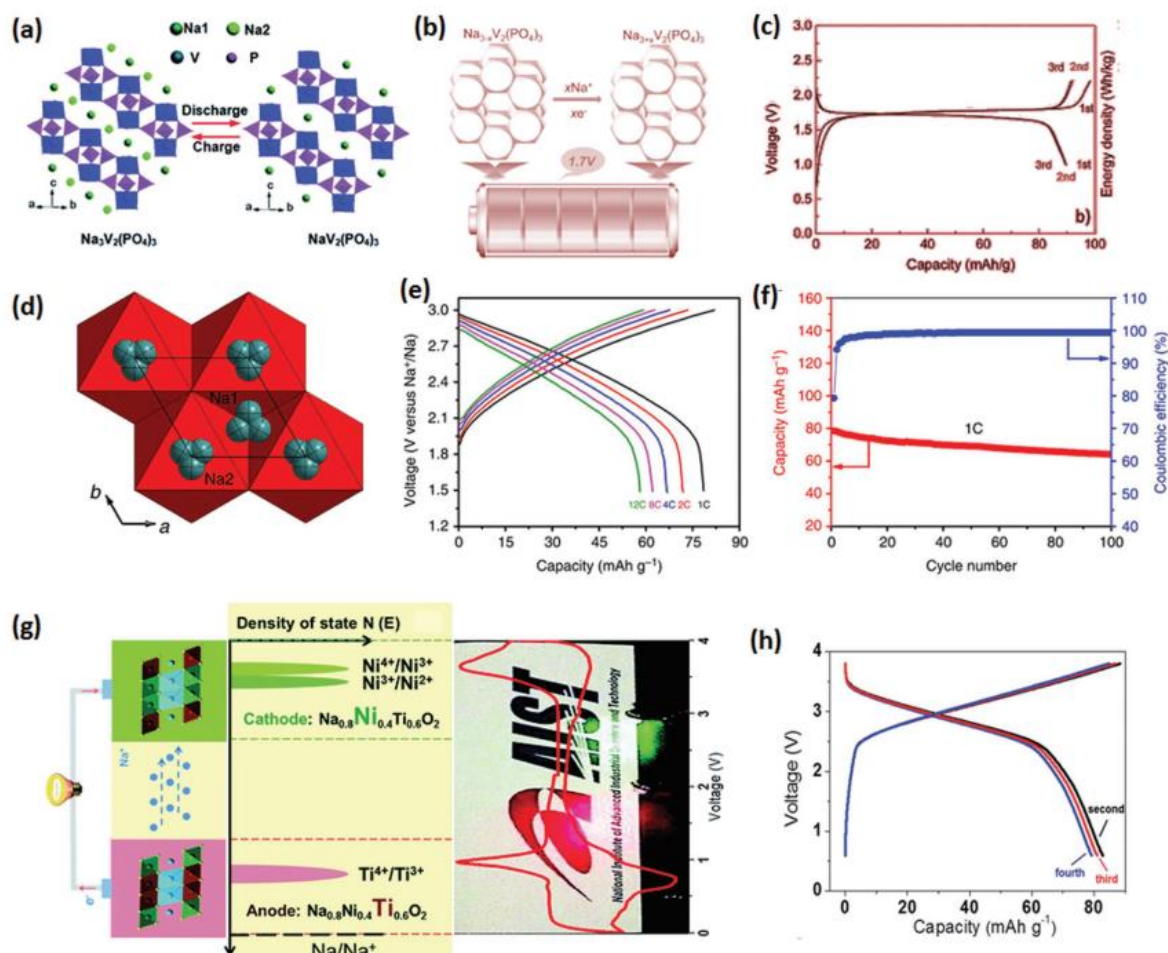


Figure 19. a,b) Schematic illustration of symmetric full sodium battery using $\text{Na}_3\text{V}_2(\text{PO}_4)_3$ for both positive and negative electrodes. c) Typical galvanostatic charging–discharging profiles of such a symmetric full sodium battery for the first three cycles at 10 C. Reproduced with permission. [65] Copyright 2016, Wiley-VCH. d) Structure of $\text{Na}_{0.6}[\text{Cr}_{0.6}\text{Ti}_{0.4}]\text{O}_2$; e) discharge profiles of $\text{Na}_{0.6}[\text{Cr}_{0.6}\text{Ti}_{0.4}]\text{O}_2/\text{Na}_{0.6}[\text{Cr}_{0.6}\text{Ti}_{0.4}]\text{O}_2$ sodium-ion full cell at various rates. f) Capacity and Coulombic efficiency versus cycle number of the $\text{Na}_{0.6}[\text{Cr}_{0.6}\text{Ti}_{0.4}]\text{O}_2/\text{Na}_{0.6}[\text{Cr}_{0.6}\text{Ti}_{0.4}]\text{O}_2$ sodium-ion full cell at the 1 C rate. Reproduced with permission. [67] Copyright 2015, Nature Publishing Group. g) Schematic illustration of the symmetric SIB design via the two redox couples of nickel and titanium in the layered material $\text{Na}_{0.8}\text{Ni}_{0.4}\text{Ti}_{0.6}\text{O}_2$ and h) charging–discharging profiles for the first three cycles. Reproduced with permission. [69]

Copyright 2015, Royal Society of Chemistry

Sb- and Sn-based anode materials have garnered attention due to their high theoretical capacity and low potential relative to Na, but they inevitably undergo enormous volume expansion during cycling due to the large ionic size of the inserted Na, destroying the anode materials and losing electrical contact, resulting in a large irreversible capacity. Before constructing the entire cell, Sb- and Sn-based anodes were presodiated to lower irreversible capacity.

NaTi₂(PO₄)₃ composite was utilised as anode and layered transition metal (M) oxides (NaM_xO₂), Prussian blue analogues, or Na₃V₂(PO₄)₃ as cathode. but these aqueous full-cell systems have fatal drawbacks of low average operating voltage (<1.5 V) and poor energy density (50 W h kg⁻¹), which restricts their practical applicability in large-scale energy storage. For large-scale electric energy storage, the aqueous system's poorly understood challenges must be resolved.

8. Nonaqueous Sodium-Ion Full-Cell System

A sodium-ion battery with sufficient energy density, safety, rate capability, and cycle life is needed for use in future energy storage systems.[178] The qualities of the active materials, cathode and anode compatibility, binder and separator choice, and electrolyte optimisation are the primary sources of these features. The active materials used in the cathode and anode of the nonaqueous sodium-ion full-cell devices may be broken down into two distinct categories: symmetric and asymmetric. This section will elaborate on the differences between the two systems.

8.1. Asymmetric Sodium-Ion Full-Cell System Based on Presodiated Anodes

The asymmetric full-cell system's high energy density is an inherent advantage over the symmetric sodium-ion full-cell system's lower energy density due to its lower operating voltage. In addition, certain alloy-based anode materials may demonstrate extraordinarily high specific capacity up to several hundred mA h g⁻¹, which can potentially boost the energy density for future practical implementation. Commercialization of the sodium-ion battery is hampered by the full-cell system's inherent problems, namely the anode material's irreversible capacity and an inadequate supply of cyclable sodium ions. The foregoing issues have prompted the development of solutions such as the presodiation procedure and the sodium compensation method. The use of sacrificial salts like NaN₃, Na₃P, or Na₂CO₃ that break down into sodium ions at a particular potential is one idea to compensate for the sodium ions in the whole cell system. [179–181] However, future commercialization may face safety concerns due to the irreversible reaction and extra product creation, such as N₂ gas. The presodiation procedure, in which sodium ions are inserted into the anode material via a half-cell system, was widely employed in the early stages of academic research due to its ability to significantly boost cycle performance and energy density. These methods have some use in gauging the electrochemical efficiency of active materials during the first stages of research. As a result, in this part, we compiled and analysed a short description of full-cell systems with a presodiated anode. Anode materials based on Sb and Sn have garnered a lot of interest because of their high theoretical capacity and low potential in comparison to Na, but they suffer from enormous volume expansion during cycling due to the large ionic size of the inserted Na, leading to the destruction of the anode materials and the loss of electrical contact, and thus a large irreversible capacity.[182] Before constructing the entire cell, presodiation using Sb- and Sn-based anodes were used to lower the full cell's irreversible capacity.[183–190]

Yu's team, for instance, suggested a complete cell made of NiSb//Na_{0.4} Mn_{0.54} Co_{0.46} O₂ that has a reversible capacity of 301 mA h g⁻¹ a current density of 300 mA gSb⁻¹, and retains 75% of its original capacity after 20 cycles.

[185] Due to their high power and cycle stability, full-cell SIBs based on presodiated transition-metal oxides that exhibit intercalation and conversion processes have also gained significant interest. In terms of rate capability and cycle stability, the $\text{Na}_2\text{Ti}_3\text{O}_7//\text{VOPO}_4$ and $\text{Na}_2\text{Ti}_3\text{O}_7//\text{Na}_{2/3}\text{Ni}_{1/3}\text{Mn}_{2/3}\text{O}_2$ complete cells performed very well.[191,192] In comparison to conventional LIBs, $\text{Na}_2\text{Ti}_3\text{O}_7//\text{VOPO}_4$ full-cell SIBs provided a much higher energy density, at 220 W h kg^{-1} . Since Na is lost during the creation of the solid electrolyte interphase (SEI) layer, hard carbon (HC) has been presodiated to improve the subpar initial coulombic efficiency and cycle life of the whole cell.[193–199] When used as an anode in a complete cell system, presodiated hard carbon may achieve the same high electrochemical performance as a pure sodium metal anode. As an added bonus, complete cell SIBs using an ether-based electrolyte have found success using graphite as the anode, which is the norm for LIBs. [194,195] The complete cell with precycled $\text{Na}_{1.5}\text{VPO}_{4.8}\text{F}_{0.7}$ Cathode and natural graphite anode could generate 120 W h kg^{-1} of energy with an average discharge voltage of 2.92 V .[200] Due to the sophisticated fabrication process and tight fabrication environment, anode presodiation and cathode precycling raise battery production costs. They're not industrial-grade.

8.2. Asymmetric Sodium-Ion Full-Cell System Using Pristine Anodes

Asymmetric complete cells with immaculate electrodes were constructed utilising commercial lithium-ion battery knowledge and procedures, and some successes were achieved. This fabrication technique is more industrially feasible and can immediately convert into industrial output. This system will be divided into carbonaceous and noncarbonaceous anodes. Table 2.

8.3. Asymmetric Sodium-Ion Full-Cell with Noncarbonaceous Anodes

The high-energy sodium-ion batteries, alloy-based anodes offer great potential due to their very high specific capacity. For instance, Sb, which has a high theoretical capacity of 660 mA h g^{-1} , has consistently been used as an anode material. Cao's team produced a whole sodium-ion battery, $\text{Sb/C}//\text{Na}_3\text{Ni}_2\text{SbO}_6$, with a 2.4 V discharge voltage and 90% of the reversible capacity of the $\text{Na}_3\text{Ni}_2\text{SbO}_6$ cathode at the 0.1 C rate (Figure 20 a).[201] After being cycled 50 times at 0.1 C , this complete cell maintained around 70% of its original capacity. Combining a $\text{P2-Na}_{2/3}\text{Ni}_{1/3}\text{Mn}_{2/3}\text{O}_2$ cathode with a Sb nanorod array anode resulted in an average operating voltage of 2.9 V , as well as enhanced capacity retention and rate capability. After 110 cycles at a current density of 0.5 A g^{-1} , the complete cell's capacity was around 620 mA h g^{-1} based on the weight of the Sb anode, which corresponds to a capacity retention of almost 94% (Figure 4b).[202]

Additionally, Yang's team produced $\text{Sb@TiO}_{2-x}//\text{Na}_3\text{V}_2(\text{PO}_4)_3\text{-C}$ sodium-ion full-cell batteries, which provided 151 W h kg^{-1} of energy at a power density of 21 W kg^{-1} (Figure 20c).[203] Furthermore, various anode types were employed as anode in full-cell systems and exhibited high compatibility with the cathode materials, including sulphide (rGO/Sb₂S₃, as shown in Figure 20d)[204,205] and transition metal oxide ($\text{Na}_{0.66}[\text{Li}_{0.22}\text{Ti}_{0.78}]\text{O}_2$, as shown in Figure 20e). Based on the Sb₂S₃ anode, the energy density of the reduced graphene oxide (rGO)/Sb₂S₃// $\text{Na}_{2/3}\text{Ni}_{1/3}\text{Mn}_{2/3}\text{O}_2$ system might approach 80 W h kg^{-1} .

When considering anode mass, high rate performance (88 mA h g⁻¹ at 50 C), and long-term cycling life (80% capacity retention over 1000 cycles at 10 C), a FeSe₂//Na₃V₂(PO₄)₃ complete cell with additional Na₃V₂(PO₄)₃ showed a high discharge capacity of 128 mA h g⁻¹ at 0.1 C. Full-cell systems still have a fatal flaw because to the exceedingly poor initial coulombic efficiency of alloy-based anodes. This necessitates a substantially higher concentration of cyclable sodium ion from the cathode materials, which poses a significant problem for currently available cathode materials and drastically reduces the efficiency and usefulness of the cathode material.

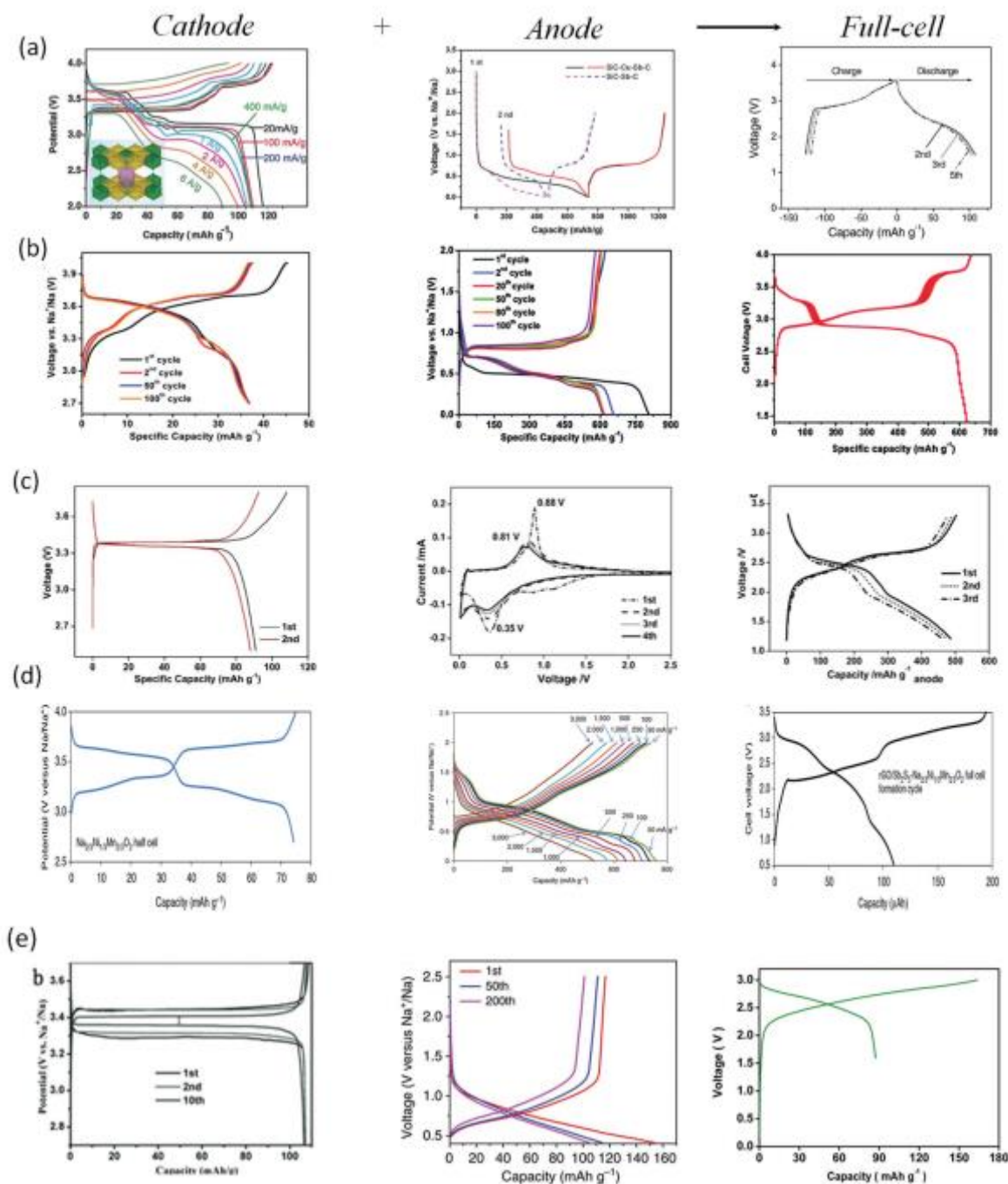


Figure 20. a) Charge and discharge profiles of Sb/C//Na₃Ni₂SbO₆ full SIB. Na₃Ni₂SbO₆ structure schematic diagram as inset image.

Reproduced with permission.[201] Copyright 2014, Wiley-VCH. b) Charge and discharge profiles of $\text{Sb//Na}_{2/3}\text{Ni}_{1/3}\text{Mn}_{2/3}\text{O}_2$ full cell at a current density of 0.5 A g^{-1} (relative to the anode weight). Reproduced with permission.[202] Copyright 2015, Royal Society of Chemistry. c) Charge and discharge profiles of full-cell $\text{Sb@TiO}_{2-x}\text{//Na}_3\text{V}_2(\text{PO}_4)_3\text{-C}$ battery, where the gravimetric capacity, power, and energy density are estimated based on the total masses of Sb@TiO_{2-x} and $\text{Na}_3\text{V}_2(\text{PO}_4)_3\text{-C}$. Reproduced with permission.[206] Copyright 2016, Wiley-VCH. d) Charge and discharge profiles of full-cell $\text{rGO/Sb}_2\text{S}_3\text{//Na}_{2/3}\text{Ni}_{1/3}\text{Mn}_{2/3}\text{O}_2$. Reproduced with permission.[207] Copyright 2013, Nature Publishing Group. e) Charge and discharge profiles of full-cell $\text{Na}_{0.66}[\text{Li}_{0.22}\text{Ti}_{0.78}]\text{O}_2\text{//Na}_3\text{V}_2(\text{PO}_4)_3\text{/C}$. Reproduced with permission.[208] Copyright 2013, Nature Publishing Group.

A high-capacity matching rate between the cathode and anode will generate a thicker coating layer on the cathode material, which can readily detach from the current collector during lengthy cycling. Even in the commercial lithium-ion battery system, the huge volume changes in alloy-based anode materials during discharge and charge operations will worsen this behaviour.

8.4. Asymmetric Sodium-Ion Full-Cell System with Carbonaceous Anode

The use of noncarbonaceous materials as an anode indicates better capacity or excellent rate capability; nevertheless, the inherent high irreversible capacity and poor energy density caused by the low operating voltage ($<3.0 \text{ V}$) remain problems. Because of their plentiful resources, low cost, renewability, industrial feasibility, and the relevant high electrochemical properties, carbonaceous materials like hard carbon are seen as one of the most promising types of anode for SIBs, which are based on the mature techniques for the commercial lithium-ion battery. As can be seen in Figure 5, for instance, significant progress has been made in the last few years in the sodium-ion full-cell system that couples layer-structured transition metal oxide cathodes with hard carbon anodes.[209,132–148] The work of Komaba et al.

reported a hard carbon// $\text{NaNi}_{1/2}\text{Mn}_{1/2}\text{O}_2$ cell with an operating voltage of 3 V at 1 C rate and an estimated specific energy density of 60% of the graphite// LiCoO_2 system.[216] The hard carbon// $\text{Na}[\text{Li}_{0.05}(\text{Ni}_{0.25}\text{Fe}_{0.25}\text{Mn}_{0.5})_{0.95}]\text{O}_2$ complete cell suggested by Oh et al. retains 76% capacity across 200 cycles at 0.5 C , as illustrated in Figure 21a,b.[217] As shown in Figure 21 c–f, Hu's group built the $\text{HC//Na}_{7/9}\text{Cu}_{2/9}\text{Fe}_{1/9}\text{Mn}_{2/3}\text{O}_2$ and $\text{HC//Na}_{0.9}[\text{Cu}_{0.22}\text{Fe}_{0.30}\text{Mn}_{0.48}]\text{O}_2$ complete cells, with energy densities of 195 and 210 W h kg^{-1} estimated on the cathode and anode's total mass.[218, 219] Figure 21 f indicates that the $\text{HC//Na}_{0.9}[\text{Cu}_{0.22}\text{Fe}_{0.30}\text{Mn}_{0.48}]\text{O}_2$ complete cell retains capacity after 100 cycles.[229] Yu et al. announced a pouch-type hard carbon// C-NaCrO_2 complete cell with 90% capacity retention after 300 cycles in 2015.[220] Tarascon's group recently produced a series of complete Na-ion cells employing carbon negative electrodes and composite positive electrodes consisting of $\text{Na}_{0.67}[\text{Fe}_{0.5}\text{Mn}_{0.5}]\text{O}_2$, $\text{Na}[\text{Fe}_{0.5}\text{Mn}_{0.5}]\text{O}_2$, and $\text{Na}[\text{Fe}_{0.5}\text{Mn}_{0.5}]\text{O}_2 + 10 \text{ wt}\% \text{ Na}_3\text{P}$. [227] Due to the usage of Na_3P as a sacrificial Na source in a complete Na-ion cell, the $\text{C//Na}[\text{Fe}_{0.5}\text{Mn}_{0.5}]\text{O}_2 + 10 \text{ wt}\% \text{ Na}_3\text{P}$ cell had the greatest electrochemical performance. After 20 cycles, this complete cell's reversible capacity stabilised at 131 mA h g^{-1} from 155 mA h g^{-1} .

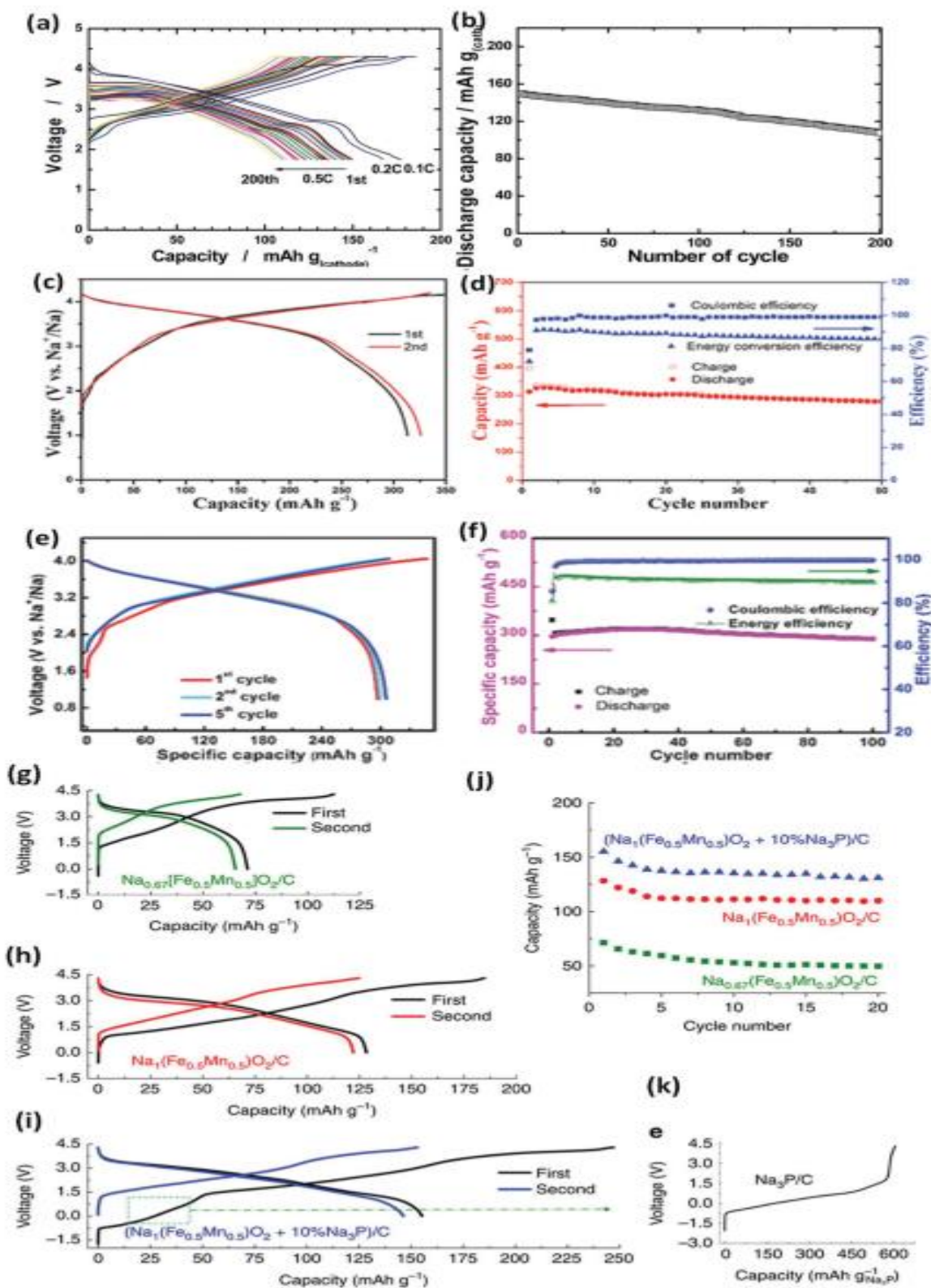


Figure 21. a,b) Charge/discharge curves and cycling data for hard carbon//Na[Li_{0.05}(Ni_{0.25}Fe_{0.25}Mn_{0.5})_{0.95}]O₂ full cell measured at 0.1, 0.2, and 0.5 C-rate. Reproduced with permission, [217] Copyright 2014, American Chemical Society. c,d) Charge/discharge curves and cycling data for HC//Na_{7/9}Cu_{2/9}Fe_{1/9}Mn_{2/3}O₂ full cell. Reproduced with permission [218]

[218] Copyright 2015, Wiley-VCH. e,f) Charge/discharge curves and cycling data for HC//Na_{0.9}Cu_{0.22}Fe_{0.30}Mn_{0.48}O₂ full cell. Reproduced with permission. [219] Copyright 2015, Wiley-VCH. Charge/discharge curves for g) C//Na_{0.67}[Fe_{0.5}Mn_{0.5}]O₂ full cell and h) C//Na[Fe_{0.5}Mn_{0.5}]O₂. i) Charge/discharge curves for C//Na[Fe_{0.5}Mn_{0.5}]O₂ + 10 wt%Na₃P cells at the 0.1 C rate. j) The capacity retention for three full cells from (g)–(i). Reproduced with permission. [73] Copyright 2016, Nature Publishing Group.

The airstable rhombohedral-structured sodium iron hexacyanoferrate (R-Na_{1.92}Fe[Fe(CN)₆])cathode and commercial hard carbon anode are utilised. Due to the R-Na_{1.92}Fe[Fe(CN)₆], high sodium-ion concentration, the entire cell had an initial charge capacity of 153.1 mA h g⁻¹ and a discharge capacity of 119.4 mA h g⁻¹, resulting in a 78% initial coulombic efficiency and 94% capacity retention after 50 cycles. Interstitial H₂O on this sort of structure degrades electrochemical characteristics, according to this group. Removal of interstitial H₂O revealed a novel dehydrated Na₂MnFe(CN)₆ phase with distinct electrochemical behaviour from the hydrated phase and a high reversible capacity at 3.5 V with outstanding rate and cycle performance.

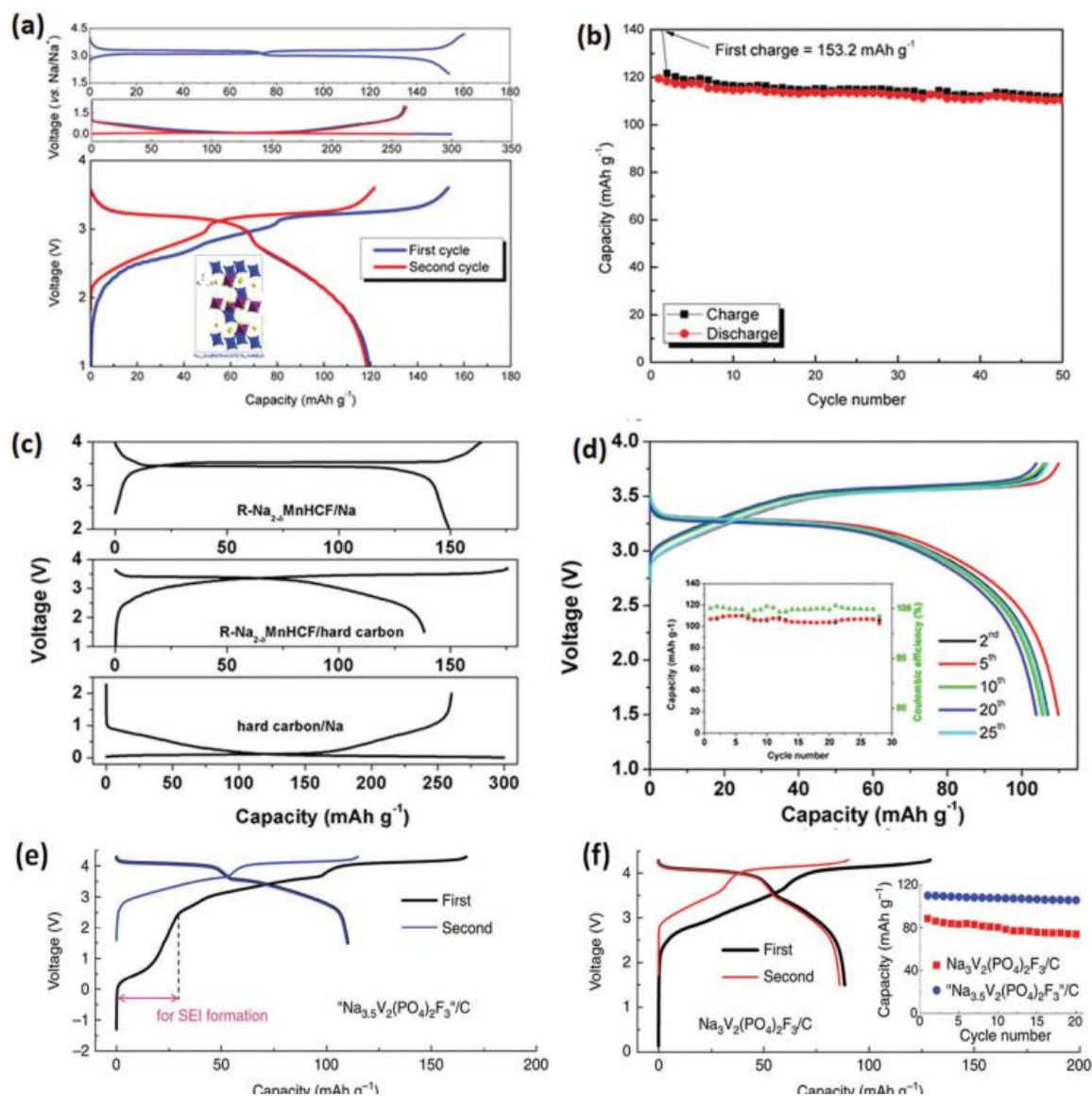


Figure 22. a) Galvanostatic charge and discharge curves of R-Na_{1.92}Fe[Fe(CN)₆]/Na, hard carbon/Na half cells, and R-Na_{1.92}Fe[Fe(CN)₆]/hard carbon full cell at a current of 10 mA g⁻¹ at the first cycle. b) Capacity retention of a R-Na_{1.92}Fe[Fe(CN)₆]/hard carbon full cell over 50 cycles. It was charged/ discharged at the current of 10 mA g⁻¹. Reproduced with permission.[224] Copyright 2015, American Chemical Society. c) The initial charge/discharge galvanostatic curves of the R-Na_{2-δ} MnHCF/Na half-cell, where MnHCF = manganese hexacyanoferrate, hard-carbon/R-Na_{2-δ} MnHCF full cell, and hard-carbon/Na half-cell. d) Charge and discharge curves of a hard-carbon/Na_xMnHCF full cell for the first 25 cycles. The full cell was cycled in the range of 3.8–1.5 V at a charge and discharge current density of 100 mA g⁻¹. The inset of (d) shows the capacity retention and Coulombic efficiency during cycling. Reproduced with permission.[223] Copyright 2015, American Chemical Society. e,f) Charge/discharge curves of C//Na_{3.5}V₂(PO₄)₂F₃ and C// Na₃V₂(PO₄)₂F₃. The inset of (f) shows the cycling performance. Reproduced with permission.[227] Copyright 2016, Nature Publishing Group.

The use of hard carbon as the anode, the full cell system achieved a reversible capacity of 140 mA h g⁻¹ at a charge and discharge current density of 100 mA g⁻¹ in the 3.8–1.5 V range.[223] Many other materials have been combined into full-cell systems using hard carbon as the anode, including layer-structured metal oxides and Prussian blue equivalents. As can be seen in Figure 22 e,f, the presence of sacrificial Na in the compound results in an initial capacity near 0.5 V, which is associated with the removal of Na from Na_{3.5} V₂(PO₄)₂F₃ to compensate for SEI formation at the negative electrode, and a subsequent rise in potential, which is also associated with the removal of Na from the compound. The total charging capacity of this cell is 167 mA h g⁻¹, while the discharge capacity is 110 mA h g⁻¹, which is an increase of 24% over the standard Na₃V₂(PO₄)₂F₃ cell. And only lately, complete SIBs with organic negative electrodes were recorded. [225,226] Na₂BDC//Na_{0.75}Mn_{0.7}Ni_{0.23}O₂ and NaHBDC//Na_{0.75}Mn_{0.7}Ni_{0.23}O₂ were reported by Abouimrane et al.[225] in complete cells that contained Na_{0.75}Mn_{0.7}Ni_{0.23}O₂ and NaHBDC//Na_{0.75}Mn_{0.7}Ni_{0.23}O₂, respectively. As measured by the anode current density at 50 cycles, the NaHBDC//Na_{0.75}Mn_{0.7}Ni_{0.23}O₂ complete cell maintains an operating voltage of 3.6 V and a discharge capacity of more than 268 mA h g⁻¹, which is 96% of the initial discharge capacity (280 mA h g⁻¹).

9. Analysis of SIB cell characteristics

Having introduced the various electrolyte materials and ideas, we will now examine their actual performance in living cells. As the interfaces/interphases with the electrodes are of utmost significance, the SEI and SL are highlighted, along with the thermal stability, before placing the few real SIB efforts into context. Having introduced the various electrolyte materials and ideas, we will now examine their actual performance in living cells. As the interfaces/interphases with the electrodes are of utmost significance, the SEI and SL are highlighted, along with the thermal stability, before placing the few real SIB efforts into context.

9.1 SEI and SL Morphology and structure

Characterising the SEI is a challenging undertaking for LIBs for the same reason that the analytical conditions/sample preparation processes may have a major effect on the data obtained and the conclusions drawn. [230] A wide variety of methods (XPS, IR, TOF-SIMS, DSC, ARC, HRTEM, etc.) have been used to investigate the SEI composition for SIB cells in light of this prior knowledge. Similar molecules (i.e. M_2CO_3 , $ROCO_2M$, $CH_2-CO-O-$, ester linkages, (M = Li or Na)) were found for both LIB and SIB cells in a comparative XPS and TOF-SIMS investigation of completely sodiated or lithiated HC electrodes in 1 M $AClO_4$ in PC (A = Li, Na, Fig. 23).

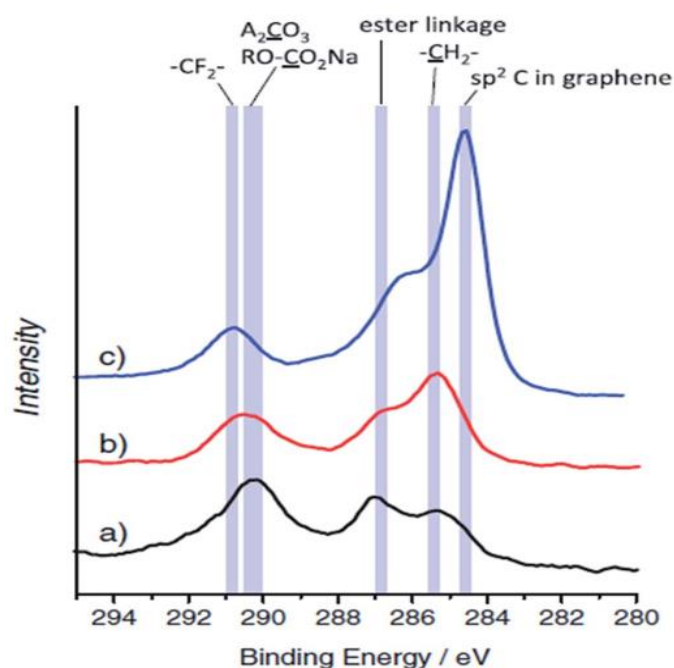


Fig. 23 XPS C1s spectra for HC electrodes tested in: (a) sodium and (b) lithium cells after the first cycle, and (c) pristine electrode. Reproduced with permission,[240] Copyright 2011, Wiley-VCH.

However, the proportions are different, with a far higher number of inorganic compounds (such as Na_2O^+ , Na_2OH^+ , Na_2Cl^+ , $Na_3CO_3^+$) identified for the SIB cells than the "organic" ones (such as $C_4H_3^+$, $C_2H_5O_3^+$, $C_2H_2O_5Li_3^+$, $Li_3CO_3^+$). found for the LIB cells.[231] Our own research[232] shows that the presence of EC in the electrolyte leads to an increase in the quantity of C-O environment of carbon (Fig. 24), which we ascribe to the ring opening of EC and the production of PEO oligomeric/polymeric species. There was no appreciable shift in SEI composition after adding DMC to lower electrolyte viscosity [233]. [232] There have been reports of noncarbonaceous negative electrodes with similar SEI compositions.[234] Using Fourier transform infrared spectroscopy, we were able to identify sodium alkoxides and alkyl carbonates in the SEI produced by dissolving 1 M $NaPF_6$ in an EC: EMC (3: 7) electrolyte.

Studies using other than XPS, [235–239] Using alloys (Sn, Mo₃Sb₇, Cu₂Sb, Sb, and In) as negative electrode materials and 1 M NaClO₄ in PC as an electrolyte, results show that carbonate-rich layers (>5 nm) completely cover the electrode after full discharge (0 V vs. Na⁺/Na), but become thinner or cracked after charging the electrodes to 2 V vs. Na⁺/Na.

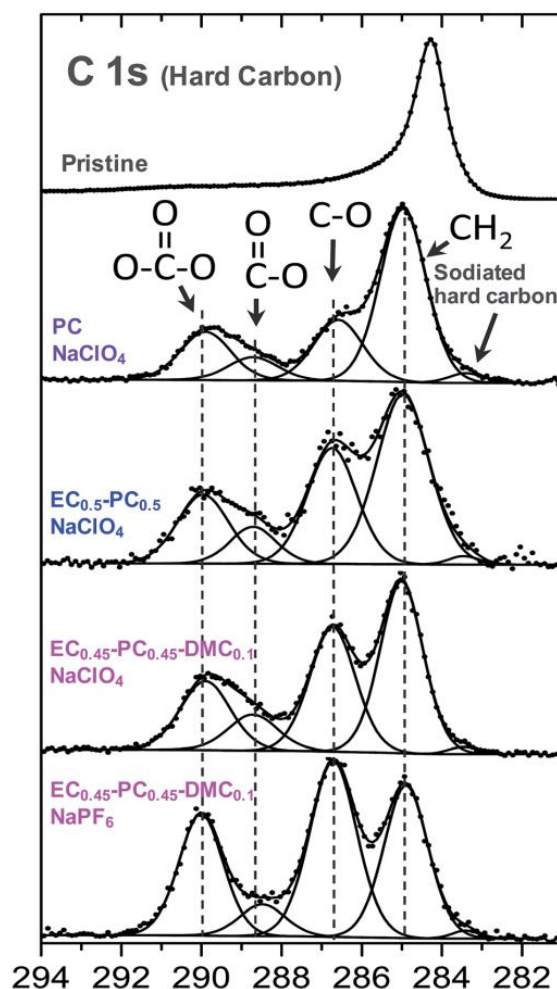


Fig. 24 XPS C1s spectra of pristine HC powder and of HC electrodes after discharge of Na/HC cells down to 3 mV vs. Na⁺/Na in various electrolytes. Reproduced with permission from The Royal Society of Chemistry.[241]

Recent work by Philippe et al. [242] used NaClO₄ and LiClO₄ in EC: DEC as electrolytes, and sodium and lithium, respectively, as counter electrodes, to perform a depth-sensitive XPS investigation of the SEI layers generated onto Fe₂O₃ electrodes by altering the photon intensity. The SEI produced in the sodium cell is thicker and more rich in inorganic species, which is different from what was found for HC negative electrodes[243]. The depth profile showed that lithium-containing SEI has a layered structure, while sodium-containing SEI has a more uniform distribution of the components.[242]

HRTEM showed a substantial change in SEI morphology on sodiated or lithiated HC electrodes employing NaClO₄ and LiClO₄ in PC electrolytes.[243] The earlier SEI surface was rough and non-uniform, whereas the later was smooth and significantly thicker.

EC has been reintroduced as a co-solvent for SIB electrolytes because it stabilises SEI by forming ether functionalities upon reduction. [241]

The surface layers (SLs) formed by electrolyte stability vs. the positive electrode have not been studied extensively, and LIBs are no exception. [244,245] After the first complete oxidation to 4.3 V vs. Na⁺/Na, Na₃V₂(PO₄)₂F₃ developed an extremely thin SL (ref. 241). Further research are planned to determine the electrode/electrolyte reactivity at high potentials. Recent investigations show better electrochemical stability vs. oxidation for both EC:PC and ethylmethyl sulfone (EMS)-based electrolytes [256], although the latter still has limited stability upon reduction. NaClO₄ or NaBF₄ in PC resulted in low Coulombic efficiency and poor capacity retention for Na₃V₂(PO₄)₃, whereas NaFSI in PC or EC : DEC electrolytes and NaPF₆ in DEC electrolytes produced superior results. [247] NaPF₆ in EC electrolytes frequently has superior Coulombic efficiency and capacity retentions than NaClO₄ in PC electrolytes.

However, half cell experiments must be interpreted with caution due to the sodium counter electrode's significant reactivity with the electrolyte, which may reduce Coulombic efficiency.[248,249]

Finally, Weadock et al. [250] used colloidal probe AFM to measure the SEI's mechanical characteristics (Young's modulus) on a Cu electrode cycled in a 1 M NaPF₆ in EC: DEC electrolyte. The heterogeneous SEI's Young's modulus ranged from 50 to 500 MPa across a 25 x 25 mm surface area. At this point, it is clear that this kind of local analysis will provide a deeper understanding of SEI properties for SIBs and LIBs, complementing results from the most commonly used SEI characterization methods (e.g. XPS, EIS, FTIR, etc.), which only provide averaged information.

9.2 Thermal stability

The thermal stability of the electrolyte (see Section 3.1) is a key design element. It is mostly governed by salt and solvents, however particular additions may be used to prevent adverse effects. However, complete SIB cells' thermal stability is more complicated due to the quality of the electrode–electrolyte interfaces and the SEI's involvement.

The SEI breaks down/cracks when heated, and exothermic interactions between the electrode and electrolyte generate a new SEI. In the following cycle, thermal breakdown of the reformed SEI and binder reactions create heat.[251] Heat is generated on the positive electrode by thermal breakdown of the active material, oxygen evolution, and solvent exothermic processes.[252]

All of the exothermic processes listed might cause battery pack thermal runaway. Thus, a safety figure of merit is the energy released by the reaction between fully charged electrodes (highest reactive state) and the electrolyte at increased temperatures. The current knowledge and recommended methods to measure thermal stability have been directly translated from LIBs to SIBs due to the electrolytes' commonalities. However, only a few electrolyte/electrode combinations have been tested by DSC or ARC.

ARC tests are performed on entire cells and cell components under adiabatic circumstances, whereas DSC measures the thermal response of individual and chosen combinations of cell components across a wide temperature range at a predetermined rate. The cell heating rate depends on the cell's inherent heat-generating processes and thermal heat capacitance.[253]

For HC electrodes, 1 M NaPF₆ in EC : PC has the greatest exothermic peak onset temperature and lowest enthalpy of reaction. The first attribute is the SEI's increased thermal stability, which is higher for NaPF₆ than NaClO₄-based electrolytes. The solvent employed also has a modest influence, EC_{0.5} : DEC_{0.5} < PC < EC : PC. [254]The SEI constructed using EC:PC has improved thermal stability. Fully sodiated HC in 1 M NaPF₆ in EC: PC has a comparable total heat produced and a greater exothermic peak onset temperature as lithiated graphite. Comparative DSC measurements for completely lithiated and sodiated HC electrodes in various electrolytes corroborate this pattern.136 However, ARC research [255,256]

appear to imply that graphite, lithiated in 1 M LiPF₆ in EC : DEC, is thermally more stable than HC sodiated in 1 M NaPF₆, due to LiPF₆'s reduced thermal stability. Moving to the positive electrodes, a variety of SIB layered positive electrode materials (Na_xFeO₂, Na_xCoO₂, Na_xCrO₂, Na_xNi_{0.5}Mn_{0.5}O₂ have been studied using DSC or ARC, with the main exothermic process being the active material decomposition involving oxygen release and solvent combustion, similar to LiCoO₂ in LIBs.[261] However, no comprehensive investigation has examined how the electrolyte or SL affect the overall heat production for SIB positive electrode materials.

Real SIBs

9.3 Practical SIBs

A decade later, Barker et al. at Valence Technologies built a 3.7 V sodium ion cell using NaVPO₄F and HC as electrode materials, which was a side effect of their intense research on phosphates for lithium batteries.[264,265] The cell, tested at room temperature at C/10 with 1 M NaClO₄ in EC:DMC electrolyte, has a reversible capacity of 80 mA h g⁻¹ on the second cycle and 50% on the 30th cycle.

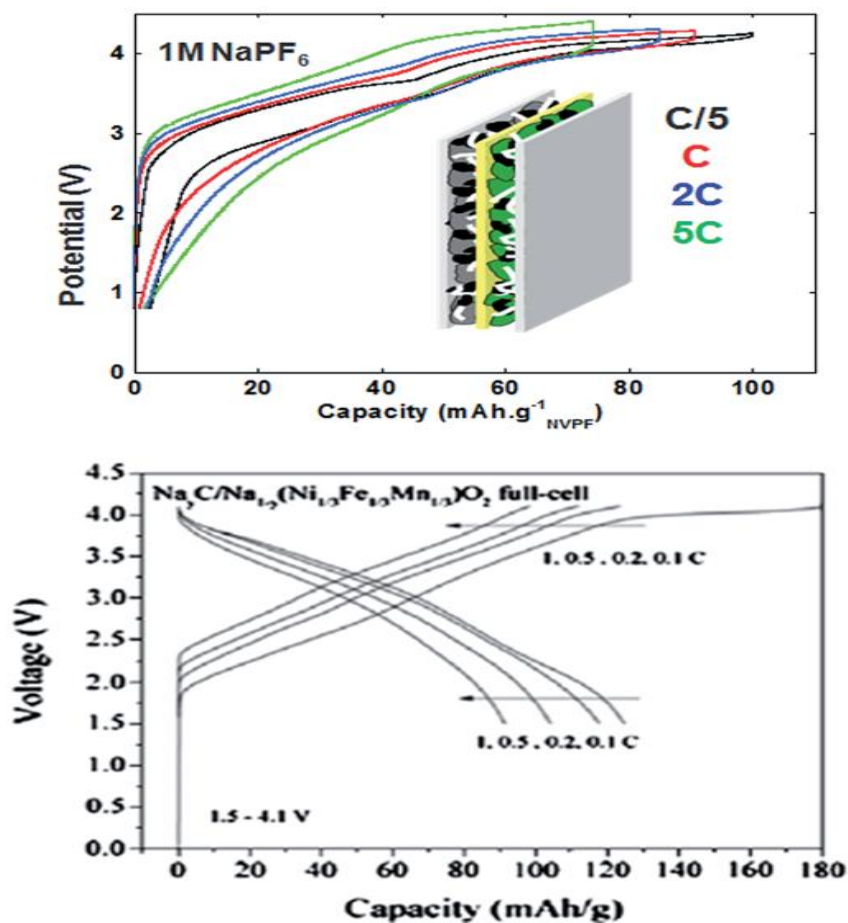


Fig. 25 Voltage versus capacity profiles for HCkNVPF full Na-ion cells cycled in 1 M NaPF₆ in EC_{0.45} : PC_{0.45} : DMC_{0.1} (reproduced with permission from The Royal Society of Chemistry [241]) and Na_yC|Na_{1-y}[Ni_{1/3}Fe_{1/3}Mn_{1/3}]O₂ (y = 0.46) cell using 1 M NaClO₄ in PC as the electrolyte recorded at different rates (reproduced with permission,[267] Copyright 2012, Elsevier).

The cycling performance of an HC|Na[Ni_{0.5}Mn_{0.5}]O₂ cell employing 1 M PC solutions of various salts (NaClO₄, NaPF₆, or NaTFSI) was reported by Komaba et al. [266] another 8-9 years later. All cells had starting capacities more than 200 mA h per (g carbon) at 1 C rate with an operating voltage of 3 V, however only the cell containing NaClO₄ lost less than 30% of its original capacity after 50 cycles, while the cells containing NaPF₆ or NaTFSI maintained 70% of their initial capacity. For a Na_yC|Na_{1-y}[Ni_{1/3}Fe_{1/3}Mn_{1/3}]O₂ (y = 0.46) cell operating at 2.75 V utilising 1 M NaClO₄ in PC as the electrolyte, Johnson et al. [267] accomplished a stable capacity of 100 mA h per (g cathode active material) for 150 cycles at 0.5 C rate. Reversible capacities ranged from 130 mA h g⁻¹ to 94 mA h g⁻¹ in a range of rate capability tests between 0.1 and 1 C (see Fig. 25). Carbon-coated Fe₃O₄ anode, Na[Ni_{0.25}Fe_{0.5}Mn_{0.25}]O₂ layered cathode, and NaClO₄ in FEC/EMS as the electrolyte were used to create a complete SIB, as described by Oh et al. This battery had a reversible operating voltage of around 2.4 V, a capacity of about 130 mAh per (g cathode active material), a capacity retention of 76.1% after 150 cycles, and a Coulombic efficiency close to 100%.[268] Recent reports have also shown that full SIBs may be achieved using organic negative electrodes (mono- or di-sodium

terephthalate) with $\text{Na}_{0.75}\text{Mn}_{0.7}\text{Ni}_{0.23}\text{O}_2$ as the positive electrode in 1 M NaPF_6 in EC: EMC. After 50 cycles, the discharge capacity of this SIB, which has an operating voltage of 3.6 V, was about 268 mA h per (g cathode active material).[269]

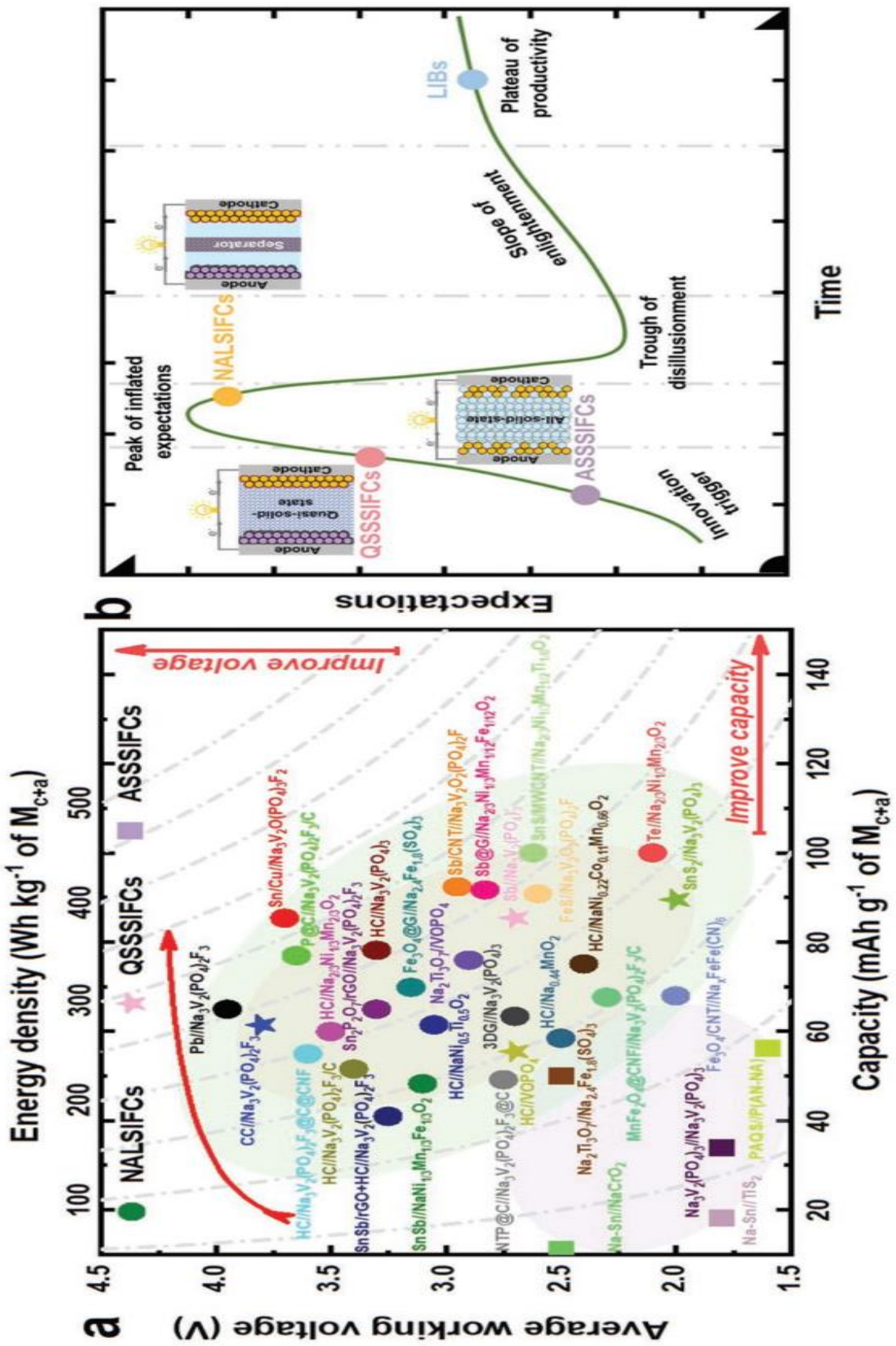
Some of us reported on complete $\text{HC}|\text{Na}_3\text{V}_2(\text{PO}_4)_2\text{F}_3$ (NVPF) cells [241] utilising 1 M NaClO_4 or NaPF_6 in $\text{EC}_{0.45} : \text{PC}_{0.45} : \text{DMC}_{0.10}$ as the electrolyte. The average potential was 3.75 V and the theoretical energy density was similar to graphite|LFP LIB cells. A steady capacity of 97 mA h per (g positive active material) for 120 cycles at C/5, a Coulombic efficiency >98.5%, and excellent performance at high rates were observed (Fig. 25).

Industrial R&D has also been partially shared. Some reports on Sumitomo's manufacturing of $\text{HC}|\text{NaFe}_{0.4}\text{Mn}_{0.3}\text{Ni}_{0.3}\text{O}_2$ coin cells and laminated SIBs employing 1 M NaPF_6 in PC as the electrolyte without FEC additive are available. Press releases are difficult to analyse.[270] These SIBs have excellent cycle life and rate capabilities, however measures to compare them to LIB cells are absent. SIBs performed better in heating and overcharging tests, since 200% overcharge only caused swelling without burst or ignite. Faradion's 3Ah SIB pouch cells with an HC negative electrode, layered positive electrode material, and an electrolyte based on NaPF_6 dissolved in a carbonate solvent mixture seem to perform similarly to LIB cells. [271]

10 Enhancing SIFCs

summarises capacity and energy density gains for the three complete cell types mentioned. Fig. a ASSSIFCs have high safety and low sodium consumption, but larger interfacial impedance causes greater polarisation and unoptimized loading (cathode, anode, and electrolyte) lower energy density, average voltage, and capacity. ASSSIFCs, like all-solid-state sodium metal batteries, still need improvement. NALSIFCs, on the other hand, have improved energy density and power density to 300 W h kg^{-1} based on cathode and anode mass. QSSSIFCs have considerable application potential and should be investigated further to optimise cycle performance and energy density. The technological maturity curve and industrialization stage may depict three complete cells (Figure 26).

Despite the longevity of studies on solid-state electrolytes, ASSSIFCs are currently mostly in the trigger era of technological birth. QSSSIFCs are becoming increasingly popular as their small interfacial impedance and high stability are thought to have a significant impact on enhancing electrochemical performance. This has led some to predict that QSSSIFC research will soon reach its peak. Research on NALSIFCs has made tremendous strides thanks to the foundational work done in LIBs. The current state of commercial SIFC development has been elaborated upon in the Introduction, and it should be noted that many different firms and research institutions have contributed to this effort.



Thus, its peak of output should develop the quickest of the three. In order to increase the whole cell's energy density, power density, and long-cycle stability, it is required to conduct a thorough examination of the most important aspects and tactics that impact these attributes. Next, for the benefit of those about to embark on or already immersed in SIFCs research, we will provide a comprehensive summary of how various modifications to the interface, electrode material choice, capacity matching, electrolyte optimisation, and sodium compensation can improve full-cell performance.

11. The Role of Cell dimensions

The modelling stacked pouch cells, it becomes clear how crucial a number of elements are in determining the impact of design choices on specific energy. For instance, the size of the cell may have a major influence on the specific energy provided by a set of electrode coatings thanks to thoughtful design. The amount of packaging needed is directly proportional to the surface area of the electrodes. However, the incremental increase in the amount of packing material needed due to a given increase in cell thickness is negligible. With an increase in electrode area comes a decrease in the 'extra' anode area needed to keep the cathodes in the right place. Our model estimates a specific energy of 139.2 W h kg⁻¹ when applied to a 15 A h cell (with cathode dimensions equal to an A5 sized sheet of paper). The cell capacity is increased by a factor of two when the cathode active area is increased to that of an A4-sized sheet, however the anticipated specific energy only increases marginally to 140.4 W h kg⁻¹ when the same design parameters are used. However, the specific energy is expected to grow by more than 5% when the cell thickness is doubled (i.e., the number of electrode layers is increased) to achieve a doubling of capacity. The limitations of a particular cell design contribute to this tendency. For instance, while determining the maximum cell thickness, one must take into account the drawability of the laminated aluminium foil packaging and the material's ability to properly close cells.[149] In addition to these mechanical restraints, there are others that are necessary for safe operation and others that arise from the performance requirements of a particular application. The active material coating, for instance, requires thick enough current collecting foils and tab terminals to withstand the requisite rates. Similarly, the separator must be thick enough and strong enough to electrically isolate the electrode layers, while also being porous enough to facilitate ionic conductivity. However, a separator that is too thick can have a negative effect on performance by decreasing the electrolyte's effective ionic conductivity and adding unnecessary mass and volume to the cell design. Once these realistic limitations are considered, it becomes apparent that reducing the volume of electrochemically inert components would improve a cell's specific energy output.

11 Summary and Future

SIBs are promising candidates to replace costly LIBs due to their low cost, abundant sodium resources, and superior safety properties. Academic research on active materials for SIBs began in 2010. A commercially viable sodium ion full-cell system should be prioritised at this time. The aqueous and symmetric systems' extremely low energy density makes them unsuitable for large-scale electric energy storage compared to commercial LIBs, despite their low cost and long cycling life.

For 10 kW storage, auxiliary supplies such the current collector, electrolyte, and packaging will account for most of the system cost. The severe environmental criteria for production and their compliant methods would considerably raise the fabrication cost for the presodiation process and sodium compensation technique.[162,167–169] Commercial full-cell design includes capacity balancing between the cathode and the anode, finding a stable electrolyte solution, choosing additives, binders, and separators, as well as the production costs of active materials for the electrodes and battery manufacturing. Academic and industry organisations must work closely to apply full-cell SIBs. The foundation for SIB production is selecting proper active materials. Thus, this section will briefly evaluate cathode and anode materials using the following criteria:

- (1) stability, which implies the active ingredients shouldn't degrade too quickly in air or have a low sensitivity to moisture or carbon dioxide;

Figure 26 displays the results of an investigation into four potential cathode materials. Polyanionic cathode materials are often vanadium or cobalt-containing phosphate or pyrophosphate-based compounds with excellent industrial feasibility and cycle performance.

Future large-scale use in energy storage raises worries about the expense and environmental friendliness of using vanadium, cobalt, or other rare metals. Prussian blue alternatives offer the benefits of being inexpensive and having a long cycle life, but their poor specific capacity and high susceptibility to interstitial water absorption severely limit their potential for mass manufacture. High rechargeable capacities and strong cycling performance have been seen in a variety of P2-type layered transition metal oxides, which have been investigated as cathode materials for full-cell SIBs. However, actual complete cell construction is hampered by the P2-type layered cathode's inherent characteristics caused by its sodium deficit. To get over the issue of the P2-type layered cathode's initial irreversible capacity, the suitable sacrificial agents Na_3P and Na_2NiO_2 are used

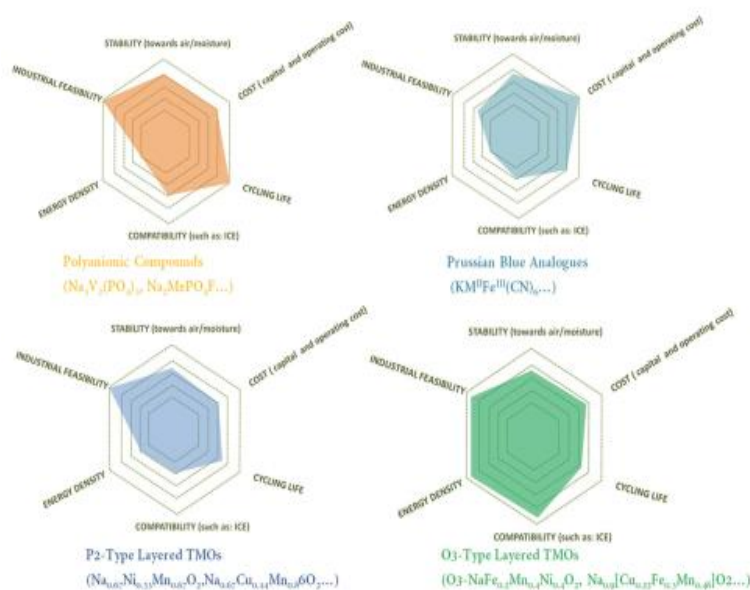


Figure 26. A brief evaluation of the different types of cathode materials (ICE: initial coulombic efficiency)

The first cycle coulombic efficiency and inadequate specific capacity achieved by using sacrificial agents to boost the irreversible capacity of P2-type cathodes fall short of what is needed to build functional SIBs. Benefiting from a high initial coulombic efficiency, a high specific capacity, and excellent compatibility with the anode, O3-type layered transition metal compounds have a high energy density due to their high operating potential. Furthermore, the established methods for lithium-ion battery materials may be simply adapted to achieve industrial viability. However, there are still certain problems that require fixing.

For instance, the generation of NaOH during the hydration of layered oxides reduces the electrode's electrochemical performance, which is a problem during both manufacture and storage

The large volume changes in these anode materials during the sodiation/desodiation process is an intrinsic problem in practical SIBs, but based on the discussion on anode materials (Figure 8), the nanostructured metals/alloys, and the metal sulphides, selenides, and oxides can offer high capacity or relatively stable cycling performance without the formation of sodium dendrites on discharge due to their high operating potential. In addition, there are significant challenges that must be addressed, such as the nanostructured anode materials' high prices and the poor initial coulombic efficiency.

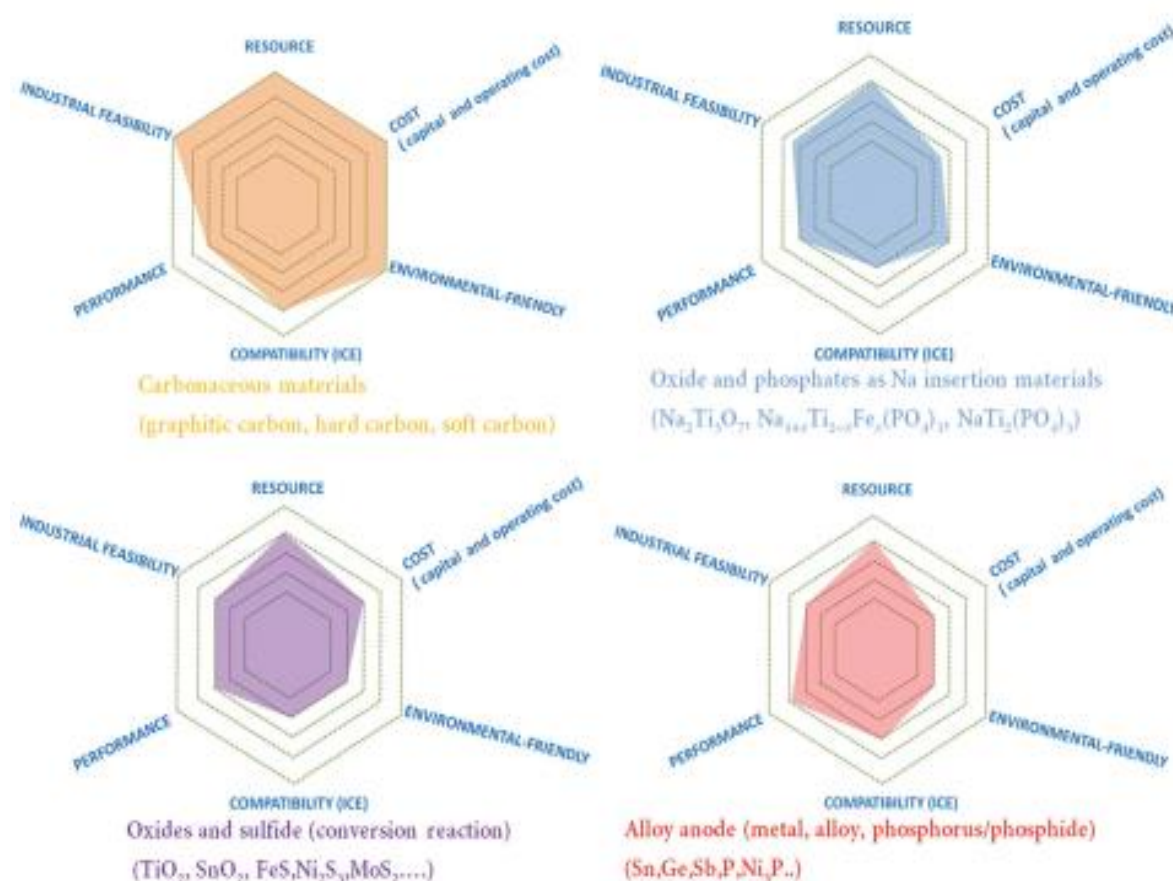


Figure 27. Evaluation of different types of anode materials (ICE: initial coulombic efficiency).

Titanium phosphate anode full-cell SIBs have high rate capability and long-term cycling stability, but their low operating voltage of 1.5-2.5 V and poor energy density make them unsuitable for high-energy SIBs. Increasing the energy density in SIBs necessitates the use of anode materials with a low operating potential, which allows for a higher operation voltage. The first commercial anode material for full SIBs is hard carbon, which provides a high practical capacity above 300 mA h g⁻¹ at a low operating potential of 0 V, as well as a high first-cycle coulombic efficiency above 80% and excellent cycling stability.

Figure 28 summarises the scholarly literature on complete SIBs, showing that those built with an O3-type layered oxide cathode and a hard carbon anode had the highest operational voltage and energy density. Overall, the O3-type layered cathode and hard carbon anode complete cell would be a good option for real-world SIBs. Several sodium ion full-cell systems, coupled with O3-type layered oxide cathode and hard carbon anode, have previously been developed in Hu's group, including hard carbon//Na_{7/9} Cu_{2/9} Fe_{1/9} Mn_{2/3} O₂ and hard carbon//Na_{0.9} Cu_{0.22} Fe_{0.3} Mn_{0.48} O₂.

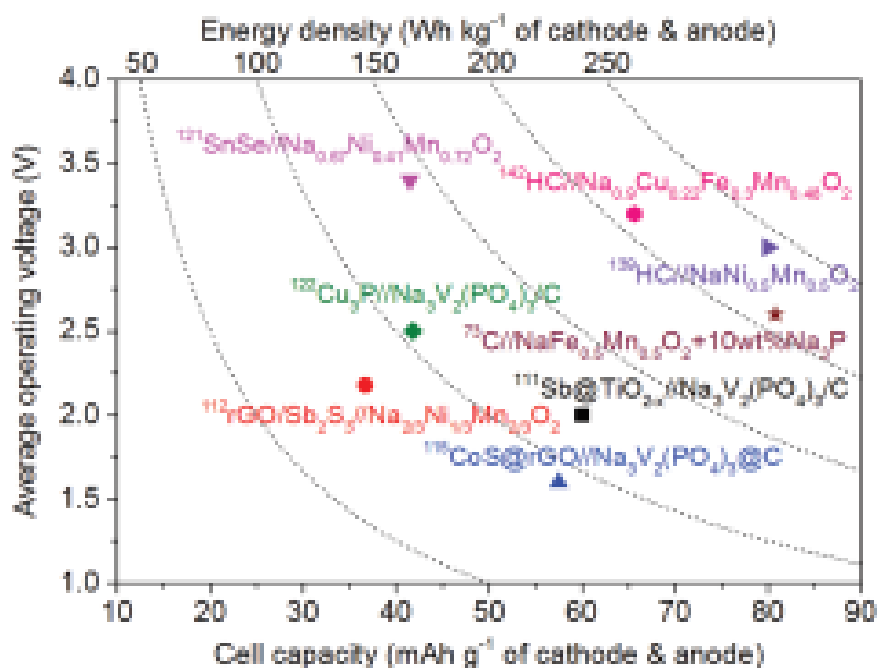


Figure 28. The energy density and average operating voltage of typical organic full-cell SIBs performed well in electrochemistry. In particular, it was discovered that copper can be integrated into layered structures and that the Cu²⁺/Cu³⁺ redox pair underlies its electrochemical activity. This discovery is important because it shows that copper may be used in place of more expensive and poisonous nickel or cobalt to create layered oxides with the same Na storing capability as those materials. While progress has been made and demand is rising, there are still some lingering problems with this system that will need to be addressed in the road. These include (a) the formation of sodium dendrites on the surface of the hard carbon anode at low voltage, (b) improving the anode's initial coulombic efficiency, and (c) using rational materials design to control the hygroscopic characteristic, phase transformation, and operating potential of an O3-type layered cathode.

Key components for SIBs include electrolytes, separators, and binders in addition to the electrode materials.

The usage of complete SIBs with electrolytes like NaClO_4 and NaPF_6 is common in academic research. Komaba et al. found that when 1 m NaPF_6/PC was used in an $\text{HC}/\text{Na}[\text{Ni}_{0.5}\text{Mn}_{0.5}]\text{O}_2$ full cell, the reversible capacity was higher and the cycling performance was better than when 1 m NaClO_4/PC was used. [138] In contrast, Poncelet et al. discovered that complete cells of hard carbon/ $\text{Na}_3\text{V}_2(\text{PO}_4)_2\text{F}_3$ incubated with 1 m NaPF_6 (98%, Aldrich) in $\text{EC}_{0.45}:\text{PC}_{0.45}:\text{DMC}_{0.1}$ solution exhibited significant polarisation when compared to cells incubated with 1 m NaClO_4 (98%, Aldrich) under the same conditions.

Poorly purified NaPF_6 salt may be to blame for the extreme polarisation, however commercial batteries are restricted from using NaClO_4 -based electrolyte solutions due to explosion risks. [168] The presence of PC solvent in the electrolyte necessitates the employment of glass fibre as the separator in cells. It is possible that the energy density of SIBs might decrease if glass fibre were used in their construction. Because of this, practical SIBs need an electrolyte composed of NaPF_6 salt in an organic solution free of the PC solvent that would otherwise breakdown the PP membrane.

The binder for the powdered electrode material is another key component in the development of functional SIBs. Carboxymethyl cellulose (CMC) binder has the potential to enhance the SEI passive layer on the anode, hence decreasing the irreversible capacity and increasing the cycle life of the cell. Considering manufacturing costs and creating eco-friendly SIBs, the CMC binder is preferable to the poly(vinylidene fluoride), poly(acrylic acid), and sodium alginate alternatives when it comes to electrodes. In addition to the aforementioned materials, the rational design of full cells is required to bring about the practical applications of SIBs in large-scale electric energy storage. These parameters and factors include the conductive additives, current collectors, electrolyte additives, cell configuration type (cylindrical, prismatic, and pouch), environmental conditions for operation, etc.

The energy density of complete cells has traditionally been exaggerated in terms of the gravimetric capabilities of the active components. When all parts of the battery system are considered, the energy density is much lower than that of commercial LIBs. Therefore, SIBs need to carefully optimise the combination of all components and rational cell design in order to make the most of their material superiority and find a good balance between the performance and cost of the batteries, so that they can eventually compete with state-of-the-art LIBs. Second, due to its relatively low volumetric energy density, sodium-ion batteries will never be able to compete with lithium-ion batteries in demanding applications such as portable devices and electromobility. Because of this, the real market for sodium-ion batteries will be in the application of large energy storage systems, and the most promising direction for developing a practical sodium-ion battery is to achieve thousands of cycles at moderate rates. The commercialization of sodium-ion full-cell systems is heavily dependent on their cycling performance and their ability to meet the needs of large energy storage systems.

References

- [1] Z. G. Yang, J. L. Zhang, M. C. W. Kintner-Meyer, X. C. Lu, D. W. Choi, J. P. Lemmon, J. Liu, *Chem. Rev.* **2011**, *111*, 3577.
- B. Dunn, H. Kamath, J. M. Tarascon, *Science* **2011**, *334*, 928.
- J. B. Goodenough, K. S. Park, *J. Am. Chem. Soc.* **2013**, *135*, 1167.
- Y. Liang, W.-H. Lai, Z. Miao, S.-L. Chou, *Small* **2018**, *14*, 1702514
- K. Chayambuka, G. Mulder, D. L. Danilov, P. H. L. Notten, *Adv. Energy Mater.* **2018**, *8*, 1800079
- C. Vaalma, D. Buchholz, M. Weil, S. Passerini, *Nat. Rev. Mater.* **2018**, *3*, 18013
- W. Ren, Z. Zhu, Q. An, L. Mai, *Small* **2017**, *13*, 1604181
- H. Kim, H. Kim, Z. Ding, M. H. Lee, K. Lim, G. Yoon, K. Kang, *Adv. Energy Mater.* **2016**, *6*, 1600943.
- Y. Liang, W.-H. Lai, Z. Miao, S.-L. Chou, *Small* **2018**, *14*, 1702514.
- H. Kim, H. Kim, Z. Ding, M. H. Lee, K. Lim, G. Yoon, K. Kang, *Adv. Energy Mater.* **2016**, *6*, 1600943.
- Y. Zhao, L. P. Wang, M. T. Sougrati, Z. Feng, Y. Leconte, A. Fisher, M. Srinivasan, Z. Xu, *Adv. Energy Mater.* **2017**, *7*, 1601424.
- M. Á. Muñoz-Márquez, D. Saurel, J. L. Gómez-Cámer, M. CasasCabanas, E. Castillo-Martínez, T. Rojo, *Adv. Energy Mater.* **2017**, *7*, 1700463.
- Y. Xiao, S. H. Lee, Y.-K. Sun, *Adv. Energy Mater.* **2017**, *7*, 1601329.
- M. Lao, Y. Zhang, W. Luo, Q. Yan, W. Sun, S. X. Dou, *Adv. Mater.* **2017**, *29*, 1700622.
- H. Hou, X. Qiu, W. Wei, Y. Zhang, X. Ji, *Adv. Energy Mater.* **2017**, *7*, 1602898.
- W. Malik, P. Dhanya, G. Yogesh, S. Neha, O. Satishchandra, *ChemSusChem* **2018**, *11*, 506.
- D. Su, K. Kretschmer, G. Wang, *Adv. Energy Mater.* **2016**, *6*, 1501785.
- H. Kim, J. Hong, Y.-U. Park, J. Kim, I. Hwang, K. Kang, *Adv. Funct. Mater.* **2015**, *25*, 534.
- C.-H. Wang, C.-H. Yang, J.-K. Chang, *Chem. Commun.* **2016**, *52*, 10890.
- R. Mogensen, J. Maibach, A. J. Naylor, R. Younesi, *Dalton Trans.* **2018**, *47*, 10752.
- J. Y. Jang, H. Kim, Y. Lee, K. T. Lee, K. Kang, N.-S. Choi, *Electrochem. Commun.* **2014**, *44*, 74.
- H. Che, S. Chen, Y. Xie, H. Wang, K. Amine, X.-Z. Liao, Z.-F. Ma, *Energy Environ. Sci.* **2017**, *10*, 1075.
- A. Ponrouch, R. Dedryvere, D. Monti, A. E. Demet, J. M. A. Mba, L. Croguennec, C. Masquelier, P. Johansson, M. R. Palacin, *Energy Environ. Sci.* **2013**, *6*, 2361.
- A. Ponrouch, E. Marchante, M. Courty, J.-M. Tarascon, M. R. Palacin, *Energy Environ. Sci.* **2012**, *5*, 8572.
- J. Zhang, D.-W. Wang, W. Lv, S. Zhang, Q. Liang, D. Zheng, F. Kang, Q.-H. Yang, *Energy Environ. Sci.* **2017**, *10*, 370.
- P. Bai, Y. He, P. Xiong, X. Zhao, K. Xu, Y. Xu, *Energy Storage Mater.* **2018**, *13*, 274.

27. K. Vignarooban, R. Kushagra, A. Elango, P. Badami, B. E. Mellander, X. Xu, T. G. Tucker, C. Nam, A. M. Kannan, *Int. J. Hydrogen Energy* **2016**, *41*, 2829.
28. J. Y. Jang, Y. Lee, Y. Kim, J. Lee, S.-M. Lee, K. T. Lee, N.-S. Choi, *J. Mater. Chem. A* **2015**, *3*, 8332.
29. Y.-E. Zhu, L. Yang, X. Zhou, F. Li, J. Wei, Z. Zhou, *J. Mater. Chem. A* **2017**, *5*, 9528.
30. L. G. Chagas, D. Buchholz, L. Wu, B. Vortmann, S. Passerini, *J. Power Sources* **2014**, *247*, 377.
31. C. Vidal-Abarca, P. Lavela, J. L. Tirado, A. V. Chadwick, M. Alfredsson, E. Kelder, *J. Power Sources* **2012**, *197*, 314.
32. C.-H. Wang, Y.-W. Yeh, N. Wongittharom, Y.-C. Wang, C.-J. Tseng, S.-W. Lee, W.-S. Chang, J.-K. Chang, *J. Power Sources* **2015**, *274*, 1016.
33. G. Yan, D. Alves-Dalla-Corte, W. Yin, N. Madern, G. Gachot, J.-M. Tarascon, *J. Electrochem. Soc.* **2018**, *165*, A1222.
34. L. Xia, L. Yu, D. Hu, G. Z. Chen, *Mater. Chem. Front.* **2017**, *1*, 584.
35. A. Bhide, J. Hofmann, A. K. Duerr, J. Janek, P. Adelhelm, *Phys. Chem. Chem. Phys.* **2014**, *16*, 1987
36. S. Kuze, J.-i. Kageura, S. Mastumoto, T. Nakayama, M. Makidera, M. Saka, T. Yamaguchi, T. Yamamoto, K. Nakane, *Sumitomo Kagaku* **2013**, *2013*, 1.
37. L. Wang, J. Song, R. Qiao, L. A. Wray, M. A. Hossain, Y.-D. Chuang, W. Yang, Y. Lu, D. Evans, J.-J. Lee, S. Vail, X. Zhao, M. Nishijima, S. Kakimoto, J. B. Goodenough, *J. Am. Chem. Soc.* **2015**, *137*, 2548.
38. K. Smith, J. Treacher, D. Ledwoch, P. Adamson, E. Kendrick, *ECS Trans.* **2017**, *75*, 13.
39. A. Bauer, J. Song, W. Pan, P. Wei, J. Barker, Y. Lu, *Adv. Energy Mater.* **2018**, *8*, 1702869.
40. X. Cao, A. Pan, S. Liu, J. Zhou, S. Li, G. Cao, J. Liu, S. Liang, *Adv. Energy Mater.* **2017**, *7*, 1700797
41. H. Li, L. Peng, Y. Zhu, D. Chen, X. Zhang, G. Yu, *Energ. Environ. Sci.* **2016**, *9*, 3399
42. W. Ren, Z. Zheng, C. Xu, C. Niu, Q. Wei, Q. An, K. Zhao, M. Yan, M. Qin, L. Mai, *Nano Energy* **2016**, *25*, 145.
43. K. Saravanan, C. W. Mason, A. Rudola, K. H. Wong, P. Balaya, *Adv. Energy Mater.* **2013**, *3*, 444
44. a) N. Wang, Z. Bai, Y. Qian, J. Yang, *Adv. Mater.* **2016**, *28*, 4126; b) D. Chao, C. H. M. Lai, P. Liang, Q. Wei, Y. S. Wang, C. R. Zhu, G. Deng, V. V. T. Doan-Nguyen, J. Lin, L. Mai, H. J. Fan, B. Dunn, Z. X. Shen, *Adv. Energy Mater.* **2018**, *8*, 1800058; c) Y. Fang, L. Xiao, J. Qian, Y. Cao, X. Ai, Y. Huang, H. Yang, *Adv. Energy Mater.* **2016**, *6*, 1502197; d) K. Chihara, A. Kitajou, I. D. Gocheva, S. Okada, J. I. Yamaki, *J. Power Sources* **2013**, *227*, 80.
45. W. Ren, X. Yao, C. Niu, Z. Zheng, K. Zhao, Q. An, Q. Wei, M. Yan, L. Zhang, L. Mai, *Nano Energy* **2016**, *28*, 216.
46. J. Zhang, Y. Fang, L. Xiao, J. Qian, Y. Cao, X. Ai, H. Yang, *ACS Appl. Mater. Interfaces* **2017**, *9*, 7177.
47. Huang Zhang, Bingsheng Qin, Daniel Buchholz, and Stefano Passerini , High-Efficiency Sodium-Ion Battery Based on NASICON Electrodes with High Power and Long Lifespan

48. B. Zhang, G. Rousse, D. Foix, R. Dugas, D. A. D. Corte, J.-M. Tarascon, *Adv. Mater.* 2016, 28, 9824.
49. J. Barker, M. Y. Saidi and J. L. Swoyer, US Pat., 6872492, 2005,(priority date April 4, 2002).
50. J. Barker, US Pat., 9608269, 2017(priority date September 30, 2011).
51. J. Barker, WO Application, 2013114102, 2015(priority date February 1, 2012).
52. H. Kim, G. Yoon, I. Park, K.-Y. Park, B. Lee, J. Kim, Y.-U. Park, S.-K. Jung, H.-D. Lim, D. Ahn, S. Lee and K. Kang, *Energy Environ. Sci.*, 2015, 8, 3325–3335.
53. P. Barpanda, G. Oyama, S.-i. Nishimura, S.-C. Chung and A. Yamada, *Nat. Commun.*, 2014, 5, 4358.
54. J. Barker, R. J. Heap, N. Roche, C. Tan, R. Sayers and Y. Liu, *ECS Meeting Abstracts*, 2013, MA2013–02, 367.
55. J. Barker and R. Heap, US Pat., 10115966, 2018(priority date March 23, 2012)
56. J. Barker and R. Heap, WO Application, 2014009724, 2014(priority date July 10, 2012).
57. J. Barker and R. Heap, US Pat., Application 20160329564, 2016(priority date January 9, 2014).
58. J. Barker and R. Heap, US Pat., 9774035, 2017(priority date July 10, 2012).
59. R. Sayers, J. Barker and R. Heap, US Pat., 10196280, 2019(priority date May 22, 2014)
60. C. Delmas, C. Fouassier and P. Hagenmuller, *Physica B+C*, 1980, 99, 81–85.
61. C. Delmas, D. Carlier and M. Guignard, *Adv. Energy Mater.*, 2021, 11(2), 2001201
62. J. Barker and R. Heap, US Pat., 9774035, 2017(priority date July 10, 2012)
63. J. Barker and R. Heap, US Pat., Application 20160329564, 2016(priority date January 9, 2014).
64. M. Keller, D. Buchholz and S. Passerini, *Adv. Energy Mater.*, 2016, 6, 1501555.
65. D. Zhou, J. Wang, X. Liu, X. He, F. Sun, V. Murzin, G. Schumacher, X. Yao, M. Winter and J. Li, *J. Power Sources*, 2020, 473, 228557.
66. X. Ding, X. Huang, J. Jin, H. Ming, L. Wang, J. Ming, *Electrochim. Acta* 2018, 260, 882.
67. B. Zhang, C. M. Ghimbeu, C. Laberty, C. Vix-Guterl, J.-M. Tarascon, *Adv. Energy Mater.* 2016, 6, 1501588.
68. J. Ming, H. Ming, W. Yang, W.-J. Kwak, J.-B. Park, J. Zheng, Y.-K. Sun, *RSC Adv.* 2015, 5, 8793.
69. B. Shen, M. Xu, Y. Niu, J. Han, S. Lu, J. Jiang, Y. Li, C. Dai, L. Hu, C. Li, *ACS Appl. Mater. Interfaces* 2018, 10, 502
70. L. Wang, J. Song, R. Qiao, L. A. Wray, M. A. Hossain, Y.-D. Chuang, W. Yang, Y. Lu, D. Evans, J.-J. Lee, S. Vail, X. Zhao, M. Nishijima, S. Kakimoto, J. B. Goodenough, *J. Am. Chem. Soc.* 2015, 137, 2548
71. A. Rudola, K. Du, P. Balaya, *J. Electrochem. Soc.* 2017, 164, A1098
72. C.-H. Wang, C.-H. Yang, J.-K. Chang, *Chem. Commun.* 2016, 52, 10890
73. I. Hasa, S. Passerini, J. Hassoun, *RSC Adv.* 2015, 5, 48928.
74. Q. Yang, P.-F. Wang, J.-Z. Guo, Z.-M. Chen, W.-L. Pang, K.-C. Huang, Y.-G. Guo, X.-L. Wu, J. Zhang, *ACS Appl. Mater. Inter-faces* 2018, 10, 34272.
75. L. Shi, W. Wang, J. Ding, *Ceram. Int.* 2018, 44, 13609.

76. W. Wang, L. Shi, D. Lan, Q. Li, J. Power Sources 2018, 377, 1.
77. J.-Y. Hwang, S.-T. Myung, J. U. Choi, C. S. Yoon, H. Yashiro, Y.-K. Sun, J. Mater. Chem. A 2017, 5, 23671
78. D. Zheng, S. Sun, W. Fan, H. Yu, C. Fan, G. Cao, Z. Yin and X. Song, The Journal of Physical Chemistry B, 2005, 109, 16439-16443
79. X. Jian, M. Jiang, Z. Zhou, M. Yang, J. Lu, S. Hu, Y. Wang and D. Hui, Carbon, 2010, 48, 4535-4541
80. Y. Zhong, X. Xia, J. Zhan, X. Wang, J. Tu, J. Mater. Chem. A **2016**, 4, 11207.
81. S. Zhang, Y. Liu, N. Zhang, K. Zhao, J. Yang, S. He, J. Power Sources **2016**, 329, 1.
82. J.-Y. Hwang, S.-T. Myung, J. U. Choi, C. S. Yoon, H. Yashiro, Y.-K. Sun, J. Mater. Chem. A **2017**, 5, 23671.
83. P. Hou, J. Yin, X. Lu, J. Li, Y. Zhao, X. Xu, *Nanoscale* **2018**, 10, 6671.
84. J. A. Rudola, K. Du, P. Balaya, J. Electrochem. Soc. 2017, 164, A1098. [72] X. Ding, X. Huang, J. Jin, H. Ming, L. Wang, J. Ming, Electrochim. Acta 2018, 260, 882
85. J. Song, L. Wang, Y. Lu, J. Liu, B. Guo, P. Xiao, J.-J. Lee, X.-Q. Yang, G. Henkelman, J. B. Goodenough, J. Am. Chem. Soc. 2015, 137, 2658
86. K. Moyer, J. Donohue, N. Ramanna, A. P. Cohn, N. Muralidharan, J. Eaves, C. L. Pint, *Nanoscale* 2018, 10, 13335.
87. H. Banda, D. Damien, K. Nagarajan, M. Hariharan, M. M. Shaijumon, J. Mater. Chem. A 2015, 3, 10453.
88. A. Li, Z. Feng, Y. Sun, L. Shang, L. Xu, J. Power Sources 2017, 343, 424
89. R. E. Franklin and J. T. Randall, Proc. R. Soc. London, Ser. A, 1951, 209, 196–218.
90. D. A. Stevens and J. R. Dahn, J. Electrochem. Soc., 2000, 147, 1271
91. D. A. Stevens and J. R. Dahn, J. Electrochem. Soc., 2001, 148, A803.
92. D. A. Stevens and J. R. Dahn, J. Electrochem. Soc., 2000, 147, 1271
93. Y. Morikawa, S.-i. Nishimura, R.-i. Hashimoto, M. Ohnuma and A. Yamada, *Adv. Energy Mater.*, 2020, 10, 1903176.
94. S. Alvin, D. Yoon, C. Chandra, H. S. Cahyadi, J.-H. Park, W. Chang, K. Y. Chung and J. Kim, Carbon, 2019, 145, 67– 81.
95. J. M. Stratford, P. K. Allan, O. Pecher, P. A. Chater and C. P. Grey, Chem. Commun., 2016, 52, 12430–12433.
96. R. V'ali, A. J'anes, T. Thomberg and E. Lust, *Electrochim. Acta*, 2017, 253, 536–544
97. B.-H. Hou, Y.-Y. Wang, J.-Z. Guo, Y. Zhang, Q.-L. Ning, Y. Yang, W.-H. Li, J.-P. Zhang, X.-L. Wang, X.-L. Wu, *ACS Appl. Mater. Interfaces* 2018, 10, 3581.
98. B.-H. Hou, Y.-Y. Wang, J.-Z. Guo, Q.-L. Ning, X.-T. Xi, W.-L. Pang, A.-M. Cao, X. Wang, J.-P. Zhang, X.-L. Wu, *Nanoscale* 2018, 10, 9218.
99. Y. Liu, N. Zhang, X. Liu, C. Chen, L.-Z. Fan, L. Jiao, *Energy Storage Mater.* 2017, 9, 170.
100. Y. Lu, P. Zhou, K. Lei, Q. Zhao, Z. Tao, J. Chen, *Adv. Energy Mater.* 2017, 7, 1601973.
101. A. Kamiyama, K. Kubota, D. Igarashi, Y. Youn, Y. Tateyama, H. Ando, K. Gotoh and S. Komaba, *Angew. Chem., Int. Ed.*, 2021, DOI: 10.1002/anie.202013951.
102. R. Sayers, J. Barker and A. Rudola, WO Application, 2020120967, 2020(priority date December 13, 2018).

103. J. Barker and Y. Liu, US Pat., Application 20180301696, 2018(priority date October 6, 2015).
104. X. Li, P. Yan, M. H. Engelhard, A. J. Crawford, V. V. Viswanathan, C. Wang, J. Liu, V. L. Sprenkle, *Nano Energy* 2016, 27, 664.
105. H. Che, S. Chen, Y. Xie, H. Wang, K. Amine, X.-Z. Liao, Z.-F. Ma, *Energy Environ. Sci.* 2017, 10, 1075.
106. A. Ponrouch, E. Marchante, M. Courty, J.-M. Tarascon, M. R. Palacin, *Energy Environ. Sci.* 2012, 5, 8572.
107. C. Vidal-Abarca, P. Lavela, J. L. Tirado, A. V. Chadwick, M. Alfredsson, E. Kelder, *J. Power Sources* 2012, 197, 314.
108. G. G. Eshetu, M. Martinez-Ibañez, E. Sánchez-Diez, I. Gracia, C. Li, L. M. Rodriguez-Martinez, T. Rojo, H. Zhang, M. Armand, *Chem. - Asian J.* 2018, 13, 2770.
109. M. S. Ding, K. Xu, T. R. Jow, *J. Electrochem. Soc.* 2000, 147, 1688.
110. N. Takenaka, H. Sakai, Y. Suzuki, P. Uppula, M. Nagaoka, *J. Phys. Chem. C* 2015, 119, 18046.
111. Y. Lee, J. Lee, J. Lee, K. Kim, A. Cha, S. Kang, T. Wi, S. J. Kang, H.-W. Lee, N.-S. Choi, *ACS Appl. Mater. Interfaces* 2018, 10, 15270.
112. H. Che, J. Liu, H. Wang, X. Wang, S. S. Zhang, X.-Z. Liao, Z.-F. Ma, *Electrochem. Commun.* 2017, 83, 20.
113. J. Y. Jang, Y. Lee, Y. Kim, J. Lee, S.-M. Lee, K. T. Lee, N.-S. Choi, *J. Mater. Chem. A* 2015, 3, 8332.
114. A. Ponrouch, D. Monti, A. Boschini, B. Steen, P. Johansson, M. R. Palacin, *J. Mater. Chem. A* 2015, 3, 22
115. H. Che, S. Chen, Y. Xie, H. Wang, K. Amine, X. Liao, Z.-F. Ma, *Energy Environ. Sci.* 2017, 10, 1075
116. L. Zhao, J. Zhao, Y. S. Hu, H. Li, Z. Zhou, M. Armand, L. Chen, *Adv. Energy Mater.* 2012, 2, 962.
117. J. Y. Hwang, S. T. Myung, Y. K. Sun, *Chem. Soc. Rev.* 2017, 46, 3529 S. Komaba, W. Murata, T. Ishikawa, N. Yabuuchi, T. Ozeki, T. Nakayama, A. Ogata, K. Gotoh, K. Fujiwara, *Adv. Funct. Mater.* 2011, 21, 3859.
118. A. Ponrouch, R. Dedryvere, D. Monti, A. E. Demet, J. M. A. Mba, L. Croguennec, C. Masquelier, P. Johansson, M. R. Palacin, *Energy Environ. Sci.* 2013, 6, 2361
119. C. Ding, T. Nohira, R. Hagiwara, A. Fukunaga, S. Sakai, K. Nitta, *Electrochim. Acta* 2015, 176, 344
120. I. Hasa, S. Passerini, J. Hassoun, *J. Power Sources* 2016, 303, 203.
121. C. H. Wang, C.-H. Yang, J.-K. Chang, *Chem. Commun.* 2016, 52, 10890.
122. H. Che, S. Chen, Y. Xie, H. Wang, K. Amine, X. Liao, Z.-F. Ma, *Energy Environ. Sci.* 2017, 10, 1075.
123. H. Gao, W. Zhou, K. Park, J. B. Goodenough, *Adv. Energy Mater.* 2016, 6, 1600467.
124. A. Hayashi, K. Noi, A. Sakuda, M. Tatsumisago, *Nat Commun.* 2012, 3, 856
125. Y. Noguchi, E. Kobayashi, L. S. Plashnitsa, S. Okada, J.-I. Yamaki, *Electrochim. Acta* 2013, 101, 59.

126. J.-K. Kim, Y. J. Lim, H. Kim, G. B. Cho, Y. Kim, *Energy Environ. Sci.* **2015**, *8*, 3589.
127. H. Gao, L. Xue, S. Xin, K. Park, J. B. Goodenough, *Angew. Chem., Int. Ed.* **2017**, *56*, 5541
128. A. Ponrouch, E. Marchante, M. Courty, J. M. Tarascon and M. R. Palacín, *Energy Environ. Sci.*, **2012**, *5*, 8572
129. S. Y. Hong, Y. Kim, Y. Park, A. Choi, N. S. Choi and K. T. Lee, *Energy Environ. Sci.*, **2013**, *6*, 2067
130. L. J. Krause, W. Lamanna, J. Summerfield, M. Engle, G. Korba, R. Loch and R. Atanasoski, *J. Power Sources*, **1997**, *68*, 320.
131. D. J. Vevlin and P. Herley, *React. Solids*, **1987**, *3*, 75.
132. T. Evans, J. Olson, V. Bhat and S.-H. Lee, *J. Power Sources*, **2014**, *269*, 616.
133. A. Bhide, J. Hofmann, A. K. Durr, J. Janek and P. Adelhelm, *Phys. Chem. Chem. Phys.*, **2014**, *16*, 1987
134. P. Johansson, H. Markusson, P. Jacobsson and M. Armand, *Phys. Chem. Chem. Phys.*, **2004**, *6*, 895.
135. J. Scheers, P. Johansson, P. Szczecinski, W. Wieczorek, M. Armand and P. Jacobsson, *J. Power Sources*, **2010**, *195*, 6081.
136. A. Plewa-Marczewska, T. Trzeciak, A. Bitner, L. Niedzicki, M. Dranka, G. Z. Zukowska, M. Marcinek and W. Wieczorek, *Chem. Mater.*, **2014**, *26*, 4908.
137. L. Niedzicki, G. Z. Zukowska, M. Bukowska, P. Szczecinski, S. Grugeon, S. Laruelle, M. Armand, S. Panero, B. Scrosati, M. Marcinek and W. Wieczorek, *Electrochim. Acta*, **2010**, *55*, 1450.
138. J. Scheers, D.-H. Lim, J.-K. Kim, E. Paillard, W. A. Henderson, P. Johansson, J.-H. Ahn and P. Jacobsson, *J. Power Sources*, **2014**, *251*, 451.
139. R. G. Pearsons, *J. Am. Chem. Soc.*, **1963**, *85*, 3533
140. E. Jónsson and P. Johansson, *Phys. Chem. Chem. Phys.*, **2012**, *14*, 10774.
141. Thematic issue *MRS Bull.*, **2013**, *38*, 7. The whole issue deals with ionic liquids.
142. M. Armand, F. Endres, D. R. MacFarlane, H. Ohno and B. Scrosati, *Nat. Mater.*, **2009**, *8*, 621.
143. D. Monti, E. Jónsson, M. R. Palacin and P. Johansson, *J. Power Sources*, **2014**, *245*, 630.
144. L. U. Subasinghe, G. S. Reddy, A. Rudola and P. Balaya, *J. Electrochem. Soc.*, **2020**, *167*, 110504.
145. K. Du, C. Wang, L. U. Subasinghe, S. R. Gajella, M. Law, A. Rudola and P. Balaya, *Energy Storage Materials*, **2020**, *29*, 287–299.
146. A. Tripathi, A. Rudola, S. R. Gajella, S. Xi and P. Balaya, *J. Mater. Chem. A*, **2019**, *7*, 25944–25960.
147. T. Broux, F. Fauth, N. Hall, Y. Chatillon, M. Bianchini, T. Bamine, J.-B. Leriche, E. Suard, D. Carlier, Y. Reynier, L. Simonin, C. Masquelier and L. Croguennec, *Small Methods*, **2019**, *3*, 1800215.
148. S. Mariyappan, T. Marchandier, F. Rabuel, A. Iadecola, G. Rouse, A. V. Morozov, A. M. Abakumov and J.-M. Tarascon, *Chem. Mater.*, **2020**, *32*, 1657–1666.

149. J.-K. Kim, Y. J. Lim, H. Kim, G.-B. Cho, Y. Kim, *Energy Environ. Sci.* **2015**, *8*, 3589.
150. D. Zhang, X. Cao, D. Xu, N. Wang, C. Yu, W. Hu, X. Yan, J. Mi, B. Wen, L. Wang, L. Zhang, *Electrochim. Acta* **2018**, *259*, 100.
151. A. Hayashi, K. Noi, N. Tanibata, M. Nagao, M. Tatsumisago, *J. Power Sources* **2014**, *258*, 420.
152. R. P. Rao, H. Chen, L. L. Wong, S. Adams, *J. Mater. Chem. A* **2017**, *5*, 3377
153. L. Zhang, K. Yang, J. Mi, L. Lu, L. Zhao, L. Wang, Y. Li, H. Zeng, *Adv. Energy Mater.* **2015**, *5*, 1501294.
154. **J. W. Heo, A. Banerjee, K. H. Park, Y. S. Jung, S.-T. Hong**, *Adv. Energy Mater.* **2018**, *8*, 1702716.
155. **A. Banerjee, K. H. Park, J. W. Heo, Y. J. Nam, C. K. Moon, S. M. Oh, S.-T. Hong, Y. S. Jung**, *Angew. Chem., Int. Ed.* **2016**, *55*, 9634.
156. D. Zhang, X. Cao, D. Xu, N. Wang, C. Yu, W. Hu, X. Yan, J. Mi, B. Wen, L. Wang, L. Zhang, *Electrochim. Acta* **2018**, *259*, 100.
157. **A. Banerjee, K. H. Park, J. W. Heo, Y. J. Nam, C. K. Moon, S. M. Oh, S.-T. Hong, Y. S. Jung**, *Angew. Chem., Int. Ed.* **2016**, *55*, 9634
158. N. Tanibata, T. Matsuyama, A. Hayashi, M. Tatsumisago, *J. Power Sources* **2015**, *275*, 284
159. K. Noi, Y. Nagata, T. Hakari, K. Suzuki, S. Yubuchi, Y. Ito, A. Sakuda, A. Hayashi, M. Tatsumisago, *ACS Appl. Mater. Interfaces* **2018**, *10*, 19605.
160. **Z. Zhang, K. Xu, X. Rong, Y.-S. Hu, H. Li, X. Huang, L. Chen**, *J. Power Sources* **2017**, *372*, 270
161. **J. van den Broek, S. Afyon, J. L. M. Rupp**, *Adv. Energy Mater.* **2016**, *6*, 1600736.
162. X. Y. Wu, Y. L. Cao, X. P. Ai, J. F. Qian, H. X. Yang, *Electrochem. Commun.* **2013**, *31*, 145.
163. D. J. Kim, Y. H. Jung, K. K. Bharathi, S. H. Je, D. K. Kim, A. Coskun, J. W. Choi, *Adv. Energy Mater.* **2014**, *4*, 1400133.
164. X. Y. Wu, M. Y. Sun, Y. F. Shen, J. F. Qian, Y. L. Cao, X. P. Ai, H. X. Yang, *ChemSusChem* **2014**, *7*, 407.
165. Z. Hou, X. Li, J. Liang, Y. Zhu, Y. Qian, *J. Mater. Chem. A* **2015**, *3*, 1400.
166. K. Nakamoto, Y. Kano, A. Kitajou, S. Okada, *J. Power Sources* **2016**, *327*, 327.
167. Y. Wang, L. Mu, J. Liu, Z. Yang, X. Yu, L. Gu, Y.-S. Hu, H. Li, X. Q. Yang, L. Chen, X. Huang, *Adv. Energy Mater.* **2015**, *5*, 1501005.
168. X. Q. Shan, D. S. Charles, Y. K. Lei, R. M. Qiao, G. F. Wang, W. L. Yang, M. Feyngenson, D. Su, X. W. Teng, *Nat. Commun.* **2016**, *7*, 13370.
169. Q. Zhang, C. Y. Liao, T. Y. Zhai, H. Q. Li, *Electrochim. Acta* **2016**, *196*, 470.
170. B. Zhao, Q. Wang, S. Zhang, C. Deng, *J. Mater. Chem. A* **2015**, *3*, 12089.
171. Y. S. Wang, J. Liu, B. J. Lee, R. M. Qiao, Z. Z. Yang, S. Y. Xu, X. Q. Yu, L. Gu, Y. S. Hu, W. L. Yang, K. Kang, H. Li, X. Q. Yang, L. Q. Chen, X. J. Huang, *Nat. Commun.* **2015**, *6*, 12089.
172. Z. Li, D. Young, K. Xiang, W. C. Carter, Y. M. Chiang, *Adv. Energy Mater.* **2013**, *3*, 290.

173. M. Pasta, C. D. Wessells, N. Liu, J. Nelson, M. T. McDowell, R. A. Huggins, M. F. Toney, Y. Cui, *Nat. Commun.* **2014**, *5*, 3007.
174. H. Gao, J. B. Goodenough, *Angew. Chem., Int. Ed.* **2016**, *55*, 12768.
175. L. Chen, H. Z. Shao, X. F. Zhou, G. Q. Liu, J. Jiang, Z. P. Liu, *Nat. Commun.* **2016**, *7*, 11982.
176. H. Pan, Y.-S. Hu, L. Chen, *Energy Environ. Sci.* **2013**, *6*, 2338.
177. Y. Wang, J. Yi, Y. Xia, *Adv. Energy Mater.* **2012**, *2*, 830.
178. S. Y. Hong, Y. Kim, Y. Park, A. Choi, N.-S. Choi, K. T. Lee, *Energy Environ. Sci.* **2013**, *6*, 2067.
179. S. Kuze, J. I. Kageura, S. Matsumoto, T. Nakayama, M. Makidera, M. Saka, T. Yamaguchi, T. Yamamoto, K. Nakane, *SUMITOMO KAGAKU.* **2013**, *2013*, 1.
180. <http://www.faradion.co.uk/technology/sodium-ion-technology/> (accessed: May, 2015).
181. <http://www2.cnrs.fr/en/2659.htm> (accessed: November, 2015).
182. H. Kang, Y. Liu, K. Cao, Y. Zhao, L. Jiao, Y. Wang, H. Yuan, *J. Mater. Chem. A* **2015**, *3*, 17899.
183. I. Hasa, J. Hassoun, Y.-K. Sun, B. Scrosati, *ChemPhysChem* **2014**, *15*, 2152.
184. I. Hasa, S. Passerini, J. Hassoun, *RSC Adv.* **2015**, *5*, 48928.
185. J. Liu, Z. Yang, J. Wang, L. Gu, J. Maier, Y. Yu, *Nano Energy* **2015**, *16*, 389.
186. F. Wan, J. Z. Guo, X. H. Zhang, J. P. Zhang, H. Z. Sun, Q. Yan, D. X. Han, L. Niu, X. L. Wu, *ACS Appl. Mater. Interfaces* **2016**, *8*, 7790.
187. M. Walter, S. Doswald, M. V. Kovalenko, *J. Mater. Chem. A* **2016**, *4*, 7053.
188. N. Wang, Z. Bai, Y. Qian, J. Yang, *ACS Appl. Mater. Interfaces* **2017**, *9*, 447.
189. X. Rui, W. Sun, C. Wu, Y. Yu, Q. Yan, *Adv. Mater.* **2015**, *27*, 6670.
190. W. Sun, X. Rui, D. Zhang, Y. Jiang, Z. Sun, H. Liu, S. Dou, *J. Power Sources* **2016**, *309*, 135.
191. H. Li, L. Peng, Y. Zhu, D. Chen, X. Zhang, G. Yu, *Energy Environ. Sci.* **2016**, *9*, 3399.
192.] J. Ni, S. Fu, C. Wu, Y. Zhao, J. Maier, Y. Yu, L. Li, *Adv. Energy Mater.* **2016**, *6*, 1502568.
193. D. Kim, E. Lee, M. Slater, W. Lu, S. Rood, C. S. Johnson, *Electrochem. Commun.* **2012**, *18*, 66.
194. H. Wang, Y. Xiao, C. Sun, C. Lai, X. Ai, *RSC Adv.* **2015**, *5*, 106519.
195. H. Wang, M. Gu, J. Jiang, C. Lai, X. Ai, *J. Power Sources* **2016**, *327*, 653.
196. L. Wu, D. Buchholz, C. Vaalma, G. A. Giffin, S. Passerini, *ChemElectroChem* **2016**, *3*, 292.
197. W. Ren, X. Yao, C. Niu, Z. Zheng, K. Zhao, Q. An, Q. Wei, M. Yan, L. Zhang, L. Mai, *Nano Energy* **2016**, *28*, 216.
198. X. Li, P. Yan, M. H. Engelhard, A. J. Crawford, V. V. Viswanathan, C. Wang, J. Liu, V. L. Sprenkle, *Nano Energy* **2016**, *27*, 664.
199.] E. de la Llave, V. Borgel, K. J. Park, J. Y. Hwang, Y. K. Sun, P. Hartmann, F. Chesneau, D. Aurbach, *ACS Appl. Mater. Interfaces* **2016**, *8*, 1867
200. H. Kim, J. Hong, Y.-U. Park, J. Kim, I. Hwang, K. Kang, *Adv. Funct. Mater.* **2015**, *25*, 534.

201. D. Yuan, X. Liang, L. Wu, Y. Cao, X. Ai, J. Feng, H. Yang, *Adv. Mater.* **2014**, *26*, 6301.
202. L. Liang, Y. Xu, C. Wang, L. Wen, Y. Fang, Y. Mi, M. Zhou, H. Zhao, Y. Lei, *Energy Environ. Sci.* **2015**, *8*, 2954.
203. N. Wang, Z. Bai, Y. Qian, J. Yang, *Adv. Mater.* **2016**, *28*, 4126
204. Y. Xiao, S. H. Lee, Y. K. Sun, *Adv. Energy Mater.* **2017**, *7*, 1601329.
205. H. Kang, Y. Liu, K. Cao, Y. Zhao, L. Jiao, Y. Wang, H. Yuan, *J. Mater. Chem. A* **2015**, *3*, 17899.
206. N. Wang, Z. Bai, Y. Qian, J. Yang, *Adv. Mater.* **2016**, *28*, 4126.
207. D. Y. W. Yu, P. V. Prikhodchenko, C. W. Mason, S. K. Batabyal,
208. Y. S. Wang, X. Q. Yu, S. Y. Xu, J. M. Bai, R. J. Xiao, Y. S. Hu, H. Li, X. Q. Yang, L. Q. Chen, X. J. Huang, *Nat. Commun.* **2013**, *4*, 2365.
209. B. Zhang, R. Dugas, G. Rousse, P. Rozier, A. M. Abakumov, J. M. Tarascon, *Nat. Commun.* **2016**, *7*, 10308.
210. P. Han, X. Han, J. Yao, Z. Liu, X. Cao, G. Cui, *Electrochem. Commun.* **2015**, *61*, 84.
211. Z. Zhu, F. Cheng, Z. Hu, Z. Niu, J. Chen, *J. Power Sources* **2015**, *293*, 626.
212. Z. Yuan, L. Si, X. Zhu, *J. Mater. Chem. A* **2015**, *3*, 23403.
213. Y. Niu, M. Xu, C. Cheng, S. Bao, J. Hou, S. Liu, F. Yi, H. He, C. M. Li, *J. Mater. Chem. A* **2015**, *3*, 17224.
214. Y. Dong, S. Li, K. Zhao, C. Han, W. Chen, B. Wang, L. Wang, B. Xu, Q. Wei, L. Zhang, X. Xu, L. Mai, *Energy Environ. Sci.* **2015**, *8*, 1267.
215. B. Zhang, C. M. Ghimbeu, C. Laberty, C. Vix-Guterl, J.-M. Tarascon, *Adv. Energy Mater.* **2016**, *6*, 1501588.
216. S. Komaba, W. Murata, T. Ishikawa, N. Yabuuchi, T. Ozeki, T. Nakayama, A. Ogata, K. Gotoh, K. Fujiwara, *Adv. Funct. Mater.* **2011**, *21*, 3859.
217. S. M. Oh, S. T. Myung, J. Y. Hwang, B. Scrosati, K. Amine, Y. K. Sun, *Chem. Mater.* **2014**, *26*, 6165.
218. S. Y. Xu, X. Y. Wu, Y. M. Li, Y. S. Hu, L. Q. Chen, *Chin. Phys. B* **2014**, *23*, 118202.
- 219.
220. Y. Li, Z. Yang, S. Xu, L. Mu, L. Gu, Y.-S. Hu, H. Li, L. Chen, *Adv. Sci.* **2015**, *2*, 1500031.
221. L. Mu, S. Xu, Y. Li, Y. S. Hu, H. Li, L. Chen, X. Huang, *Adv. Mater.* **2015**, *27*, 6928.
222. C. Y. Yu, J. S. Park, H. G. Jung, K. Y. Chung, D. Aurbach, Y. K. Sun, S. T. Myung, *Energy Environ. Sci.* **2015**, *8*, 2019.
223. T. Yang, T. Qian, M. Wang, X. Shen, N. Xu, Z. Sun, C. Yan, *Adv. Mater.* **2016**, *28*, 539.
224. H. Wang, X. Z. Liao, Y. Yang, X. M. Yan, Y. S. He, Z. F. Ma, *J. Electrochem. Soc.* **2016**, *163*, A565.
225. J. Song, L. Wang, Y. Lu, J. Liu, B. Guo, P. Xiao, J. J. Lee, X. Q. Yang, G. Henkelman, J. B. Goodenough, *J. Am. Chem. Soc.* **2015**, *137*, 2658.

226. L. Wang, J. Song, R. Qiao, L. A. Wray, M. A. Hossain, Y. D. Chuang, W. Yang, Y. Lu, D. Evans, J. J. Lee, S. Vail, X. Zhao, M. Nishijima, S. Kakimoto, J. B. Goodenough, *J. Am. Chem. Soc.* **2015**, *137*, 2548.
227. A. Abouimrane, W. Weng, H. Eltayeb, Y. Cui, J. Niklas, O. Poluektov, K. Amine, *Energy Environ. Sci.* **2012**, *5*, 9632.
228. H. Wang, P. Hu, J. Yang, G. Gong, L. Guo, X. Chen, *Adv. Mater.* **2015**, *27*, 2348
229. B. Zhang, R. Dugas, G. Rousse, P. Rozier, A. M. Abakumov, J. M. Tarascon, *Nat. Commun.* **2016**, *7*, 10308
230. P. Verma, P. Maire and P. Novák, *Electrochim. Acta*, 2010, *55*, 6332.
231. C. Vidal-Abarca, P. Lavela, J. L. Tirado, A. V. Chadwick, M. Alfredsson and E. Kelder, *J. Power Sources*, 2012, *197*, 314.
232. A. Ponrouch, R. Dedryvere, D. Monti, J. M. Ateba Mba, L. Croguennec, C. Masquelier, P. Johansson and M. R. Palacín, *Energy Environ. Sci.*, 2013, *6*, 2361.
233. L. Vogdanis, B. Martens, H. Uchtmann, F. Hensel and W. Heitz, *Makromol. Chem.*, 1990, *191*, 465.
234. A. Abouimrane, W. Weng, H. Eltayeb, Y. Cui, J. Niklas, O. Poluektov and K. Amine, *Energy Environ. Sci.*, 2012, *5*, 9632
235. L. Baggetto, P. Ganesh, R. P. Meisner, R. R. Unocic, J. C. Jumas, C. A. Bridges and G. M. Veith, *J. Power Sources*, 2013, *234*, 48.
236. L. Baggetto, E. Allcorn, R. R. Unocic, A. Manthiram and G. M. Veith, *J. Mater. Chem. A*, 2013, *1*, 11163.
237. L. Baggetto, E. Allcorn, A. Manthiram and G. M. Veith, *Electrochem. Commun.*, 2013, *27*, 168.
238. L. Baggetto, P. Ganesh, C. N. Sun, R. A. Meisner, T. A. Zawodzinski and G. M. Veith, *J. Mater. Chem. A*, 2013, *1*, 7985.
239. S. A. Webb, L. Baggetto, C. A. Bridges and G. M. Veith, *J. Power Sources*, 2014, *248*, 1105.
240. S. A. Webb, L. Baggetto, C. A. Bridges and G. M. Veith, *J. Power Sources*, 2014, *248*, 1105.
241. A. Ponrouch, R. Dedryvere, D. Monti, J. M. Ateba Mba, L. Croguennec, C. Masquelier, P. Johansson and M. R. Palacín, *Energy Environ. Sci.*, 2013, *6*, 2361.
242. B. Philippe, M. Valvo, F. Lindgren, H. Rensmo and K. Edstrom, *Chem. Mater.*, 2014, *26*, 5028.
243. S. Komaba, W. Murata, T. Ishikawa, N. Yabuuchi, T. Ozeki, T. Nakayama, A. Ogata, K. Gotoh and K. Fujiwara, *Adv. Funct. Mater.*, 2011, *21*, 3859.
244. D. Aurbach, B. Markovsky, M. D. Levi, E. Levi, A. Schetchter, M. Moshkovich and Y. Cohen, *J. Power Sources*, 1999, *81–82*, 95.
245. K. Edstrom, T. Gustafsson and J. O. Thomas, *Electrochim. Acta*, 2004, *50*, 397.
246. S. M. Oh, S. T. Myung, C. S. Yoon, J. Lu, J. Hassoun, B. Scrosati, K. Amine and Y. K Sun, *Nano Lett.*, 2014, *14*, 1620.
247. Z. Jian, W. Han, X. Lu, H. Yang, Y.-S. Hu, J. Zhou, Z. Zhou, J. Li, W. Chen, D. Chen and L. Chen, *Adv. Energy Mater.*, 2013, *3*, 156.
248. T. D. Hatchard and M. N. Obrovac, *J. Electrochem. Soc.*, 2014, *161*, A1748.
249. A. Rudola, D. Aurbach and P. Balaya, *Electrochem. Commun.*, 2014, *46*, 56.

250. N. Weadock, N. Varongchayakul, J. Wan, S. Lee, J. Seog and L. Hu, *Nano Energy*, 2013, 2, 713.
251. H. Yang, H. Bang, K. Amine and J. Prakash, *J. Electrochem. Soc.*, 2005, 152, A73.
252. D. D. MacNeil and J. R. Dahn, *J. Electrochem. Soc.*, 2002, 149, A912.
253. D. Doughty and E. P. Roth, *Interface*, 2012, 21, 37.
254. A. Ponrouch, E. Marchante, M. Courty, J. M. Tarascon and M. R. Palacín, *Energy Environ. Sci.*, 2012, 5, 8572.
255. X. Xia, M. N. Obrovac and J. R. Dahn, *Electrochem. SolidState Lett.*, 2011, 14, A130.
256. X. Xia and J. R. Dahn, *J. Electrochem. Soc.*, 2012, 159, A515.
257. J. Zhao, L. Zhao, N. Dimov, S. Okada and T. Nishida, *J. Electrochem. Soc.*, 2013, 160, A3077.
258. X. Xia and J. R. Dahn, *J. Electrochem. Soc.*, 2012, 159, A647.
259. X. Xia and J. R. Dahn, *Electrochem. Solid-State Lett.*, 2012, 15A1.
260. X. Xia and J. R. Dahn, *J. Electrochem. Soc.*, 2012, 159, A1048.
261. D. D. MacNeil and J. R. Dahn, *J. Electrochem. Soc.*, 2002, 149, A912.
262. L. W. Shacklette, T. R. Jow and L. Townsend, *J. Electrochem. Soc.*, 1985, 135, 2669.
263. Y. Ma, M. M. Doeff, S. J. Visco and L. J. De Jonghe, *J. Electrochem. Soc.*, 1993, 140, 2726.
264. J. Barker, Y. Saily and J. L. Swoyer, US Patent 2002/0192553.
265. Barker, Y. Saily and J. L. Swoyer, *Electrochem. Solid-State Lett.*, 2003, 6, A1.
266. R. Alcantara, P. Lavela, G. F. Ortiz and J. L. Tirado, *Electrochem. Solid-State Lett.*, 2005, 8, A222.
267. D. Kim, E. Lee, M. Slater, W. Lu, S. Rood and C. S. Johnson, *Electrochem. Commun.*, 2012, 18, 66.
268. S. M. Oh, S. T. Myung, C. S. Yoon, J. Lu, J. Hassoun, B. Scrosati, K. Amine and Y. K Sun, *Nano Lett.*, 2014, 14, 1620.
269. A. Abouimrane, W. Weng, H. Eltayeb, Y. Cui, J. Niklas, O. Poluektov and K. Amine, *Energy Environ. Sci.*, 2012, 5, 9632.
270. S. Kuze, J. I. Kageura, S. Matsumoto, T. Nakayama, M. Makidera, M. Saka, T. Yamaguchi, T. Yamamoto and K. Nakane, *Sumitomo Kagaku*, 2013, 1.
271. J. Barker, R. Heap, N. Roche, C. Tan, R. Sayers and Y. Liu, 17th IMLB, Como 10–14th June 2014, Abstract #266.
272. B. Zhang, C. M. Ghimbeu, C. Laberty, C. Vix-Guterl, J.-M. Tarascon, *Adv. Energy Mater.* **2016**, 6, 1501588.
273. G. Singh, B. Acebedo, M. C. Cabanas, D. Shanmukaraj, M. Armand, T. Rojo, *Electrochem. Commun.* **2013**, 37, 61.
274. M. Sathiya, J. Thomas, D. Batuk, V. Pimenta, R. Gopalan, J. M. Tarascon, *Chem. Mater.* **2017**, 29, 5948.
275. B. Zhang, R. Dugas, G. Rousse, P. Rozier, A. M. Abakumov, J. M. Tarascon, *Nat. Commun.* **2016**, 7, 10308.